
ΠΑΝΕΠΙΣΤΗΜΙΟ ΚΡΗΤΗΣ
UNIVERSITY OF CRETE


# *Dynamics and linear viscoelasticity of polymeric assemblies at high pressures*

***Nikolaos A. Burger***

***Supervisor:*** *Prof. Dimitris Vlassopoulos*

***Co-supervisor:*** *Dr. Benoit Loppinet*

*Heraklion, September 2020*

***University of Crete***

*Department of Materials Science and Technology*

*FORTH - IESL*

# ***Acknowledgements***

First and foremost, I would like to thank Benoit Loppinet and Dimitris Vlassopoulos who provided me the opportunity to continue my studies under their supervision in the lab, giving me the chance to work in this amazing project. I leave the lab (for the time being) having in my mind the best memories which had been emerged by our perfect cooperation. They had an inexhaustible patience and appetite to transport the necessary supplies for my future with their unique way. They were great supervisors and amazing persons, too.

I would like to give very special thanks to Gerhard Meier for the nice discussions, the perfect biscuits and for his contribution in this work. He was always willing to help. I am delighted to have met him. George Petekidis for the nice discussions and the great collaboration in my first try as teacher assistant. With his way was helped to be a nice experience for me. To Nikos Hadjichristidis & Laurent Bouteiller and in their students for providing the materials used in this thesis.

To Antonis, not only his contribution in the project (always willing to help) and our nice discussions but also for his contribution in my life outside the lab. He was a pedagogue for me. I'd really like to thank Athanasios Bogris, for the perfect collaboration in my first years in the lab.

I'd really like to thank, King and Mohan**,** for the nice and helpful conversations. Furthermore, I'd like to thank all of group mates Panagiota, Katerina, Alan, Daniele, Ameur, Katerina, Nikos, Antje, Dimitra, Consi, Moudi, Captain, Antonio!! and Stelios for the great environment.

Following with the friends I need permission from the ecological ministration to write for them, I would like to thank from my bottom of my heart Nikos, what the heck-leave it, Manos you should call Stelios father at some point, Stelios peees, Aris(?), my lovely school teacher Kostas, George I will wait for your wedding, doctor Stavros – after all I will be doctor before you 're', Kostakis no comment for you sweetheart, Nikos and his 'pipila' courses, Vasilis Vrasidas & his cat Haris, Antonis I am waiting to return in Ethia, Christina and who is ok? Antonis without kir, Manos 'be PANATHINAIKOS', don't forget the lovely grandpas Jokerako & Stef, the albino rabbits Eva, Erinni & Niki, as well as Maria, Depi, Dr Kostakis, Gaitazi, Johnny tyraki, Aggelos, Petros,

Aristotelis ole, Periklis & Eleni for the amazing time with so many laughs, fights, drinks & adventures where we pass together in the island (as well as away from this) since I was came here.

Last but definitely not least, I'd like to thank my mother Eleni, my brother Alexandro, my grand mother Eva and the aunts Senti & Rena because they were always willing to help as well as supporting me with their valuable advice.

*This thesis is dedicated to my good friend Panagiotis Asmanis*

**ΠΑΝΕΠΙΣΤΗΜΙΟ ΚΡΗΤΗΣ**
**ΣΧΟΛΗ ΘΕΤΙΚΩΝ ΚΑΙ ΤΕΧΝΟΛΟΓΙΚΩΝ ΕΠΙΣΤΗΜΩΝ**
**ΤΜΗΜΑ ΕΠΙΣΤΗΜΗΣ ΚΑΙ ΤΕΧΝΟΛΟΓΙΑΣ ΥΛΙΚΩΝ**

*Ηράκλειο, 3 Σεπτεμβρίου 2020*

**Πρακτικά Εξεταστικής Επιτροπής**

**του Μεταπτυχιακού Φοιτητή Νικολάου Αθανάσιου Μπούρκερ για την απόκτηση Διπλώματος Μεταπτυχιακών Σπουδών**

Ο ***κ Νικόλαος Αθανάσιος Μπούρκερ,*** μεταπτυχιακός φοιτητής του Προγράμματος Μεταπτυχιακών Σπουδών του Τμήματος Επιστήμης και Τεχνολογίας Υλικών του Πανεπιστημίου Κρήτης, παρουσίασε υπό μορφή σεμιναρίου σε ανοικτό ακροατήριο που πραγματοποιήθηκε με τηλεδιάσκεψη σύμφωνα με α) την παρ. 1 του άρθρ.12 της από 11.3.2020 Πράξης Νομοθετικού Περιεχομένου (Α'55), και τις οδηγίες εφαρμογής Α Δ1α/Γποικ.28237/5.5.2020 Κ.Υ.Α (Β'1699), ΑΔΑ: ΨΠ7046ΜΤΛΗ-43Φ στις **3 Σεπτεμβρίου 2020**, την ερευνητική του εργασία με τίτλο:

**«High-pressure light scattering and microrheology: application to supramolecular and associating polymer solutions»**

**«Σκέδαση φωτός και μικροreολογία σε υψηλή πίεση: εφαρμογή σε υπερμοριακά και συσσωματούμενα πολυμερικά διαλύματα»**

Η τριμελής εξεταστική επιτροπή έκρινε την εν γένει παρουσίαση και ερευνητική εργασία του υποψηφίου πολύ καλή και προτείνει ομόφωνα την απονομή του Διπλώματος Μεταπτυχιακών Σπουδών.

Η Τριμελής Επιτροπή

**Δημήτριος Βλασσόπουλος (Επιβλέπων)**
Καθηγητής, Τμήμα Επιστήμης και Τεχνολογίας Υλικών, Πανεπιστημίου Κρήτης

**Benoit Loppinet**
Ερευνητής Β', Ινστιτούτο Ηλεκτρονικής Δομής και Λέιζερ, Ίδρυμα Τεχνολογίας Έρευνας, Ηράκλειο Κρήτης

**Γεώργιος Πετεκίδης**
Καθηγητής Τμήματος Επιστήμης και Τεχνολογίας Υλικών Πανεπιστημίου Κρήτης

# CONTENTS

# ***Introduction***

## I. High-hydrostatic pressure

The role of pressure, and especially high hydrostatic pressure (HHP) has long been considered in science and technology. HHP typically ranges from 100 bar to 100 kbar, or equivalently from $10^7$ Pa to $10^{10}$ Pa (1bar=$10^5$ Pa). The studies rely on the development of compressor and cells able to reach pressure up to 1000 GPa. An important contribution was done by Bridgeman that was rewarded by the Nobel prize in Physics in 1946.

The effects of high hydrostatic pressure (HHP) have been considered in physics chemistry and also biology [1-6]. The on-going development of high-pressure instruments and apparatus lead to many studies [7-12]. The development of megabar diamond anvil cells, known as DAC (Fig 1 and table 1) and its use with synchrotron radiation improved the last twenty years. Targeting increase of the upper pressure limit, have opened a new window of opportunities [10, 13-22]. Using HHP, one may expect that many new materials and new phases are to be discovered [23,24]. High-pressure scattering experiments (X-ray, Neutron, Infrared and Raman spectroscopy) evidenced structural and molecular characterization [25-31]. In particular pressure-induced phase transitions were observed [32]. HHP was found to have big impact on chemical processes. It affects the chemical reactions and their kinetics. Specific reactions are induced at elevated pressures, especially interesting in the context of green-chemistry [33,34]. Studies have focused both on dynamic as well as static properties [35]. Overall, pressure is essential parameter for structural but also electronic, magnetic, optical elastic properties [7,8] and HHP allows to evidence some of its effect. The existence of living organisms in deep ocean [36-42] (P~1kbar, 100MPa) calls for the understanding of biology under high pressure. Similarly, the prevailing extreme conditions closer to the nuclear highlight the importance to extract information about earth materials properties (structural-mechanical) under such conditions [43,44].

Application wise the use of HHP is covering many different fields. For example, the very important Haber–Bosch process to convert atmospheric nitrogen ($N_2$) to ammonia ($NH_3$) takes place at ~100 bar [45]. Oher significant HHP applications are pressure-induced homogenization for the production of stable emulsions, enhanced crude oil recovery, production and used of supercritical fluids, renewable energy processes [137], manufacturing or high-pressure processes for food

preservation [8,9]. The latter has been proposed as a promising industrial method for food preservation (under the acronym of HPP) as a practical alternative to conventional thermal processing as it can be applied in a big variety of products. The effect on the food taste is less than the temperature treatment [46-50]. It relies on the deactivation of the microorganisms under high pressure (~6 kbar).

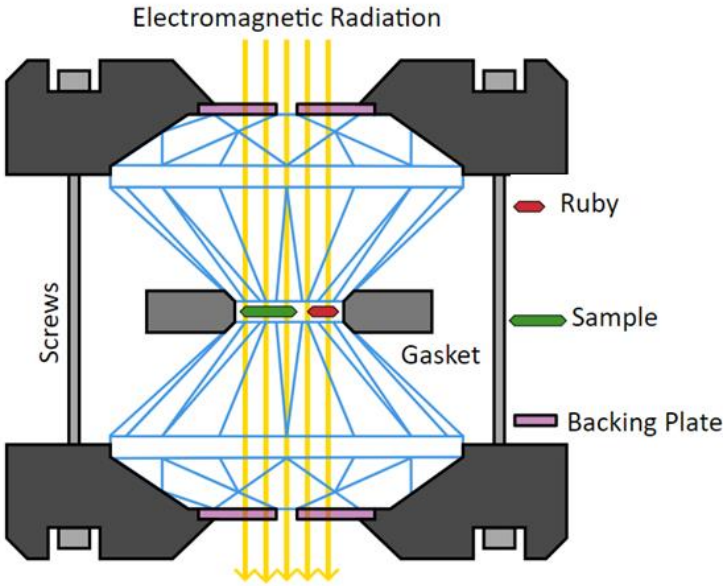


**Table 1: Characteristics and limitations of different DAC. Obtained from [7].**

| $C$ ($\mu$m) | $B$ ($\mu$m) | $A$ ($\mu$m) | $\alpha_1$° | $\alpha_2$° | $P_{max}$ (GPa) | Sample | Gasket |
|---|---|---|---|---|---|---|---|
| | | < 4 | | | 640 | Re | Re |
| 350 | 250 | 20 | 15 | 8.5 | 408 | Mo | Re |
| | 350 | 22 | | 8.5 | 364 | W | Steel |
| | | 25 | | 8 | 320 | H | Re |
| | 300 | 30 | | 8.5 | 384 | Ir | W |
| 450 | 250 | 35 | 15 | 7 | 297 | Sc | Re |
| | 300 | 40 | | 8.5 | 300 | Fe | Steel |
| | 300 | 50 | | 8.5 | 302 | CsI | Steel |
| | 300 | 75 | | 8 | 220 | Ti | Re |
| | 300 | 100 | | 8 | 241 | Ca | cBN,Re |
| | 300 | 150 | | | 190 | Mn | Steel |
| | 300 | 180 | | 1.5 | 172 | Steel | Steel |
| | 660 | 230 | | 2 | 155 | Steel | Steel |
| | | 1000 | | | 94 | $H_2O$ | Steel |

**Figure 1**: Diamond anvil cell (DAC). Cartoon adapted from Wikipedia.

Another recent application of ultra-high pressure (UHP) is the completion of phase diagram of nitrogen, helium or hydrogen. Recently, the phase diagram and stability limits of diatomic solid nitrogen were reported [51]. From spectroscopic experiments the formation of a largely amorphous new molecular phases were observed at pressures in the order of GPa [52,53]. Application of ultra-high pressures in different gases such as helium and $H_2$ lead to complex phase behavior as depicted in figure 2). J. Shi and Y. Li report the presence of two energetically stable ammonia helium compounds at high pressure [52,54]. Earlier, Liu et al. predicting plastic and superionic helium-ammonia compounds at extreme condition with the formation of eight new stable phases of the respective compounds [55]. The understating of the properties of such materials under extreme conditions attract the interest of the community due to the rich occurrence of helium and hydrogen in space. [56].

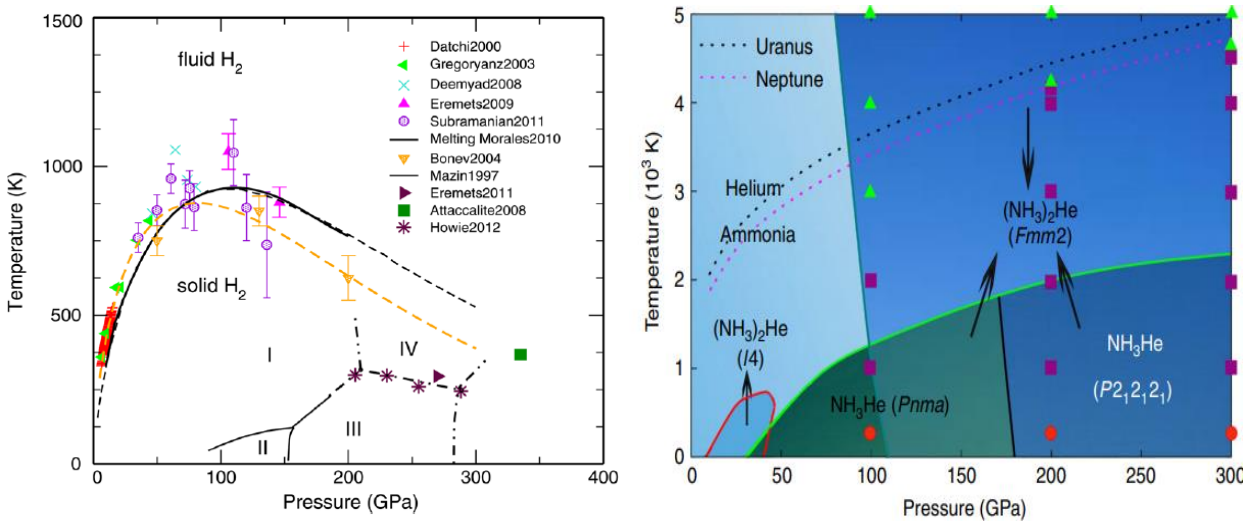


**Figure 2:** Phase diagram of a) H and b) He at T-P space. Adapted from [52,54] respectively.

## II. Compressible fluids

In this work we are concerned with complex fluids made of liquid constituents. Gases are fully and easily compressible fluids, possess no definite volume but it always expands until its volume is equal to that of the vessel. In contrast, liquids are known for the extremely low compressibility values that possess. In most cases the fluids are considered incompressible [57-61]. This general approximation is almost true, but not always. When HPP effect is considered, the incompressible hypothesis is not valid anymore. structural and dynamic changes can occur. Compressibility of

fluids is known to be relevant in many cases [62-64]. How pressure precisely alters different processes still remain under investigation. Theoretical models need to be modified to take care of compressibility and to explain such complex processes. In fluid dynamics compressible fluid means that a density gradient observed as pressure increase. Water, one of the most incompressible fluid - if not the most, has a change in specific volume ~ 0.04 $cm^3/g$ over change of pressure of $10^9$ Pa corresponding to changes in compressibility values to the 0.12 x $10^{-6}$ $bar^{-1}$ [65,66]. These small changes are found to have profound consequences. From the three common phases of water at ambient pressure, around 30 have reported at elevated pressures (~GPa) as depicted in figure 3.

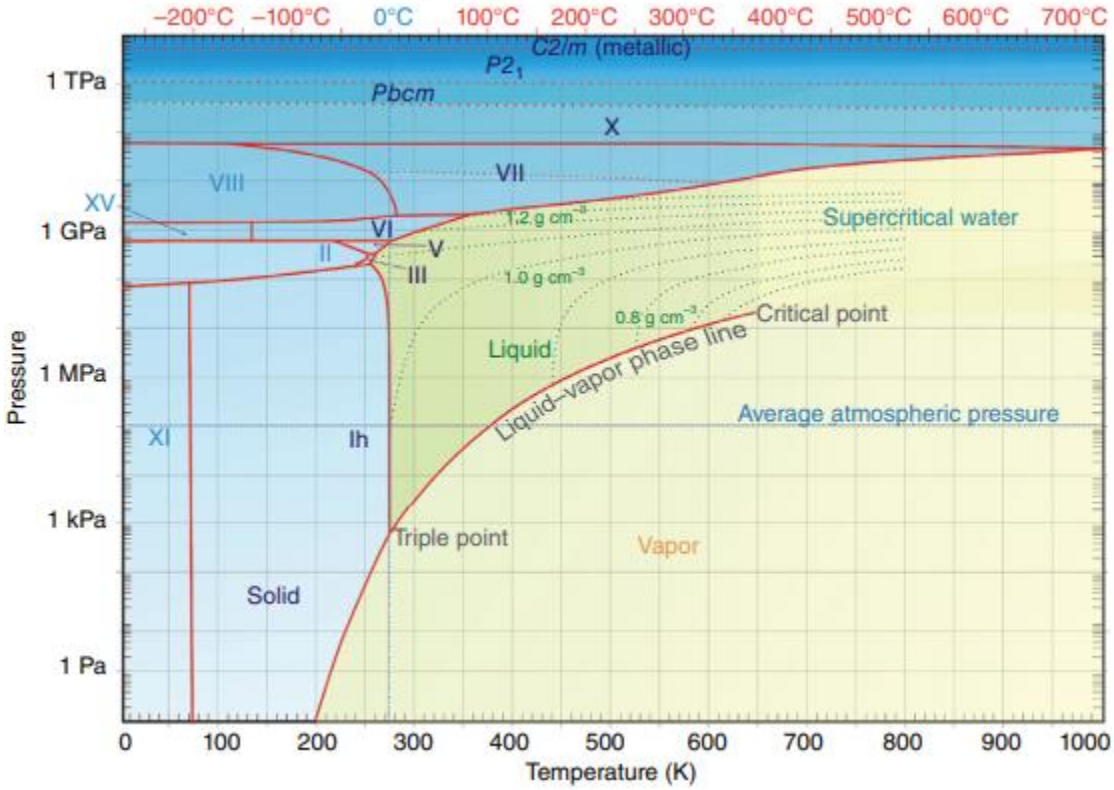


**Figure 3:** Phase diagram of water. Depicted from [66].

In the simplest form (eq.1 and 2), isothermal ($\beta_T$) and isentropic ($\beta_S$) compressibility expressed as a function of volume (V) and pressure (P). The negative value connected with the negative value of $(\frac{\theta V}{\theta P})$ as pressure increased. A standard and quite precise way for the determination of β was reported in [74]. The sound velocity c, in a fluid connected with the thermal compressibility, $\beta_T$ (eq. 3). [65, 75] is

$$\beta_T = -\frac{1}{V}\frac{\theta V}{\theta P}|_T \quad (1)$$

$$\beta_S = -\frac{1}{V}\frac{\theta V}{\theta P}|_S \quad (2)$$

$$\beta_T = -\frac{V}{c^2} + Ta^2V\frac{1}{C_p} \quad (3)$$

Dielectric constant is an alternative way to extract information about the compressibility and how the solubility of the respective substances change by pressure [76]. The pressure dependence in the density, dielectric constant, and viscosity of hydrocarbons, aqueous and organic liquids were reported in [77-79]. The increase of pressure was followed by an increase of density and dielectric constant by ~20-30% and ~11-15% respectively.

**III. Soft matter and High – pressure: a general overview**

Pressure is often considered to be a forgotten thermodynamic variable, in part because pressure-dependent experimentation is far more challenging than its temperature-dependent counterpart. Yet, over the years several investigations of static and dynamic properties of soft materials at high pressures have been reported in the literature. For example, moderate pressures of the order of 100 bar were found to influence the second virial coefficient and radius of gyration of flexible polymers in different solvents [80]. Clearly, pressure affects the miscibility in polymer mixtures, promoting miscibility in LCST polymer solutions [81-86] and in UCST polymer blends [87-89] due to volume changes on mixing. In addition, studies show that high hydrostatic pressure have a big impact on ternary systems where strange phenomena of co-solvency as well as co-non-solvency observed. The generation of true co-solvency by pressure reported in water-soluble systems e.g. PNIPAM-gels [90] as well as in non-aqueous systems such as high molecular weight polystyrene in mixtures of acetone / diethyl ether [91-94]. An explanation why pressure can ‘destroy’ the co-non-solvency effect of PNIPAM/aqeous-methanol solutions was given by [95]. In general, increase of pressure find to lead in an increase of the solubility values of the respective substances, as a result compatibilization is promoted. Patterson et al. extract values of polymer-solvent interaction parameter, ($\chi$), which is related to the difference between the solubility parameters [96]. In some exceptions, pressure-induced micro and macro-phase separation observed [97-99]. Recently, Didier Long et al. discuss the existing theoretical models and derive an analytical expression regarding blend miscibility [67-72]. Key point of the study, based on Gibbs free energy is the model of

compressible polymers. More details are discussed in chapter 3. The effects of low pressure on melt compressibility are generally in the order of 5-10% in macro-injection molding. C.Y. Yeu et al. report that the compressibility of the molten polymer plays a significant role on the flow behavior in micro-injection molding [73].

Micro-structural studies of pressure dependence in adhesive colloidal dispersions report that the spinodal temperature change by a rate dP/dT ~ 77 bar/K [100]. In physical hydrogels and proteins, the effect of pressure was extensively studied. As already mentioned in the case of coagulation of the white of the egg by pressure, different mechanisms and protein transitions was comparing with the temperature are possible to happen [101,102]. The pressure effect on the sol -gel transition of gelatin gels and similar proteins were reported [103-105]. Opposite effects such unfolding of proteins by pressure is possible also [106,107]. Recently was reported that hydrostatic pressure presents of osmotic phenomena lead to the formation of multilamellar lipid membranes [108]. More complicated is the effect of pressure on triblock copolymer micelles, where it is found to promote crystal to liquid transition, but often the micellar liquid is topologically interacting [109,110]. Furthermore, pressure is found to affect the glass transition and associated alpha relaxation (typically increasing the glass temperature) in supercooled liquids [111,112] and a wide range of shape polymeric materials with intrinsic orientational order, for which the lack of thermal energy rather than free volume is proposed to be responsible for vitrification [113]. In general, soft materials experience high pressures in a variety of applications or during their transformation, which renders relevant studies necessary. Other examples are, the use of high pressure to protein crystals from spider silk [114] and the high-pressure preparation of dairy products (emulsions) [115].

**IV. High pressure impact on the mechanical properties of soft matter systems:**

Focusing on rheology, the effects of pressure that have been addressed in the past are limited. Making rheometers working well under high pressure is not that simple. As a result, most of the studies is focus on the effect of pressure on viscosity. The pressure dependence (~10 kbar) in water viscosity for different temperatures measured in the mid of previous century [116]. Increasing pressure (up to about 4 kbar) was reported to increase the intrinsic viscosity of polymer solutions, with the Flory-Huggins coefficient exhibiting a non-monotonic dependence with a broad minimum [117]. A drastic increase of viscosity of branched polyethylenes with increasing pressure was

already reported in the late 50s [118]. Recently, pressure was reported to stabilize dynamic supramolecular assemblies of the host-guest type (enhancing their binding equilibria) and maintaining a constant viscosity (in contrast to crosslinked fluids which may suffer pressure-induced viscosity thinning) [119]; the pressure-dependent viscosity (up to 1 kbar) was measured with a Couette device and commercial cell. This study shows that pressure is an important variable that may affect supramolecular associations and their properties; hence it represents a motivation for the present work. The application of pressure was found to increase the yield stress and strain of polymeric solids undergoing tensile deformation [120]. Additional examples involve processing and capillary flow of polymer melts [121-126], drilling operations with fracturing fluids [127]. Pressure-driven devices such as capillary [121,128] and falling ball rheometers [117] have been used quite extensively. The detailed review of specialized mechanical instrumentation by Boza and Gallegos [129] provides useful information. The use of rotational instruments offers the advantage of giving access to the entire linear viscoelastic (LVE) spectrum, but is limited to relatively low pressures (typically not exceeding 200 bar although some commercial rheometer vendors offer options claimed to reach 1 kbar) and mostly with liquids [130]. An alternative approach is taking advantage of passive-microrheology by means of dynamic light scattering and diffusing wave spectroscopy. Different metallic cells for handling elevated pressures have been developed and utilized in neutron or X-ray scattering facilities [131, 132], but also coupled to static or dynamic light scattering [133-135]. DLS-based microrheological LVE data were reported in the past [109] and very recently a comprehensive study reported a robust approach to obtain reliable data with fracturing fluids for pressures up to 2 kbar using [136]. Both investigations used diffusive wave spectroscopy (DWS), i.e., DLS in the high multiple scattering limit. Hence the challenge to explore the effects of pressure on the rheology of complex fluids is worth and feasible to address.

## References


[1] W. A. Hodge, R. S. Fijan, K. L. Carlson, R. G. Burgess, W. H. Harris and R. W. Mann, "Contact pressures in the human hip joint measured in vivo", Proc. Natl. Acad. Sci. U. S. A., **83**, 2879–2883, (1986).

[2] N. J. Brooks *IUCrJ*, "Pressure effects on lipids and bio-membrane assemblies", **1**, 470 —477, (2014).

[3] N. L. C. McCarthy, O. Ces, R. V. Law, J. M. Seddon and N. J. Brooks, "Separation of liquid domains in model membranes induced with high hydrostatic pressure", Chem. Commun., 51, 8675 -8678, (2015).

[4] S. Purushothaman, P. Cicuta, O. Ces and N. J. Brooks, "Influence of High Pressure on the Bending Rigidity of Model Membranes", J. Phys. Chem. B, 119, 9805-9810, (2015).

[5] R. Winter and C. Jeworrek , Soft Matter, **"**Effect of pressure on membranes", **5**, 3157, (2009).

[6] M. Trapp, J. Marion, M. Tehei, B. Demé, T. Gutberlet and J. Peters, "High hydrostatic pressure effects investigated by neutron scattering on lipid multilamellar vesicles", *Phys. Chem. Chem. Phys.*, **15**, 2095, (2013).

[7] Ho-Kwang Mao, X. J. Chen, Y. Ding, B. Li, L. Wang, "Solids, liquids, and gases under high pressure", REV. MOD. PHYS., **90**, (2018).

[8] Ho-Kwang Mao, B. Chen, J. Chen, K. Li, J.-F. Lin, W. Yang, H. Zheng, "Recent Advances in High-Pressure Science and Technology", Matter and Radiation at Extremes (2016).

[9] Zou, G. Ma, Y. Mao, Ho-Kwang; Hemley, Russell J.; Gramsch, Stephen A. "A diamond gasket for the laser-heated diamond anvil cell", Review of Scientific Instruments. **72**, 1298. (2001).

[10] L. Dubrovinsky, N. Dubrovinskaia, V. B. Prakapenka & A. M Abakumov, "Implementation of micro-ball nanodiamond anvils for high-pressure studies above 6 Mbar", Nature Communications, **3**, 1163, (2012).

[11] Samuel Weir, "Putting the squeeze on materials", Lawrence Livermore National Laboratory, (2004).

[12] Jeanloz R., "High-Pressure Geoscience Special Feature: Achieving high-density states through shock-wave loading of precompressed samples", Proc. Natl Acad. Sci., **104**, 9172–9177 (2007).

[13] Akahama, Y., and H. Kawamura, J. Phys. Conf. Ser. **215**, 012195, (2010).

[14] Akahama, Y., and H. Kawamura, High Press. Res. **27**,473–482, (2007).

[15] Akahama, Y., H. Kawamura, and T. L. Bihan, Phys. Rev. Lett. **87**, 275503, (2001).

[16] Boehler, R.,M. Guthrie, J. J.Molaison, A. M. d. Santos, S. Sinogeikin, S. Machida, N. Pradhan, and C.A. Tulk, High Press. Res. **33**, 546–554, (2013).

[17] Fujihisa, H., and K. Takemura, Phys. Rev. B 52, 13257–13260, (1995).

[18] Sakata, M., Y. Nakamoto, K. Shimizu, T. Matsuoka, and Y. Ohishi, Phys. Rev B, **83**, 220512, (2011).

[19] Ruoff, A. L., H. Xia, H. Luo, and Y. K. Vohra, Rev. Sci. Instrum. 61, 3830–3833, (1990).

[20] H. K. Mao, & P. M. Bell, "High-pressure physics: the 1-megabar mark on the ruby R1 static pressure scale", Science **191**, 851–852, (1976).

[21] H. K. Mao, & P. M. Bell, "High-pressure physics: sustained static generation of 1.36 to 1.72 megabars", Science **200**, 1145–1147, (1978).

[22] H. K. Mao, & P. M. Bell, "Electrical resistivity measurements of conductors in the diamond-window, high-pressure cell", Rev. Sci. Instrum. **52**, 615–616, (1981).

[23] Paul F. McMillan, "New materials from high-pressure experiments", Nature materials, **1**, (2002).

[24] V.V. Brazhkin & A.G. Lyapin, "Metastable high-pressure phase of low-Z compounds: creation of a new chemistry or a prompt for old principles?", Nature materials, **3**, (2004).

[25] Eremets M., "High Pressure Experimental Methods" Oxford University Press: New York, (1996).

[26] Ruoff A. L., Xia H., Vohra Y., "Miniaturization techniques for obtaining static pressures comparable to the center of the Earth: X-ray diffraction at 416 GPa" Rew. Sci. Instr. **61**, 3830-3830, (1990).

[27] S.G. Kazarian & K.L.A. Chan, "FTIR Imaging of Polymeric Materials under High-Pressure Carbon Dioxide", Macromolecules, **37,** 579-584, (2004).

[28] Stefan Klotz, "Techniques in High Pressure Neutron Scattering", ISBN:9780429093760, 1st edition, (2012).

[29] S. S. Mitra, O. Brafman, W. B. Daniels, R. K. Crawford, "Pressure-Induced Phonon Frequency Shifts Measured by Raman Scattering", Phys. Rev., **186**, 3, (1969).

[30] J.M. Besson & R.J. Nelmes, "New developments in neutron-scattering methods under high pressure with the Paris—Edinburgh cells", Physica B: Condensed Matter, **213-214**, 31-36, (1995).

[31] J.Li, W. Zhang, P. J. M. Monteiro, “Synchrotron X-ray Raman scattering shows the changes of the Ca environment in C-S-H exposed to high pressure”, Cement and Concrete Research, **132**, (2020).

[32] X. Li, D. Chen, M. Jin, D. Ma, Y. Ge, W. Guo, H. Sun, J. Han, W. Xiao, J. Duan, Q. Wang, C. C. Liu, C. Jin, J. Zhou, J. B. Goodenough, J. Zhu & Y. Yao, “Pressure-induced phase transitions and superconductivity in a quasi–1-dimensional topological crystalline insulator α-Bi4Br4”, PNAS, **116**, 17696-17700, (2019).

[33] D. Obermayer, B. Gutmann, C. O. Kappe, “Microwave Chemistry in Silicon Carbide Reaction Vials: Separating Thermal from Nonthermal Effects”, Angew. Chem. Int. Ed., **48**, 8321-8342, (2009).

[34] M. A. Herrero, J. M. Kremsner, C. O. Kappe, “Nonthermal Microwave Effects Revisited, On the Importance of Internal Temperature Monitoring and Agitation in Microwave Chemistry”, J. Org. Chem., **73**, 36-47, (2008).

[35] P. M. Celliers, “Insulator-to-conducting transition in dense fluid helium”, Phys. Rev. Lett. **104**, 184503, (2010).

[36] I. Daniel, P. Oger & R. Winter, “Origins of life and biochemistry under high-pressure conditions”, Chem. Soc. Rev., **10**, (2006).

[37] E. G. Nisbet and N. H. Sleep, “The habitat and nature of early life”, Nature, **409**, 1083, (2001).

[38] J. T. Trevors, “The subsurface origin of microbial life on the Earth”, Research in Microbiology, **153**, 8, 487-491, (2002).

[39] R. Winter, “Synchrotron X-ray and neutron small-angle scattering of lyotropic lipid mesophases, model biomembranes and proteins in solution at high pressure”, Biochimica et Biophysica Acta (BBA) - Protein Structure and Molecular Enzymology, **1595**, 1-2, 25-184, (2002).

[40] J. D. Kramer, “Volatile element abundance patterns and an early liquid water ocean on Earth”, Precamb. Res., 126, 379, (2003).

[41] F. Ono, M. Saigusa, T. Uozumi, Y. Matsushima, H. Ikeda, N.L. Saini, M. Yamashita, “Effect of high hydrostatic pressure on to life of the tiny animal tardigrade”, J. Phys. & Chem. Sol., **69**, 9, 2297-2300, (2008).

[42] B. M. Jakosky, E. L. Shock, “The biological potential of Mars, the early Earth, and Europa”, J. Geophys. Res., 103, 19359-64, (1998).

[43] K. Fishbaugh, D. des Marais, O. Korablev, P. Lognonne and F. Raulin, “Geology and Habitability of Terrestrial Planets”, Springer, Amsterdam, (2006)

[44] M. J. Russell and N. T. Arndt, “Geodynamic and metabolic cycles in the Hadean”, Biogeosciences, **2**, 97, (2005).

[45] Carl Bosch, "Process of producing ammonia". U.S. Patent, **990**, 191, (1908).

[46] P. W. Bridgman, “The coagulation of albumin by pressure”, J. Bio. Chem., **19**, 511, (1914).

[47] F. Abe, “Piezophysiology of yeast: occurrence and significance”, Cell. Mol. Biol., **50**, 437, (2004).

[48] C. Balny, P. Masson and K. Heremans, “High pressure effects on biological macromolecules: from structural changes to alteration of cellular processes”, Biochim. Biophys. Acta, **1595**, 3, (2002).

[49] H. Ludwig, “Effects of High Pressure on Bacteria and Fungi”, Adv. High Pressure Biosc. & Biotech. II, 259-265, (2003).

[50] J. Torrent, C. Balny, R. Lange, “High Pressure Modulates Amyloid Formation”, Prot. & Pept. Let., **13**, 3, 271-277, (2006).

[51] E. Gregoryanz, A. F. Goncharov, R. J. Hemley, & H. K. Mao, “High-pressure amorphous nitrogen”, PHYS. REV. B, **64**, 052103, (2001).

[52] J.M. McMahon, M. A. Morales, C. Pierleoni, and D. M. Ceperley, “The properties of hydrogen and helium under extreme conditions”, Rev. Mod. Phys. **84**, 1607–1653, (2012).

[53] J. Shi, W. Cui, J. Hao, M. Xu, X. Wang, Y. Li, “Formation of ammonia-helium compounds at high pressure”, Nature Communications, **11**, 3164, (2020).

[54] R.R. Mattsson, T.R. Nettelmann, & French M. “The phase diagram of water and the magnetic fields of Uranus and Neptune”, Icarus **211**, 798–803 (2011).

[55] C. Liu et al., “Topologically frustrated ionisation in a water-ammonia ice mixture”, Nat. Commun. **8**, 1065, (2017).

[56] L. Koci, R. Ahuja, A. B. Belonoshko and B. Johansson, “Study of the high-pressure helium phase diagram using molecular dynamics”, J. Phys.: Condens. Matter, **19**, 016206, (2007).

[57] P. J. Flory, “Principles of Polymer Chemistry”, Cornell University Press: Ithaca, (1953).

[58] P. J. Flory, “Thermodynamics of High Polymer Solutions”, J. Chem. Phys., **9**, 660-661, (1943).

[59] M. L. Huggins, “Solutions of Long Chain Compounds”, J. Chem. Phys., **9**, 440– 449, (1941).

[60] M. L. Huggins, “Some Properties of Solutions of Long-chain Compounds.”, J. Phys. Chem., **46**, 151-158, (1942).

[61] R. L. Scott, “Thermodynamics of high polymer solutions. VI. The compatibility of copolymers”, J. Polym. Sci., **9**, 423-432, (1952).

[62] K. Gekko & Y. Hasegawa, “Compressibility-structure relationship of globular proteins”, Biochemistry, **25**, 6563–6571, (1986).

[63] J. Dudowicz & K. F. Freed, “Effect of Monomer Structure and Compressibility on the Properties of Multicomponent Polymer Blends and Solutions:1. Lattice Cluster Theory of Compressible Systems”, Macromolecules, **24**, 5076-5095, (1991).

[64] K. Y. Wei, J. A. Cuculo, & D. W. Ihm, “Effects of Pressure on the Compressibility and Crystallization of Fiber-Forming Polymers”, Mat. Sci. J. Pol. Sci. B, (1983).

[65] R.A. Fine & F. J. Millero, “Compressibility of water as a function of temperature and pressure”, J. Chem. Phys., **59**, 5529, (1973).

[66] M. F. Chaplin, “Structure and Properties of Water in its Various States”, Ency. Water: Sci. Tech. & Soc., (2019).

[67] R. H. Lacombe, I. C. Sanchez, “Statistical thermodynamics of fluid mixtures”, J. Phys. Chem., **80**, 2568– 2580, (1976).

[68] I. C. Sanchez, R. H. Lacombe, “Statistical Thermodynamics of Polymer Solutions”, Macromolecules, **11**, 1145– 1156, (1978).

[69] J. Dudowicz, K. F. Freed, “Pressure Dependence of Polymer Fluids: Application of the Lattice Cluster Theory”, Macromolecules, **28**, 6625– 6641, (1995).

[70] E. A. Clark, J. E. G. Lipson, “LCST and UCST behavior in polymer solutions and blends” Polymer, 53, 536– 545, (2012).

[71] S. Merabia, D. Long, Heterogeneous Dynamics and Pressure Dependence of the Dynamics in van der Waals Liquids” Macromolecules, **41**, 3284– 3296, (2008).

[72] E. M. Masnada, G. Julien, D.R. Long, “Miscibility Maps for Polymer Blends: Effects of Temperature, Pressure, and Molecular Weight”, J. Pol. Sci. Pol. Phys., **52**, 419-443, 2014.

[73] Q. M. P. Nguyen, X. Chen, Y. C. Lam, & C. Y. Yue, “Effects of polymer melt compressibility on mold filling in micro-injection molding”, J. Micromech. Microeng.,**21,** 095019, (2011).

[74] Landau & Lifshitz, “Course of Theoretical Physics- Statistical Physics” Pergamon Intern. Library, **5**, 54-55 & 342, (1980).

[75] Landau & Lifshitz, "Course of Theoretical Physics- Statistical Physics" Pergamon Intern. Library, **5**, (1980).
[76] J.M. St-Arnaud, T.K. Bose, R. Okambawa, & D. Ingrain, "Precise determination of the compressibility factor by using dielectric constant measurements", Fluid Phase Equilibria, **88**, 137-149, (1993).
[77] D. W. Braziera & G. R. Freeman "The effects of pressure on the density, dielectric constant, and viscosity of several hydrocarbons and other organic liquids", Canadian Journal of Chemistry, **47**, 893, (1969).
[78] Ding Pan, L. Spanu, B. Harrison, D. A. Sverjensky, & G. Gallia, "Dielectric properties of water under extreme conditions and transport of carbonates in the deep Earth", PNAS, **110**, 6646–6650, (2013).
[79] M. Dzida & U. Kaatze, "Compressibility and Dielectric Relaxation of Mixtures of Water with Monohydroxy Alcohols", J. Phys. Chem. B, **110**, 12480-12489, (2015).
[80] D. Gaeckle and D. Patterson, "Effect of Pressure on the Second Virial Coefficient and Chain Dimensions in Polymer Solutions," Macromolecules **5**, 136-141 (1972).
[81] A. Wolf, "Improvement of polymer solubility: Influence of shear and of pressure," Pure & Appl. Chem. **69**, 929-933 (1997).
[82] E. Maderek, G.V. Schulz & B.A. Wolf, "Lower critical solution temperatures of poly(decyl methacrylate) in hydrocarbons", Eur. Polym. J. **19**, 963-965, 1983.
[83] B.A. Wolf, "Thermodynamics and Rheology of Polymer Solutions", DFG, Chem. & Phys. Macrom., (1991).
[84] S. Janssen, D. Schwahn, K. Mortensen, T. Springer, "Pressure Dependence of the Flory-Huggins Interaction Parameter in Polymer Blends: A SANS Study and a Comparison to the Flory-Orwoll-Vrij Equation of State", Macromolecules, **26**, 5587-5591, (1993).
[85] J.J.L. Santos, B.S. Martin, U. Gasser & A.F. Nieves, "The effect of hydrostatic pressure over the swelling of microgel particles", Soft Matter, **7**, 6370, (2011).
[86] S. Grobelny, C. H. Hofmann, M. Erlkamp, F.A. Plamper, W. Richtering & R. Winter, "Conformational changes upon high pressure induced hydration of poly(N-isopropylacrylamide) microgels", Soft matter, **9**, 5862, (2013).
[87] M. Beiner, G. Fytas, G. Meier, and S. K. Kumar, "Pressure-Induced Compatibility in a Model Polymer Blend," Phys. Rev. Lett. **81**, 594-597 (1998).

[88] L. Zeman & D. Patterson, “Pressure Effectes in Polymer Solution Phase Equilibria. II. Systems Showing Upper and Lower Critical Solution Temperatures”, J. Phys. Chem. **76**, 1214-1219, (1971).
[89] K.S. Siow & D. Patterson, “Cloud-Point Curves in Polymer Solutions with Adjacent Upper and Lower Critical Solution Temperatures”, Macromolecules, **5**, 29-34, (1971).
[90] C. H. Hofmann, S. Grobelny, M. Erlkamp, R. Winter, “Influence of high-pressure on cononsolvency of poly(N-isopropylacrylamide) nanogels in water/methanol mixtures”, Polymer, **55**, 2000-2007, (2014).
[91] B.A. Wolf & R.J. Molinary, “True Cosolvency Acetone/Diethylether/Polystyrene”, Die Makrom. Chem., **173**, 241-245, (1973).
[92] B.A. Wolf & G. Blaum, “Pressure Influence on True Cosolvency”, Macrom. Chem., **177**, 1073-1088, (1976).
[93] B.A. Wolf & M.M. Willms, “Measured and Calculated Solubility of Polymers in Mixed Solvents: Co – nonsolvency”, Macrom. Chem., **179**, 2265-2277, (1978).
[94] G. Blaum & B.A. Wolf, “The generation of True Cosolvency by Pressure. Solubility Limits of High Molecular Weight Polystyrene in Mixtures of Acetone and Diethyl Ether”, Macromolecules, **9**, 579-582, (1976).
[95] T. E. de Oliveira, P. A. Netz, D. Mukherji, K. Kremer, “Why does high pressure destroy co-non-solvency of PNIPAm in aqeous methanol?”, Soft Matter, **12**, 43:58, (2015).
[96] I. Zeman & D. Patterson, “Effect of the solvent on Polymer Incompatibility in Solution”, Macromolecules, **5**, 513-516, (1972).
[97] V. Grinberg, A.A. Senin, N. V. Grinberg, T.V. Burova, A.S. Dudovik, S.A.Potekhin & I.Y. Erukhimovich, “High pressure effects under phase separation of aqeous solutions of poly(-isopropylacrylamide): A HS-DSC study”, Polymer, **64**, 14-18, (2015).
[98] M. Shibayama, K. Isono, S. Okabe, T. Karino & M. Nagao, “SANS Study on Pressure-Induced Phase Separation of poly(-isopropylacrylamide) aqeous Solutions ang Gels”, Macromolecules, **37**, 2909-2918, (2004).
[99] N. Osaka, S. Okabe, T. Karino, Y. Hirabaru, S. Aosima & M. Shibayama, “Micro- and Macrophase Separations of Hydrophobically Solvated Block Copolymer Aqeous Solutions Induced by pressure and temperature”, Macromolecules, **39**, 5875-5884, (2006).
[100] R. Vavrin, J. Kohlbrecher, A. Wilk, M. Ratajczyk, M. P. Lettinga, J. Buitenhuis & G. Meier, “Structure and phase diagram of an adhesive colloidal dispersion under high pressure: A small angle

neutron scattering, diffusing wave spectroscopy, and light scattering study", J.C.P., **130**, 154903, (2009).

[101] S.M. Gruner, "Soft materials and biomaterials under pressure", High-Pressure Crystallography, 543-556, (2004).

[102] S. Kunugi, K. Kameyama, T. Tada, N. Tanaka, M. Shibayama & M. Akashi, "Differences in pressure and temperature transitions of proteins and polymer gels", Braz. J. Med. Biol. Res. **38**, 1233-1238, (2005).

[103] K. Gekko & M. Fukamizu, "Effect of pressure on the sol-gel transition of gelatin", Int. J. Biol. Macromol., **7**, (1985).

[104] T. Matsunaga & M. Shibayama, "Gel point determination of gelatin hydrogels by dynamic light scattering and rheological measurements", Phys. Rev. E, **76**, 030401, (2007).

[105] Gekko, K. and Kasuya, K. Int. J. Biol. Macromol, 7, 299, (1985).

[106] M.A.Schroer, M. Paulus, C. Jeworrek, C. Krywka, S.Schmacke, Y. Zhai, D. C. Wieland, C. J.Sahle, M. Chimenti, C. A.Royer, B.G.-Moreno, M. Tolan, R. Winter, "High-Pressure SAXS Study of Folded and Unfolded Ensembles of Proteins", Biophysical Journal, **99**, 3430-3437, (2010).

[107] G.H. Hoa, C.D.Primo, I. Dondaine, S. G. Sligar, I. C. Gunsalus, P. Douzou, "Conformational Changes of Cytochromes P-450cam and P-450lin Induced by High Pressure", Biochemistry, **28**, 651-656, (1989).

[108] S. R. Al-Ayoubi, P. K. F. Schinkel, M. Berghaus, M. Herzoga & R. Winter, "Combined effects of osmotic and hydrostatic pressure on multilamellar lipid membranes in the presence of PEG and trehalose", Soft Matter, **14**, 8792-8802, (2018).

[109] C. J. Kloxin, J. H. van Zanten, "High-pressure phase diagram of an aqueous PEO-PPO-PEO triblock copolymer system via probe diffusion measurements," Macromolecules **43(4)**, 2084-2087 (2010).

[110] K. Mortensen, D. Schwahn & S. Janssen, "Pressure-induced Melting of Micellar Crystal", Phys. Rev. Let., **71**, 1728-1731, (1993).

[111] A. Patkowski, M. Paluch, H. Kriegs, "Dynamic light scattering studies of supercooled phenylphthalein–dimethylether dynamics under high pressure," J. Chem. Phys., 117(5), 2192-2198 (2002).

[112] S.W.Smith, B.D. Freeman & C. K. Hall, "Pressure-Dependent Photon Correlation Spectroscopic Investigation of Poly(propylene oxide) near the glass transition", Macromolecules, **30**, 2052-2057, (1997).

[113] G. Floudas, "Effects of pressure on systems with intrinsic orientational order," Prog. Polym. Sci. **29**, 1143–1171 (2004).

[114] H. Peng, S. Zhou, J. Jiang, T. Guo, X. Zheng, and X. Yu, "Pressure-Induced Crystal Memory Effect of Spider Silk Proteins," J. Phys. Chem. B, **113**, 4636-4641 (2009).

[115] N. K. Rastogi, K. S. M. S. Raghavarao, V. M. Balasubramaniam, K. Niranjan, D. Knorr, Opportunities and challenges in high pressure processing of foods," Crit. Rev. Food Sci. Nutr. **47(1)**, 69-112 (2007).

[116] Fisher, Knight, "Effect of Pressure on the Viscosity of Water", Nature, **207**,620-621 (1965).

[117] J. R. Schmidt and B. A. Wolf, "Pressure Dependence of Intrinsic Viscosities and Huggins Constants for Polystyrene in tert-Butyl Acetate'', Macromolecules **15**, 1192-1195 (1982).

[118] Maxwell B, "Jung A Hydrostatic pressure effect on polymer melt viscosity," Mod. Plast. **35**,174–182 (1957).

[119] Appel, E. A., Biedermann, F., Hoogland, D., del Barrio, J., Driscoll, M. D., Hay, S., Wales, D. J., and Scherman, O. A., Decoupled Associative and Dissociative Processes in Strong yet Highly Dynamic Host−Guest Complexes, J. Am. Chem. Soc. **139**, 12985-12993 (2017).

[120] A. W. Christiansen, E. Baer & S. V. Radcliffe "The mechanical behavior of polymers under high pressure," Philosophical Magazine, **24:188**, 451-467 (1971).

[121] Q. Guan, K. Shen, J. Li and J. Zhu, "Structure and properties of self-reinforced polyethylene prepared by oscillating packing injection molding under low pressure," J. App. Polym. Sci. **55**, 1797-1804 (1995).

[122] Berthe and Ph. Vergne, "High pressure rheology for high pressure lubrication: A review," J. Rheol. **34**, 1387-1414 (1990).

[123] M. A. Couch, D. M. Binding, "High pressure capillary rheometry of polymeric fluids, Polymer" **41** (16):6323-6334 (2000).

[124] S. G. Hatzikiriakos and J. M. Dealy, "Start-up Pressure Transients in a Capillary Rheometer," Polym. Eng. Sci. **34(6)**, 493-499 (1994).

[125] Mackley, M. R., P. H. J. Spitteler, "Experimental Observations on the Pressure-Dependent Polymer Melt Rheology of a Linear Low-Density Polyethylene using a Multipass Rheometer," Rheol. Acta, **35**, 202–209 (1996).

[126] F. Koran, J. M. Dealy , "A high pressure sliding plate rheometer for polymer melts," J. Rheol., **43**, 1279-1290 (1999).

[127] R. Barati, J. Liang, "A review of fracturing fluid systems used for hydraulic fracturing of oil and gas wells," J. Appl. Polym. Sci. **131(16)**, 40735 (2014).

[128] R. Cardinaels, P. Van Puyvelde, P. Moldenaers, "Evaluation and comparison of routes to obtain pressure coefficients from high-pressure capillary rheometry data," Rheol. Acta, **46**, 495 505 (2007).

[129] F. J. M. Boza and C. Gallegos, Rheology, "High Pressure Rheology', **1**, EOLSS, Paris, (2010).

[130] Y. Y. Hou, H. O. Kassim, "Instrument techniques for rheometry," Rev. Sci. Instrum. **76**, 101101 (2005).

[131] Z. Wojnarowska, M. Rams-Baron, J. Knapik-Kowalczuk, A. Połatyńska, M. Pochylski, J. Gapinski, A. Patkowski, P. Wlodarczyk, and M. Paluch, "Experimental evidence of high-pressure decoupling between charge transport and structural dynamics in a protic ionic glassformer," Sci. Rep. **7**, 7084 (2017).

[132] B. Annighöfer, A. Hélary, A. Brûlet, A. Colas de la Noue, C. Loupiac and S. Combet, "A high pressure cell using metallic windows to investigate the structure of molecular solutions up to 600 MPa by small-angle neutron scattering," Rev. Sci. Instrum. **90**, 025106 (2019).

[133] J. Kohlbrecher, A. Bollhalder, R. Vavrin, G. Meier, Rev. Sci. Instr. **78**, 125101 (2007).

[134] G. Meier, H. Kriegs, Rev. Sci. Instr. **79**, 013102 (2008).

[135] G. Meier, R. Vavrin, J. Kohlbrecher, J. Buitenhuis, M. P. Lettinga, M. Ratajczyk, Mater. Sci. Technol. **19**, 034017 (2008).

[136] K. Dennis, Y. Gao, A. Phathak, P. F. Sullivan, E. M. Furst, J. Rheol. 64, 205-212 (2020).

[137] N. Dahmen and A. Kruse, "High Pressure in Renewable Energy Processes", Chapter 10, (2012).

# ***Chapter 1: Materials and Methods***

## 1.1: Experimental Methods

In this thesis we are interested in applying and developing methods to measure dynamics under high pressure and to possibly microrheology. DLS under pressure is well established for many years. So far, the report of microrheology under high pressure are scarce, though the use of DLS under HHP for viscosimetry is well developed. An important part of this work was to identify the capacity of light scattering based microrheology and its possible implementation using the existing HP light scattering cells. Two distinct high-pressure cells are available. One gas cell with possibility of detection at 45,60, 90 scattering angle and one hydraulic transmission cell with forward and backscattering detection possibilities.

Gas cell: can be used for DLS microrheology under certain conditions for the sample (scattering is dominated by microrheology probe, not too large modulus, viscosity up to 1000 Pa*s (relaxation time <= 10s , longer time will require multispeckle which should not be an issue, preliminary test have achieved feasibility test, a proper implementation needs a proper software) .

Liquid cell: it has been used with success in case of turbid sample (DWS microrheology). The limited cell thickness (2mm) makes its application limited to “natural” DWS and microrheology (rather than probe). Microprobe DWS (with 2mm cell thickness) is limited to PS latex in water. Both backscattering and transmission can be used. The cell construction leads to very large scattering from the windows and the unavoidable interfaces. The so strong scattering prevents the single scattering limit of weakly scattering sample. In particular probe based single scattering DLS microrheology appears to be out of reach. Such application will require the reduction of windows and interface scattering. Preliminary tests to identify the source of the scattering have been done. It appears as if the scattering was coming from the polymeric film used to limit friction between the two windows (small sapphire and larger glass) using a fluid might provide a way to reduce the scattering and ensure good contact between the materials (refractive index could be selected to reduce mismatch and scattering).

### 1.1.1: High pressure Dynamic Light Scattering apparatus (Gas compressor cell)

A homemade high-pressure cell was coupled to a light scattering setup for the high-pressure (HP-DLS) experiments. Here we provide the brief description of the main components. The pressure comprises 6 optical windows corresponding to scattering angles of 45, 90 and 130º, and the light beam was focused with a convex f 400 mm lens before reaching the sample, in the middle of the cylindrical cell, .The nitrogen was compressed means of a membrane compressor [Fig.1] and entered the cell from the top. Details concerning the cell, windows and sealing are described elsewhere [26,27]. The experiments were performed for pressures ranging from 1 to 1200 bar and temperatures from 20 to $70^0$C (the latter were controlled by means of a recirculating water/alcohol bath and measured with a thermocouple attached at the surface of the sample cell). Since the pressure transmitting medium is compressed nitrogen, special care was taken for the measurement time and the selected sample volume in order to avoid diffusion of nitrogen molecules into the polymer sample up to the measurement point (where the laser enters the sample). More specifically, the diffusion coefficient of nitrogen molecules in liquids such as organic solvents, at ambient conditions (P = 1 bar, T = 20 $^0$C) is in the order of $10^{-9}$ $m^2/s$ [28], therefore for a distances of about 1 cm (between the free surface of the solution and the measurement point) the corresponding time ($t = \frac{<r^2>}{2dD}$) is in the order of days, ensuring that the measurements are unaffected by possible dilution of the sample. Further evidence is provided later where DLS data are compared at different times and pressures. A cw laser at 514.5 nm was used and the scattering angle was fixed at $\theta = 90^0$. A mono-mode optical fiber was employed to feed the scattered light into an avalanche photodiode (Perkin-Elmer) operating in photon counting mode (Fig. 1). The time autocorrelation function of the scattering intensity (intermediate scattering function, ISF) was obtained in real time by means of an ALV 5000E digital correlator. The pressure was kept constant over long times as shown in the DLS data in appendix of chapter 2.

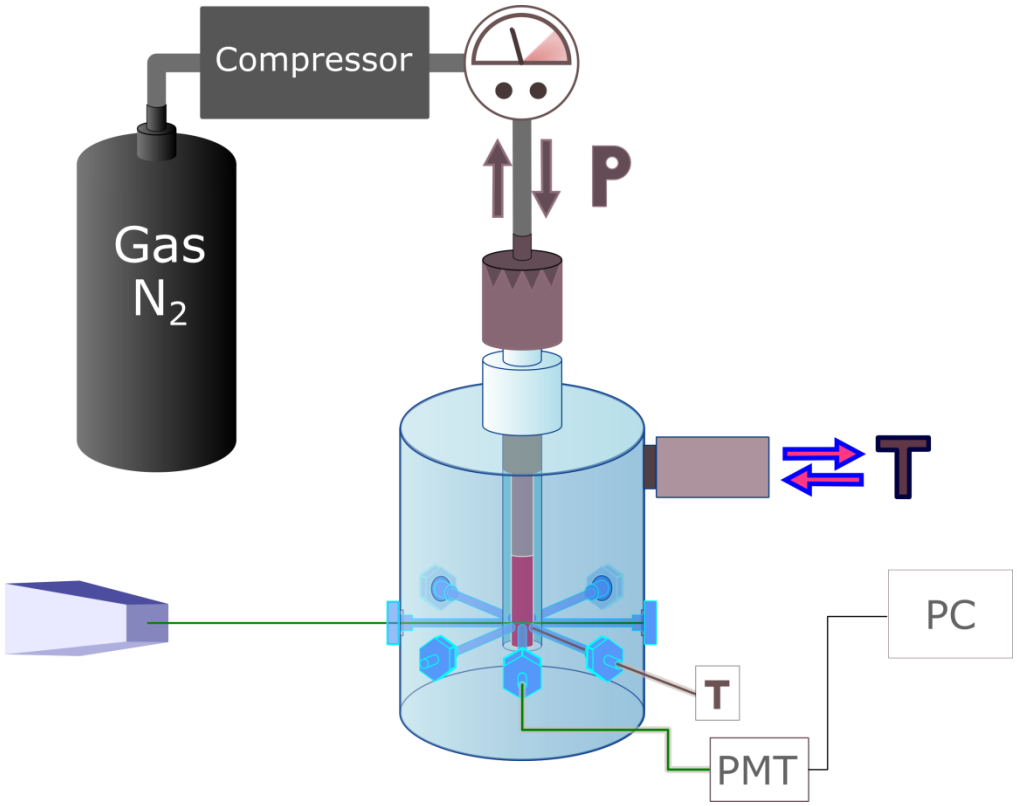


**Figure 1:** Schematic illustration of the experimental high-pressure DLS setup. Shown, out of scale are: the gas (nitrogen) tank, compressor, chamber cell with different glass windows for scattering at different fixed angled, gas inlet to DLS cell (P), inlet of recirculating fluid to cell chamber for maintaining constant temperature (T with arrows), temperature meter (T), laser with transmitted beam, scattered beam entering the photomultiplier tube (PMT), whose signal is collected and analyzed by a correlated on a PC.

### 1.1.2 High-pressure apparatus, Hydraulic compressor cell

See above, a homemade high-pressure cell was coupled to a light scattering setup (from ALV, Germany) for the high-pressure DLS (HP-DLS) experiments (Fig.2). Here we provide the brief description of the main components. The pressure transmitted medium is compressible liquid oil. Experiments were performed only in transmission and backscattering geometry. In multiple scattering limit, (DWS). Pressures ranging from 1 to 2000 bar (can increase to 5000 by addition of the bigger pressure chamber) and temperatures from 15 to $70^0$C (the latter were controlled by means of a recirculating water/alcohol bath and measured with a thermocouple attached at the surface of the sample cell).

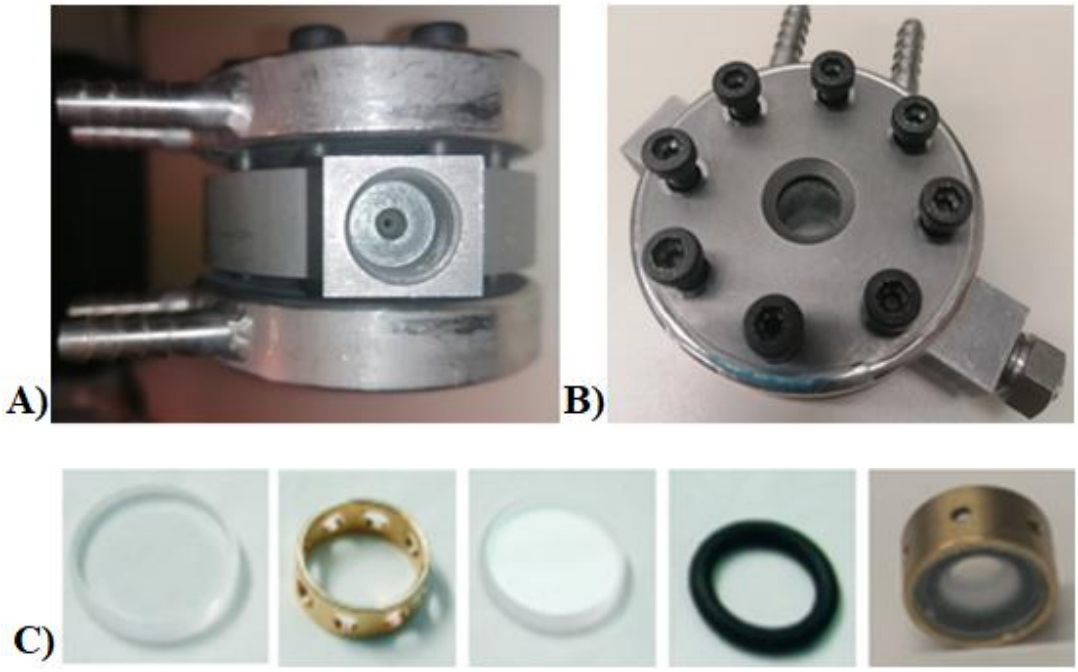


**Figure 2: a)** Details of high-pressure cell. **a)** What is seen is the steel body on which the inner cell holder lies. Mounted on that is one big sapphire which in the completely mounted state is hidden within the steel body. **b)** the sample pill located in the middle of pressure cell, between the sapphire windows in the middle of the inner cell holder. The silver ring which seals the inner volume filled with oil (and pill) against the sapphire lies around the sample pill. Also, a Teflon sealing foil is seen between sapphire and inner cell holder. **c)** Components of the pill: the brass ring with holes on the periphery, the two sapphire plates, and the O-ring. The sample in the pill is sealed against the hydraulic oil when the two sapphire plates press the O-ring against the brass ring holes from inside. **d)** Closed pill with sample inside – bubble formation is an undesired phenomenon.

The cell limited to experiments in diffusion wave spectroscopy (DWS), in other words in multiple scattering limit. The huge scattering of the sapphire windows in combination with the 8 in overall window-surfaces makes impossible measurements in single scattering limit. In addition, extra work needed in the design of the cell. The 2 mm width (sample width) makes the DWS limit difficult to achieved in a variation of polymer samples. This is ideally for emulsions and concentrated colloidal dispersions but limited in microrheology of organic based polymer solutions (specialized probes with high refractive index needed). Even now only water-based polymer solution by addition of Polystyrene spheres in the appropriate probe concentration (<=1% wt) offer multiple scattering. In

the advantages of the apparatus: the pressure transmitting medium is compressed hydraulic oil and not gas nitrogen. Long time experiments (over 1 day) under high-pressure conditions as well as fast compression and decompression are carried out. More details about the set-up described elsewhere [26]. Details for the diffusion wave spectroscopy, the determination of the l* discussed extensively in [55-60].

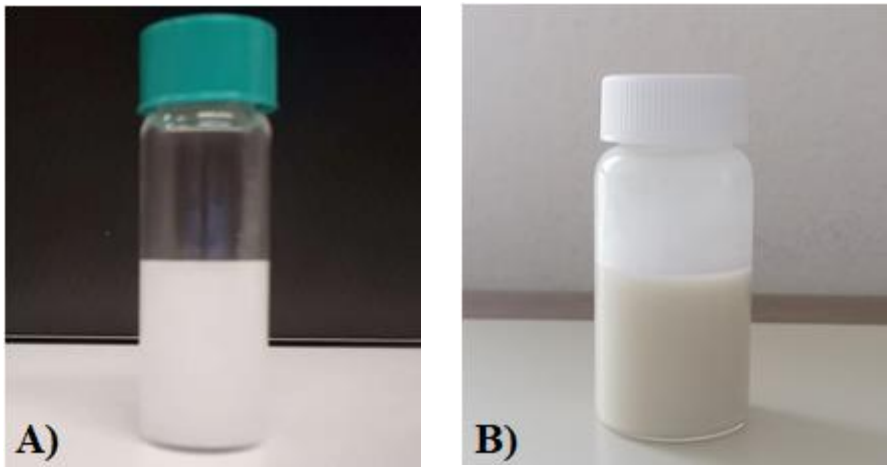


**Figure 3:** Ideally turbid samples for the liquid cell. **a)** gelatin aqueous gel addition of poly-styrene probes **b)** water-oil concentrated emulsion.

### 1.2.3 Passive Microrheology methodology

In the last 20 years microrheology has find widespread use in soft matter systems for scientific purposes. Passive microrheology, use thermal fluctuation of immersed (in the sample) colloidal probes to measure the mechanical properties of material, as a result is limited in linear (rheology) regime [29-37]. In advance, active microrheology use externally forced colloidal probes to measure the mechanical properties of the material, in linear as well as non-linear regime [38-40].

The principle of passive microrheology is that a microscopic probe larger than any length scale of the medium in which it is dispersed will undergo a Brownian motion that reflects the viscoelastic nature of the medium. It is known as the generalized Stokes Einstein equation ($D = k_B TM$), which can be expressed under the following form: MSD ~ creep compliance J(t). The aim of a microrheology experiment is to accurately measure the MSD of a probe. The MSD is simply put into creep compliance. The obtained creep compliance can then be transformed into frequency dependent complex shear modulus. The issues with microrheology have different origins. One is

the transform from time dependent creep to frequency dependent shear modulus. This is not inherent to microrheology. Another issue is the applicability of the GSER for the specific sample and probe. The post-measurement assessment of the GSER applicability is not always easy. We use colloidal probe in single scattering DLS or DWS for microrheological experiments [39,41].

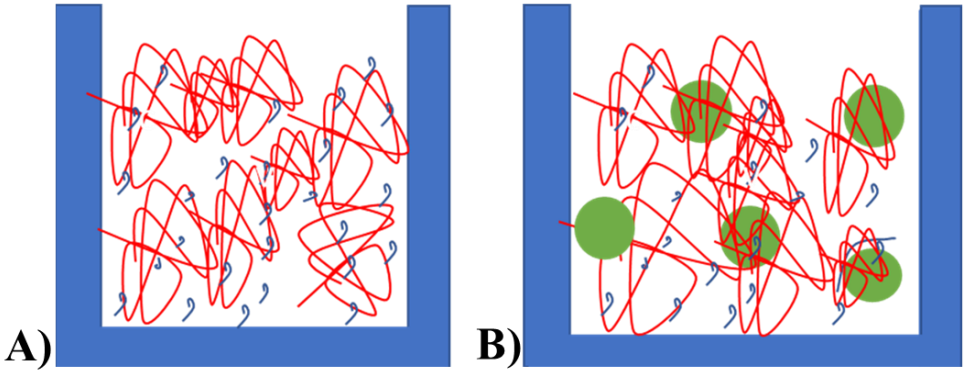


**Figure 4: a)** Cartoon of a polymer solution, red lines correspond to polymer chains, blue to solvent molecules, **b)** addition of colloidal probes (green spheres).

If the scattering of the sample is dominated by the probe , and if the probe are diluted so that the motion of two separate probes are uncorrelated, then the measured intensity autocorrelation function can be assumed to be on the form : $g(t) = f^* \exp(-q^2 \langle r^2 \rangle(t)/2)$ , f* is an experimental factor depending of the specifics illumination and detection used in the set-up. The field autocorrelation function (FAF) is obtained from the intensity autocorrelation function (IAF), using the Siegert relation. The electric field autocorrelation function $g_1(t)$ is related to the mean square displacement $\langle \Delta r^2 \rangle$ of the colloidal probe particle by $g_1(\tau, q) = exp\left(\frac{-q^2\langle \Delta r^2(\tau)\rangle}{6}\right)$ , with the scattering wave vector being $q = \frac{4\pi n}{\lambda} sin\left(\frac{\theta}{2}\right)$ . Here, $n$ is the refractive index, $\lambda$ the wavelength and $\theta$ the scattering angle. Mean square displacement (MSD) can simply be obtained as $MSD = -\frac{6}{q^2} ln(g_1)$. Using the GSER, $J(t) = \frac{\pi a}{k_B T}\langle \Delta r^2(\tau)\rangle$.

It is common practice to present linear rheological data in term of the frequency dependence of the complex modulus $G(\omega) = G'(\omega) + iG''(\omega)$. G' and G" are the in-phase elastic and out of phase viscous part of the shear modulus. They are standardly measured under small oscillatory shear in shear rheometer. A number of procedures to transform the creep compliance J(t) into shear modulus

G(ω) have been discussed in the literature. It is an ill posed problem and the transformation inevitably introduces artifacts. Recently, T. M. Squires and T.G. Mason [39], describes an alternative way to extract information about the mechanical properties of complex materials. Ideally applied in (bulk) rheological creep and microrheology measurements. This representation of the GSER converts the microscopic (measured) time-dependent mean squared displacement of the probe to the equivalent one-time dependent macroscopic creep compliance. With this path, there is no need of Laplace transformations, the frequency dependent viscoelastic spectra (G' (ω), G''(ω)) obtained through a straightforward mathematical procedure [44]. The mathematical expressions represent step by step in figure 6. All the equivalent relations represent in table 1. In the frame of this work we used the procedure which described in [61, 62].

The first theoretical description for the transformation given by T. Mason in 1995.

$$\widetilde{D}(s) = \frac{k_B T}{6\pi R s \tilde{\eta}(s)} \tag{1}$$

links the diffusion coefficient $\widetilde{D}(s)$ and the viscosity $\tilde{\eta}(s)$ as functions of the Laplace frequency s, with R the particle radius, $k_B T$ the Boltzmann constant and $T$ the absolute temperature. Assuming negligible inertial effects [42,43], one can deduce the Laplace-transformed complex modulus as

$$\tilde{G}(s) = s\tilde{\eta}(s) = \frac{s}{\pi R}\left[\frac{k_B T}{s^2\langle \Delta r^2(s)\rangle}\right] \tag{2}$$

The frequency-dependent linear viscoelastic moduli $G'$(storage) and $G''$ (loss) can be obtained from $s = i\,\omega$ and their interrelation $G^* = G' + iG''$ with $G^*$ being the complex modulus. This leads to

$$G^*(\omega) = \frac{k_B T}{\pi R i\omega F\{\langle \Delta r^2(\tau)\rangle\}} \tag{3}$$

where $F\{\langle \Delta r^2(\tau)\rangle\}$ is the one-side Fourier transform of the mean-square displacement. It has been shown that $\Delta r^2(\tau)$ can be expanded locally around $\tau = \frac{1}{\omega}$ by assuming that $\langle \Delta r^2(\tau)\rangle = \langle \Delta r^2(1/\omega)\rangle(\tau\omega)^{\alpha(\omega)}$, where the exponent $\alpha(\omega)$ is the local slope of the logarithmic time derivative of $\langle \Delta r^2(\tau)\rangle$ at $\tau = \frac{1}{\omega}$. It takes values between 0 (purely elastic material) and 1 (purely viscous) as depicted in figure # b). This leads to the following working expressions [30,31]:

$$|G^*(\omega)| = \frac{k_B T}{\pi R \langle \Delta r^2(1/\omega) \rangle \Gamma[1+\alpha(\omega)]} \quad (4)$$

$$G'(\omega) = |G^*(\omega)| cos(\pi\alpha(\omega)/2) \quad (5)$$

$$G''(\omega) = |G^*(\omega)| sin(\pi\alpha(\omega)/2) \quad (6)$$

where $\Gamma[1 + \alpha(\omega)]$ is the gamma function.

**Table 1:** Connecting macroscopic linear rheology and probe dynamics with thermal diffusion (passive) microrheology. Depicted from [39].

| Property | Symbol | Relation |
|---|---|---|
| **Linear shear rheology** | | |
| Complex shear modulus | $G^*(\omega)$ | $\tau(\omega) = G^*(\omega)\gamma(\omega)$ |
| Complex viscosity | $\eta^*(\omega)$ | $G^*(\omega) = i\omega\eta^*(\omega)$ |
| Stress relaxation modulus | $G_r(t)$ | $\tau(t) = -\int_{-\infty}^{t} G_r(t-t')\dot{\gamma}(t')dt'$ |
| Creep compliance | $J(t)$ | $\Theta(t) = \int_{-\infty}^{t} M_r(t-t')J(t')dt'$ |
| **Local probe response** | | |
| Probe mobility | $M(t)$ | $V(t) = \int_0^t M(t-t')F(t')dt'$ |
| Probe resistance | $\zeta(t)$ | $F(t) = \int_0^t \zeta(t-t')V(t')dt'$ |
| | $\tilde{\zeta}(s) = \tilde{M}^{-1}(s)$ | |
| Linear-response function | $\alpha^*(\omega)$ | $M^*(\omega) = i\omega\alpha^*(\omega)$ |
| Local transfer function | $\tilde{\chi}(s)$ | $\tilde{M}(s) = s\,\tilde{\chi}(s)$ |
| **Probe statistics** | | |
| Mean square displacement (MSD) | $\langle \Delta \mathbf{r}^2(t) \rangle$ | $\mathcal{L}\langle \Delta \mathbf{r}^2 \rangle = \frac{2Nk_BT}{s^2}\tilde{M}(s)$ |
| Positional autocorrelation (PAC) | $\langle x(0)x(t) \rangle$ | $\mathcal{L}\langle x(0)x(t) \rangle = \frac{2k_BT}{s^2}\tilde{M}(s)$ |
| Power spectral density (PSD) | $S^x(\omega) = \mathcal{F}(\langle x(0)x(t) \rangle)$ | $S^x(\omega) = \frac{2k_BT\alpha''(\omega)}{\omega}$ |
| Velocity autocorrelation (VAC) | $\langle V(0)V(t) \rangle$ | $\langle V(0)\tilde{V}(s) \rangle = \frac{s^2\langle \Delta \tilde{r}^2(s) \rangle}{2}$ |
| Time-dependent diffusivity | $D(t)$ | $\frac{d\langle \Delta \mathbf{r}^2(t) \rangle}{dt} = 2ND(t)$ |
| Two-point (coupling) MSD | $\langle \Delta x_1(0)\Delta x_2(t) \rangle$ | $\mathcal{L}\langle \Delta x_1(0)\Delta x_2(t) \rangle = \frac{2k_BT}{s^2}\tilde{M}_{12}(s)$ |

### 1.2.3.1 Viscous medium

The use of DLS / DWS and SER for measuring viscosity has long been established. Using a probe of known dimension and measuring its diffusion coefficient, the friction and the viscosity of the fluid can be obtained. The probe particle undergoes a diffusive motion and the macroscopic properties of the sample characterized by one characteristic relaxation time, the viscosity [45-49].

$$\boldsymbol{D = \frac{k_B T}{6\pi\eta\alpha}} \quad (7)$$

$$\boldsymbol{\eta = \frac{k_B T}{6\pi a D}} \quad (8)$$

Or making use of the MSD: $\boldsymbol{\eta = 6Dt = \frac{k_B T}{\pi a} \frac{1}{\frac{<\Delta r^2>(t)}{\tau}}}$, fig. 5b.

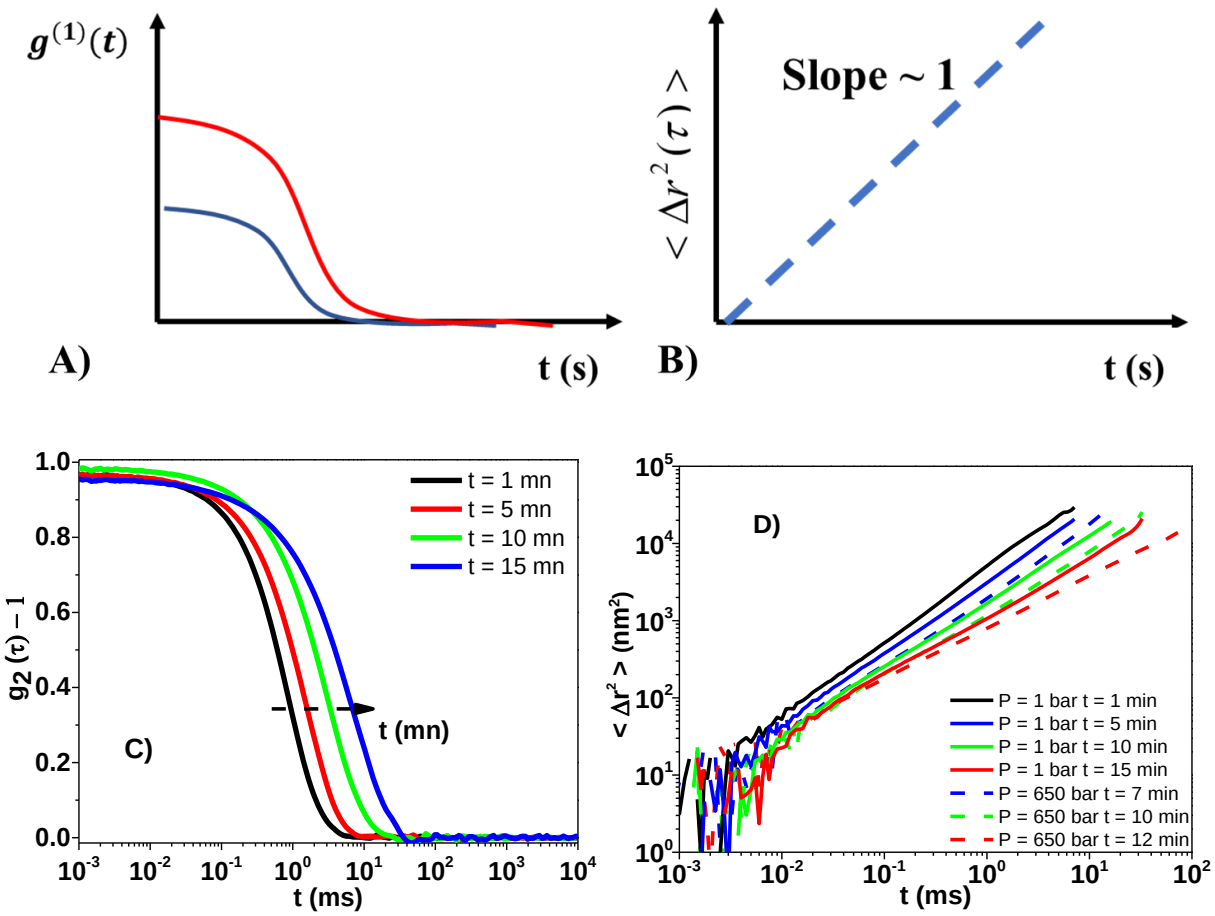


**Figure 5: a)** ISF **b)** time dependent MSD. The data is a result of probe motion (diffusive motion) in a viscous medium**, c)** ISF of gelatin/ $H_2O$/ polystyrene solutions, evolution of viscosity in gelling temperature (before gel formation) **d)** MSD of the respective ISF data. Dashed lines indicate time evolution viscosity at high pressure measurement (650 bar).

### 1.2.3.2 Viscoelastic medium: A complex fluid

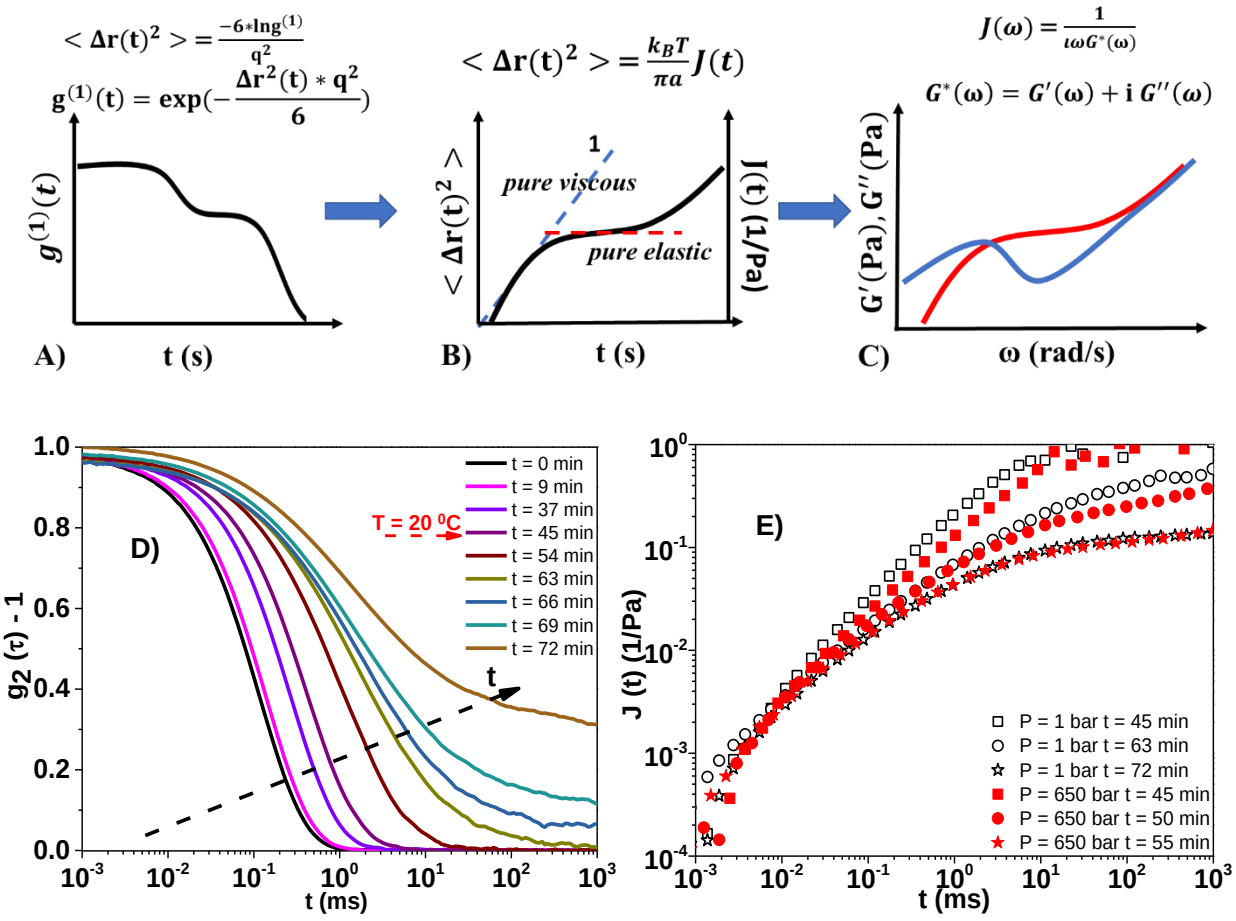


**Figure 6: a)** ISF **b)** time dependent MSD and the equivalent creep compliance **c)** frequency dependent viscoelastic spectra through the conversion of numerical routine. The data is a result of probe motion in a viscoelastic medium. **d)** ISF of gelatin/ $H_2O$/ polystyrene solutions, evolution of gelation procedure with time before and after (no relaxation time) gel formation **e)** Creep compliance of the respective data. Open symbols correspond at high pressure measurement (650 bar).

One can see that the plateau modulus will be measured by the difference of intercept between the full intercept and the measure one. This is not easy to obtain from DLS/DWS measurement. But the probe particle is not immobile at time faster than the relaxation time. It will undergo fast "rattling", "in cage" motion. That will lead to a time dependent MSD, i.e. a fast diffusion with a diffusion coefficient $D_f$. The existence of the fast motion makes it possible to measure the plateau

modulus. This highlight the fact that DLS/DWS based microrheology is a creep like measurement, more appropriate to viscous samples than to elastic samples. In that sense it might be more appropriate to call it micro-viscosimetry.

### 1.2 Technical aspect of passive microrheology – Probe characteristics

To conclude, accurate and precisely measurements of the mechanical properties in complex fluids by mean of passive microrheology requires the applicability of generalized-Stokes-Einstein relation Significant importance should be given in probe characteristics. The probes are important to be spherical, [50] monodisperse [51] (error created as the probe radius value affects the viscosity and the plateau modulus value) and under circumstances chemical modification of its surface needed. Should not induce heterogeneity either in the bulk material or in the probe surface. If the last one happens, then we can't know if we measure the self-diffusion of the probe. Characteristics of colloidal probes collected in table 2.

**Table 2:** Colloidal Probe characteristics

| Probe particles | Silica | Melamine | PS | PMMA | POLYMER | Organic solvent | $D_20$ |
|---|---|---|---|---|---|---|---|
| density ($g/cm^3$) | 1,85 | 1,51 | 1.05 | 1.19 | About 0.9-1 | ~ 0.5-0.9 | 1.11 |
| refractive index | 1,42 | 1,68 | 1,59 | 1,485 | About 1.4-1.5 | ~ 1.4 | 1.33 |
| Temperature stability ($^0C$) | 1000 | 250 | About 100 | 100 | | | |
| stability without swelling | water, alcohols, all solvents and oils | water, alcohols, all solvents and oils | Mainly water | Water and aliphatic hydrocarbons | | | |

## I. Probes Material Chemistry

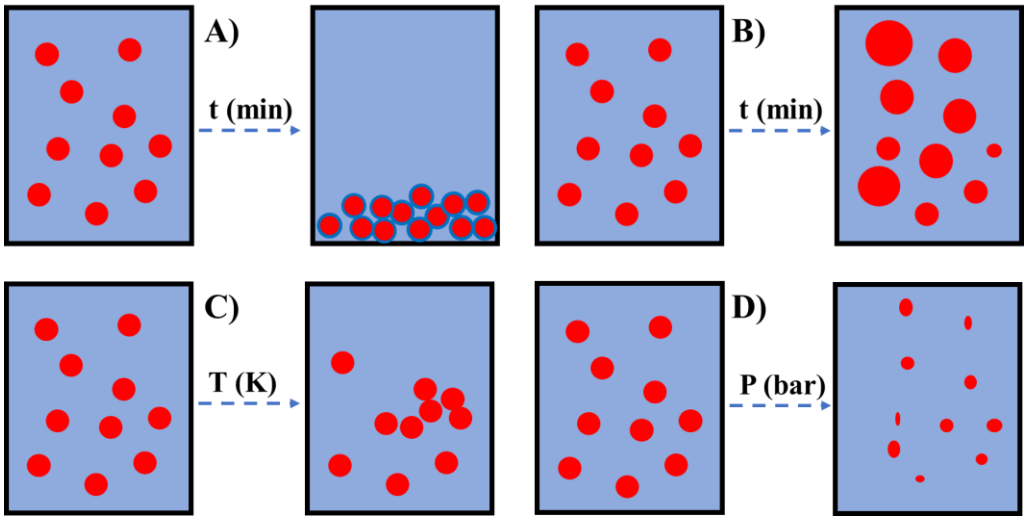


**Figure 7**: Undesirable Colloidal Probe Characteristics, **a)** sedimentation with time, **b)** swelling, **c)** destabilization by temperature, **d)** shrinking by pressure [54].

## II. Probes scattering

When microrheology experiments take place in single scattering limit the refractive index (of the probes and this of the solution) play a role. Someone should add probes which offer the necessary scattered intensity at low probe concentration. The scattering power of a probe dispersed in a medium is controlled by the probe size and the refractive index difference (contrast).

To be able to extract the probe MSD from the measured IAF, one need to make sure that the scattered intensity is dominated by the probe. The total intensity is the sum of the probe scattering and of the underlying sample scattering. We can assume the two terms to be uncorrelated $E_t = E_p + E_s$. The FAF is then the sum of two terms $< E_t(t)E_t(t+\tau) >= < E_p(t)E_p(t+\tau) > + < E_s(t)E_s(t+\tau) > = < I_p > g_p(t) + < I_s > g_s(t)$. Only if $I_p >> I_s$ can we safely extract $g_p|(t)$ . As Is and gs are known from separate measurements, one can check the fact that $I_{pt} >> I_s$ and that no strong contribution in $g_s(t)$ is visible in $g_t(t)$. As a check, one can even try to subtract the sample contribution computing $< I_t > g_t(t) - < I_s > g_s(t)$ and compare it to the measured FAF. This requirement can be difficult to meet in single scattering measurements. If the sample scattering is already large, it is not easy to add probe that will scatter enough without

providing multiple scattering. This constitutes a strong limit of single scattering microrheology. It is applicable in case of low scattering samples.

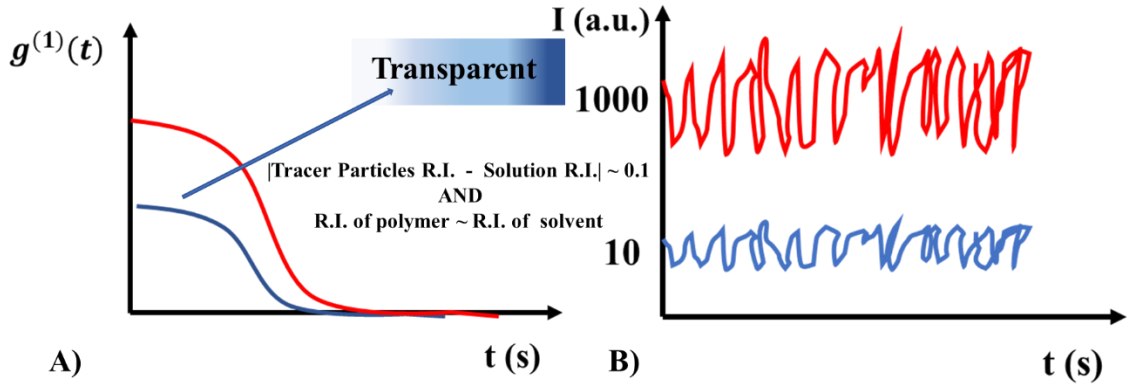


**Figure 8:** Refractive index condition. **a)** ISF of polymer solution (blue curve) and probes addition (red curve). **b)** Respective average intensity data.

**II. Size of colloidal probes**

The appropriate size of the probe in microrheology has been discussed. The GSER assume that the probe should 'feel' the material as a continuum medium. The probe size should be well above the characteristic length scales in the sample. On the upper limit of the particle radius, one need to avoid the probe sedimentation, that is achieved reasonably well if $R <= 1\ \mu m$ [52]. For example, in the case of the semi -dilute polymer solutions, the probe should be bigger than the characteristic length of the sample, (mesh -size) [53]. As shown in fig 9, different sizes can lead to difference in the apparent friction measured in the micro-rheology experiments.

$$\xi < r_{particle} < r_{cent}$$

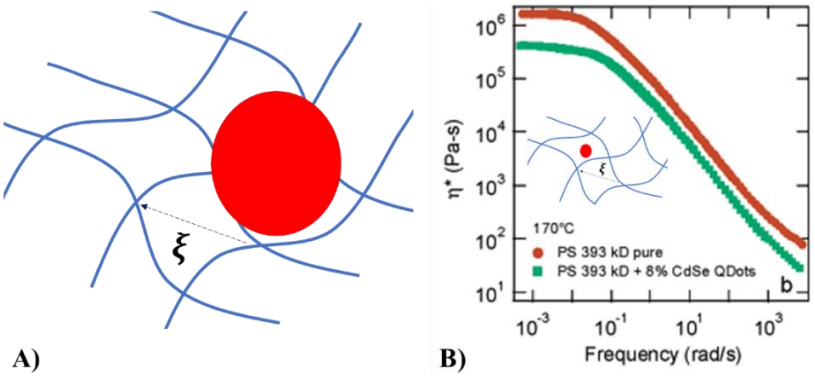


**Figure 9: a)** Colloidal probe radius higher than the characteristic length of the formatted network. **b)** Colloidal probe < 10 nm. The plot depicted by [52].

### 1.3 Microrheology by means of scattering methods

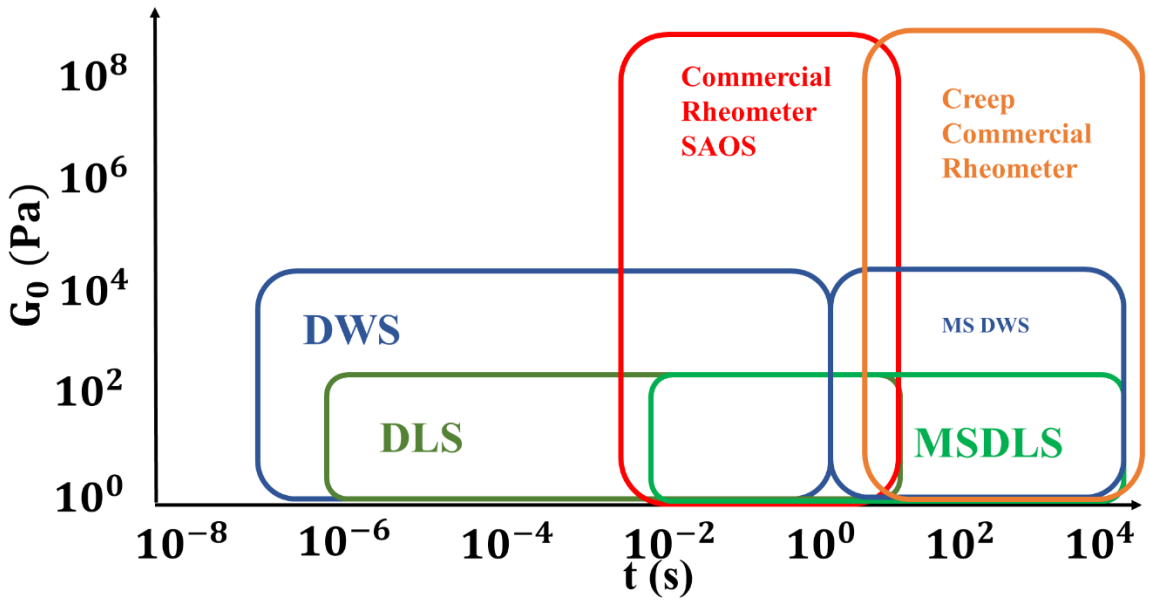


**Figure 10:** Relaxation time (connected with sample viscosity) and plateau modulus limits in Passive microrheology techniques.

## 1.4 Systems under investigation

### 1.4.1 Supramolecular (EHUT) living polymer solutions in apolar solvents

(EHUT) is a well-studied bis-urea monomer moiety **[**1**]**. In non-polar solvents, under certain conditions, EHUT self-assembles and form long self-assembly either cylindrical tubes with 3 molecules in cross section or thinner filaments with one molecule per cross section. The tube structure forms viscoelastic Maxwell-like fluids **[**2**]** and filament structure forms viscous solutions. The phase diagram of EHUT solutions in non-polar solvent toluene has been investigated extensively [3]. Toluene is slightly less apolar compared to dodecane and cyclohexane (its dielectric constant is 2.38 and relative polarity about 0.099 [4,5]). Depending on concentration and temperature EHUT solutions may be monomeric (unassembled) or form self-assembled thin filaments or tubes, under atmospheric pressure [6,7]. In dodecane, another extensively investigated, highly apolar solvent, EHUT solutions exhibit some qualitative differences in their structural and

dynamic behavior [7,8]. It turns out that this solvent, which is of worst quality for the polar parts of EHUT, stabilizes the tube structure as opposed to toluene [4]. For a 4.2 g/L solution, the transition between tube and filament takes place at 89°C. The qualitative phase diagram is sketched in Fig.2a, where the tube phase is dominant. Dodecane has been a popular choice for conventional rheological measurements, in part because of its high boiling point at atmospheric pressure [4, 9-13]. The phase behavior of EHUT solutions in cyclohexane is expected to be qualitatively similar to that in dodecane. It is shown in Fig.12b, where for the same concentration of 10 nm the tube-to-filament transition is observed at 50°C. The effects of pressure will be discussed in chapter 2. Note that there is no macroscopic evidence of phase separation in either solvent, as the samples remain visually transparent. Moreover, since the thrust of the present investigation is the effects of pressure on the EHUT-based reversible supramolecular polymers, we work in conditions of ambient humidity without considering its effects on the viscoelastic properties of the solutions [12].

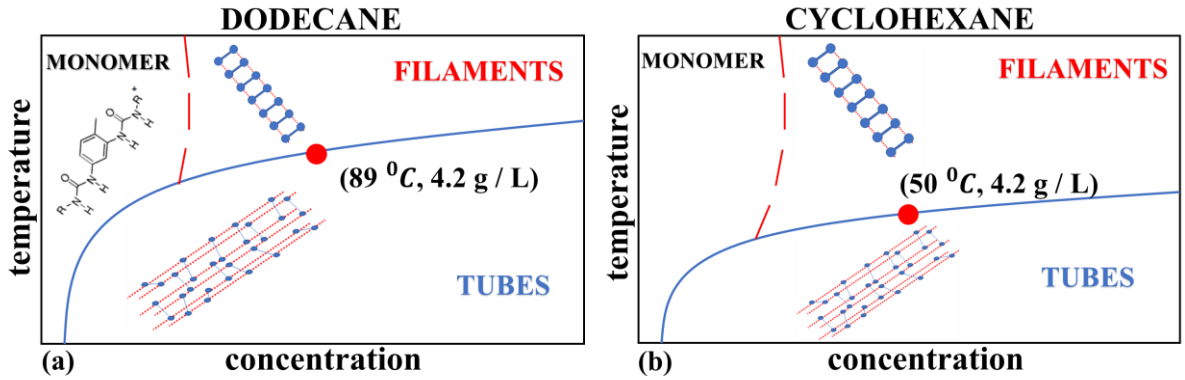


**Figure 11**: Schematic illustration of the phase diagram for EHUT solutions in non-polar solvents dodecane (a) and- cyclohexane (b), at atmospheric pressure, based on literature [33, 47]. Three regimes are identified, monomeric (unassembled), self-assembled thin filaments and self-assembled tubes. The cartoon illustrates the molecular structure of the EHUT monomer, and the self-assembled filaments and tubes (the hydrogen bonds are represented by the dotted lines connecting the urea monomers, shown by blue circles). The symbols indicate the observed structural transition from filament to tube for c=4.2 g/L (at 89 and 50 $^0$C, for dodecane and cyclohexane, respectively.

**Sample preparation**

EHUT was obtained from Prof. Laurent Bouteiller and co-workers. The synthesis of EHUT was achieved by reacting racemic 2-ethylhexylamine with 2,4-toluene diisocyanate [9,10]. Two apolar solvents were used as received, dodecane (99+ % pure) and cyclohexane (99.7 % pure), both obtained from Sigma Aldrich. Both have nearly the same dielectric constant (2.01 and 2.02, respectively, compared to the value of water, 78.5, at 25ºC) and relative (to water) polarity (about 0.01 and 0.006, respectively) [4,5]. The solutions were prepared under conditions of atmospheric humidity and temperature (about 80ºC for dodecane) and room temperature for cyclohexane, by adding the EHUT powder to the solvent [12] and stirring for at least 48 hours. For the microrheology experiments, polymethylmethacrylate (PMMA) particles were added at a volume fraction of about $10^{-4}$ vol%, to act as effective tracers for following their motion (see Methods section below). They were chemically grafted with poly-hydroxy stearic acid (PHSA) chains (of about 10nm) to ensure stability of the dispersion and their hydrodynamic radius was R=130 nm (measured with dilute regime by dynamic light scattering, DLS) and their polydispersity 10% [14]. The dual goal of adding these particles was to stay in the single scattering limit and reach a scattering intensity at least 50 times higher compared to that of EHUT solutions in the absence of particles.

### 1.4.2 Diblock Stars copolymer

Diblock stars polymer has recently been proposed as an approach to soft patchy colloids. We are concerned here with the pressure dependence of 3 arm stars. The star consists of polybutadiene (inner) and polystyrene (outer block). In highly selective solvent for the outer block and athermal for the inner, the formation of micelles observed in similar systems [15]. In proper selective solvent, the formation of large aggregates observed [16-19]. Their size depends on the selectivity change by temperature as depicted in figure 12 [20].

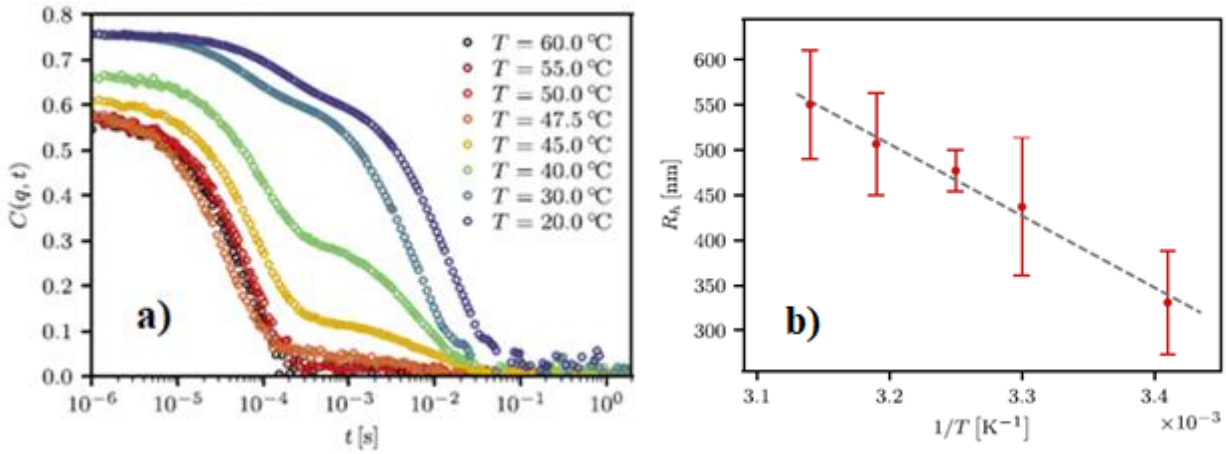


**Figure 12: a)** ISF of 3 arm diblock stars as a function of temperature in dilute regime (c*/12). For T < 47.5 the evolution of cluster observed. **b)** Evolution of Cluster hydrodynamic radius with inverse temperature. Adapted from [20].

**Sample Preparation**

Solutions were prepared by mixing an appropriate amount of telechelic star polymers (TSPs) and solvent (1-phenyldodecane) to reach a desired concentration. The sample degradation was inhibited by adding 0.1 wt% of TSP of the antioxidant BHT (2,6-Di-tert-butyl-4-methylphenol). In order to fully dissolve TSPs, methylene chloride was used as the cosolvent. Then, the cosolvent was removed under ambient conditions until constant weight was achieved. Details about the synthesis of TSPs can be found in [20]. The refractive index of phenyldodecane is n = 1.482. Before each experiment, the sample was equilibrated at T = 60 °C (above the θ-temperature of the outer PS-block) for 30 min to erase thermal history. Then, the sample was quenched to the desired temperature and equilibrated. The equilibration process was probed by measuring the ISF until it reached steady values over time. In the frame of this thesis, low molecular weight linear polystyrene and high molecular wight polybutadiene in selective solvent (phenyldodecane) studied. During their preparation in phenyldodecane solvent we keep the temperature constant at $60^0$ (for polystyrene) and 25 $^0$ (for polybutadiene).

**Table 3:** Sample characteristics

| Sample | Mw (kg/mol) | $F_{PS}$ | $F_{PB}$ |
|---|---|---|---|
| A (N.5) | 46.3 | 0.2 | 0.8 |
| B (N.6) | 40 | 0.33 | 0.67 |
| Linear PS | 126 | 100 | 0 |
| Linear PB | 1091 | 0 | 100 |

Due to the high refractive index of phenyldodecane that is close to the PMMA particles ones, microrheology DLS were not feasible. An attempt was made to use cyclohexane. We expect a similar behavior of 3 arm stars/cyclohexane solutions with the solutions of 3 arm stars / phenyldodecane, as cyclohexane is $\Theta \sim 34$ for the outer block (polystyrene) and good for the inner (polybutadiene). PMMA probes dispersed well in the solutions and the sample was looked homogenized. From the intensity correlation function, we have indications that the contribution of the sample itself in the ISF is negligible (fig.13). The scattering light is mainly from the probes and not from the sample itself. We assume that the contribution (<1%) of the sample doesn't affect the microrheology data. Finally, we use heptane (Sigma – Aldrich, 99%), a non-solvent for the polystyrene and good for the polybutadiene. Our predictions as well as literature studies clearly predict the micelles formation [21-25]. More details discussed below.

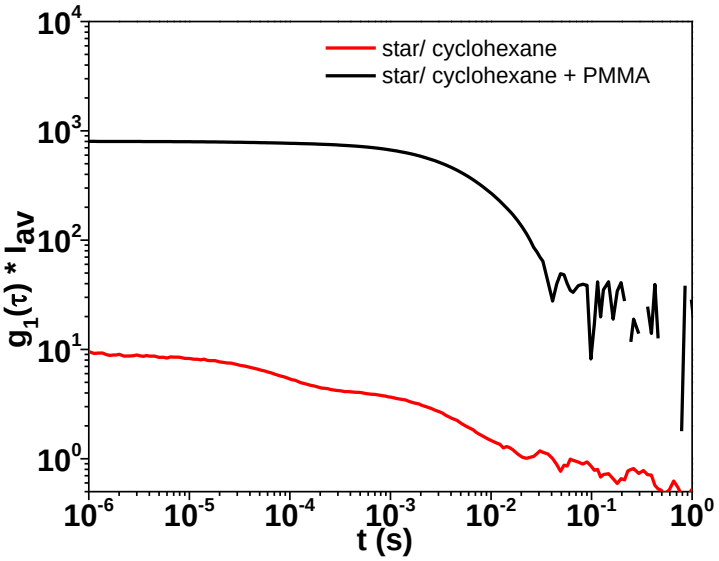


**Figure 13:** Field correlation function multiplied by the average intensity of 3 arm diblock star/ phenyldodecane solution (red line) and star/phenyldodecane/ PMMA solution (black line). (c = 2c*)

## References


[1] Simic, V., L. Bouteiller, and M. Jalabert, ‘‘Highly cooperative formation of bis-urea based supramolecular polymers,’’ Journal of the American Chemical Society **125**, 13148 13154 (2003).

[2] A. Louhichi, A. R. Jacob, L. Boutteiller, and D. Vlassopoulos, “Humidity affects the viscoelastic properties of supramolecular living polymers”, special issue on Associating polymers, J. Rheol., **61**, 1173-1182 (2017).

[3] Bellot, M., and L. Bouteiller, ‘‘Thermodynamic description of bis-urea self-assembly: competition between two supramolecular polymers,’’ Langmuir **24**, 14176-14182 (2008).

[4] Bouteiller, L., Colombani, O., Lortie, F. & Terech, P. “Thickness transition of a rigid supramolecular polymer.” J. Am. Chem. Soc. **127**, 8893–8898 (2005).

[5] Solvents and Solvent Effects in Organic Chemistry, Wiley-VCH Publishers, 3rd ed., N.Y. (2003).

[6] Shikata, T., T. Nishida, B. Isare, M. Linares, R. Lazzaroni, and L. Bouteiller, ‘‘Structure and dynamics of a bisurea-based supramolecular polymer in n-dodecane,’’ The Journal of Physical Chemistry B **112**, 8459-8465 (2008).

[7] B. G. Alvarenga, M. Raynal, L. Bouteiller, E. Sabadini, “Unexpected Solvent Influence on the Rheology of Supramolecular Polymers,” Macromolecules **50**, 6631-6636 (2017).

[8] Isare, B., Pensec, S., Raynal, M. & Bouteiller, L. “Bisurea-based supramolecular polymers: From structure to properties.” Comptes Rendus Chim. **19**, 148–156 (2016).

[9] Ducouret, G., C. Chassenieux, S. Martins, F. Lequeux, and L. Bouteiller, ‘‘Rheological characterisation of bis-urea based viscoelastic solutions in an apolar solvent,’’ Journal of colloid and interface science **310**, 624-629 (2007).

[10] Lortie, F., S. Boileau, L. Bouteiller, C. Chassenieux, B. Demé, G. Ducouret, M. Jalabert, F. Lauprêtre, and P. Terech, ‘‘Structural and rheological study of a bis-urea based reversible polymer in an apolar solvent,’’ Langmuir **18**, 7218-7222 (2002).

[11] Van der Gucht, J., N. Besseling, W. Knoben, L. Bouteiller, and M. C. Stuart, ‘‘Brownian particles in supramolecular polymer solutions,’’ Physical Review E **67**, 051106 (2003).

[12] A. Louhichi, A. R. Jacob, L. Boutteiller, and D. Vlassopoulos, “Humidity affects the viscoelastic properties of supramolecular living polymers”, special issue on Associating polymers, J. Rheol., **61**, 1173-1182 (2017).

[13] Jacob, A. R., A. P. Deshpande, and L. Bouteiller, ‘‘Large amplitude oscillatory shear of supramolecular materials,’’ Journal of Non-Newtonian Fluid Mechanics **206**, 40-56 (2014).
[14] Jacob, A. R., Moghimi, E. & Petekidis, G.” Rheological signatures of aging in hard sphere colloidal glasses.” Phys. Fluids **31**, (2019).
[15] D. Lairez, M. Adam, J.P. Carton, E. Raspaud, “Aggregation of Telechelic Triblock Copolymers: From Animals to Flowers”, Macromolecules, **30**, 6798-6809, (1997).
[16] Lo Verso, F.; Panagiotopoulos, A. Z.; Likos, C. N. Aggregation Phenomena in Telechelic Star Polymer Solutions. Phys. Rev. E 2009, 79, 010401.
[17] Lo Verso, F.; Panagiotopoulos, A. Z.; Likos, C. N. Phase Behavior of Low-Functionality, Telechelic Star Block Copolymers. Faraday Discuss. 2010, 144, 143−157.
[18] Koch, C.; Likos, C. N.; Panagiotopoulos, A. Z.; Lo Verso, F. Self-Assembly Scenarios of Block Copolymer Stars. Mol. Phys. 2011, 109, 3049−3060.
[19] Koch, C.; Panagiotopoulos, A. Z.; Lo Verso, F.; Likos, C. N. Phase Behavior of Rigid, Amphiphilic Star Polymers. Soft Matter 2013, 9, 7424−7436.
[20] Esmaeel Moghimi, Iurii Chubak, Antonia Statt, Michael P. Howard, Dimitra Founta, George Polymeropoulos, Konstantinos Ntetsikas, Nikos Hadjichristidis, Athanassios Z. Panagiotopoulos, Christos N. Likos and Dimitris Vlassopoulos, ‘Self-Organization and Flow of Low-Functionality Telechelic Star Polymers with Varying Attraction’, ACS Macro Lett., vol: 8, pp: 766−772, 2019.

[21] J. Bang, K. Viswanathan, T. P. Lodge, M. J. Park & K. Char, “Temperature-dependent micellar structures in poly(styrene-b-isoprene) diblock copolymer solutions near the critical micelle temperature”, J. Chem. Phys., **121**, 11489, (2004).

[22] J. P. Hinestrosa, J. Alonzo, M. Osa, & S. M. Kilbey II, “Solution Behavior of Polystyrene-Polyisoprene Miktoarm Block Copolymers in a Selective Solvent for Polyisoprene”, Macromolecules, **43**, 7294-7304, (2010).

[23] K. Mortensen, “Structural properties of self-assembled polymeric micelles”, Cur. Op. Col. & Int. Sci, **3**, 12-19, (1998).

[24] D. A. Vega, J. M. Sebastian, Y. L. Loo, R. A. Register, “Phase Behavior and Viscoelastic Properties of Entangled Block Copolymer Gels”, J. Pol. Sci.: Part B: Pol. Phy., **39**, 2183-2197, (2001).

[25] J. Huh, K. H. Kim, C. H. Ahn & W. H. Jo, “Micellization behavior of star-block copolymers in a selective solvent: A Brownian dynamics simulation approach”, J. Chem. Phy. **121**, 4998-5003, (2004).

[26] J. Kohlbrecher, A. Bollhalder, R. Vavrin, G. Meier, Rev. Sci. Instr. 78, 125101, 2007.

[27] G. Meier, H. Kriegs, Rev. Sci. Instr. 79, 013102, 2008.

[28] Ferrell, R. T. & Himmelblau, D. M. “Diffusion Coefficients of Nitrogen and Oxygen in Water,” J. Chem. Eng. Data **12**, 111–115 (1967).

[29] T.G. Mason and D.A. Weitz, “Optical measurements of Frequency-Dependent Linear Viscolestic Moduli of Complex Fluids”, Phys. Rev. Let., **74**, 7, (1995).

[30] John H. van Zanten and Karl P. Rufener, “Brownian motion in a single relaxation time Maxwell fluid” P. R. E, **62**, 4, (2000).

[31] Thomas G. Mason, “Estimating the viscoelastic moduli of complex fluids using generalized Stokes-Einstein equation” Rheol. Acta, **39**, 371-378, (2000).

[32] B.S. Chae and Eric M. Furst, “Probe Surface Chemistry Dependence and Local Polymer Network Structure in F-Actin Microrheology” Lungmuir, **21,** 3084-3089, (2004).

[33] D.T. Chen, E.R. Weeks, A.J. Levine, T.C. Lubensky et al., “Rheological Microscopy: Local Mechanical Properties from Microrheology” Phys. Rev. Let. **90**, 10, (2003).

[34] F.C. MacKintosh and C.F. Schmidt, “Microrheology”, Cur. Op. Col. Sci., **4**, 300-307, (1999).

[35] Z. Cheng and T.G. Mason, “Rotational Diffusion Microrheology” Phys. Rev. Let., **90**, 1, (2003).

[36] Alex J. Levine and T.C. Lubensky, “One-and Two-Particle Microrheology”, Phys. Rev. Let., **85**, 8, (2000).

[37] M.L. Gardel, M.T. Valentine, D.A. Weitz, “Chapter 1 Microrheology”, Dep. Of Physics, Cambridge MA 02138[38] N. Yang, R. Lv, J. Jia, K. Nishinari, Y. Fang, “Application of Microrheology in Food Science” Annu. Rev. Food Sci. Technol., **8**:23.1-23.29, (2017).

[39] Todd M. Squires and Thomas G. Mason, “Fluid Mechanics of Microrheology”, Annu. Rev. Fluid Mech., **42**:413-38, (2010).

[40] Roseanna N. Zia, “Active and Passive Microrheology: Theory and Simulation”, Annu. Rev. Fluid Mech., **50**: 371-405, (2010).

[41] T.B. Liverpool and F.C. Mackintosh, “Inertial Effects in the Response of Viscous and Viscoelastic Fluids”, Phys. Rev. Let., **95,** 208303, (2005).

[42] P.D. Garcia, F. Cardinaux, E. Bertseva, L. Forro, F. Scheffold, S. Jeney, “Accounting for inertia effects to access the high-frequency microrheology of viscoelastic fluids” Phys. Rev. E, **90**, 060301, (2014).

[43] E. M. Furst, T. M. Squires, Microrheology, Oxford University Press, NY 2017.

[44] R.M.L Evans, M. Tassieri, D. Auhl, T. A. Waigh, ‘Direct conversion of rheological compliance measurements into storage and loss modulus”, Phys. Rev. E, **80**, 012501, (2009).

[45] R. Brown, “A brief account of microscopical observations made in the months of June, July and August 1827, on the particles contained in the pollen of plants; and on the general existence of active molecules in organic and inorganic bodies” Phil. Mag. **4**, 161 (1828).

[46] A. Einstein, “On the Motion of Small Particles Suspended in Liquids at Rest Required by the Molecular-Kinetic Theory of Heat∗” Ann. Phys. (Berlin) **17**, 549 (1905).

[47] M. von Smoluchowski, “Zur kinetischen Theorie der Brownschen Molekular bewegung und der Suspensionen” Ann. Phys. (Berlin) **21**, 756 (1906).

[48] G. K. Batchelor, “Brownian diffusion of particles with hydrodynamic interaction”, J. Fluid Mech., **74,** 9, (1976).

[49] T. Li and M. Raizen, “Brownian motion at short time scales”, Ann. Phys. (Berlin), **525,** 4, 281-295, (2013).

[50] Bivash Ranjan Dasgupta, “Microrheology and Dynamic Light Scattering Studies of Polymer Solutions” PhD thesis, Harvard University, Cambridge, Massachusetts, (2004).

[51] DC. Morse, “Viscoelasticity of concentrated isotropic solutions of semiflexible polymers. 2. Linear response”, Macromolecules, **31**, 7044–67, (1998).

[52] Valentine MT, Kaplan PD, Thota D, Crocker JC, Gisler T, “Investigating the microenvironments of inhomogeneous soft materials with multiple particle tracking” *Phys. Rev. E* **64**, 061506, (2001).

[53] Tuteja A, Mackay ME,Narayanan S, Asokan S,Wong MS. “Breakdown of the continuum Stokes-Einstein relation for nanoparticle diffusion”, Nano Lett., **7**, 1276–81, (2007).

[54] G. Meier, J. Gapinski, M. Ratajczyk, M.P. Lettinga, K. Hirtz, E. Banachowicz, A. Patkowski, "Nano-Viscosity of supercooled liquid measured by fluorescence correlation spectroscopy: Pressure and temperature dependence and the density scaling", J. Chem. Phys. **148**, 094201, (2018).
[55] D. A. Weitz & D.J. Pine, "Diffusing-wave spectroscopy", Chapter 16, 655-699, (1993).
[56] P.D. Kaplan, M.H. Kao, A.G. Yodh & D.J. Pine, "Geometric constraints for the desigh of diffusing-wave spectroscopy experiments", Appl. Opt. **32**, 3828-3836, (1993).
[57] G. Maret, "Diffusing-wave spectroscopy", Cur. Op. Col. Int. Sci. **2**, 251-257, (1997).
[58] C. Zhang, M. Reufer, D. Gaudino & F. Scheffold, "Improved diffusing wave spectroscopy based on the automized determination of the optical transport and absorption mean free path", J. Kor. Aus. Rheol. (2017).
[59] D.J. Pine, D.A. Weitz, P.M. Chaikin & E. Herbolzheimer, "Diffusing wave spectroscopy", Phys. Rev. Let. **60**, 1134-1137, (1988).
[60] Z. Fahimi, F. J. Aangenendt, P. Voudouris, J. Mattsson & H. M. Wyss, "Diffusing-wave spectroscopy in a standard dynamic light scattering setup", Phys. Rev. E, **96**, 062611, (2017).
[61] J. WEESE, "A regularization method for nonlinear ill–posed problems", Comput. Phys. Commun., **77**, 429–440, (1993).
[62] J. HONERKAMP & J. WEESE, "A nonlinear regularization method for the calculation of relaxation spectra", Rheol. Acta, **32**, 65–73, (1993).

# *Chapter 2: Dynamics and Structure properties of Supramolecular Living Polymers at high pressures.*

## I. INTRODUCTION

The supramolecular chemistry that is central to organization and communication in living cells relies on hydrogen bonding, hydrophobic, and other non-covalent interactions between biomolecules. [16-19]. The presence of supramolecular materials in nature is a good answer in the question: "do wo need another class of polymers?" [21]. This kind of polymers differ with the conventional one in the way that this connected. In one hand we meet the stiff and difficult to break (difficulties in processing procedures) covalent connected (spaghetti-like) macromolecules, on the other hand small molecules (N ~ 10) are connected (weaker) one to each other through hydrogen bonding, π-π stacking, hydrophobic and other non-covalent interactions which depicted at figure 1.

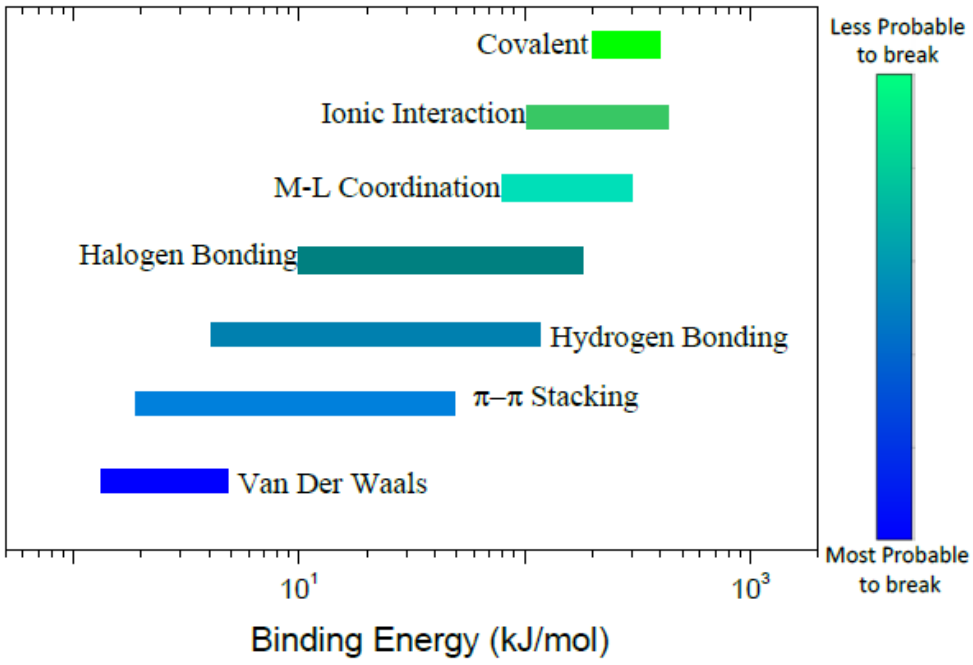


**Figure 1.** Binding energy ranges of different types of secondary interactions, in kJ/mol (about 0.4 kT at room temperature). The color bar represents the probability of a bond breaking spontaneously due to thermal fluctuations. Adapted from [16].

An example of hydrogen bonding system illustrated in figure 2a. Because supramolecular assemblies (made by building units) connected by means of non-covalent interactions the bonds can break spontaneously, considered and often called living polymers. [6-8]. These molecules find

to be easily processable due to the reversibility of this specific type of bonding. These great materials are not only easily processable but also recyclable and well-known for the self -healing properties. Under certain conditions offer mechanical properties equivalent with the common plastics and elastomers [9,10,20].

In addition to the above, the synthesis of functional supramolecular polymers remains challenging. The manipulation of DNA for materials purposes offers great opportunities in natural science. The scientists try to taking advantage the unique molecular recognition of DNA in order to make materials with high specificity and structural control [22,23]. In nowadays self-assembly materials with programmable properties synthesized (fig. 2) [67-69].

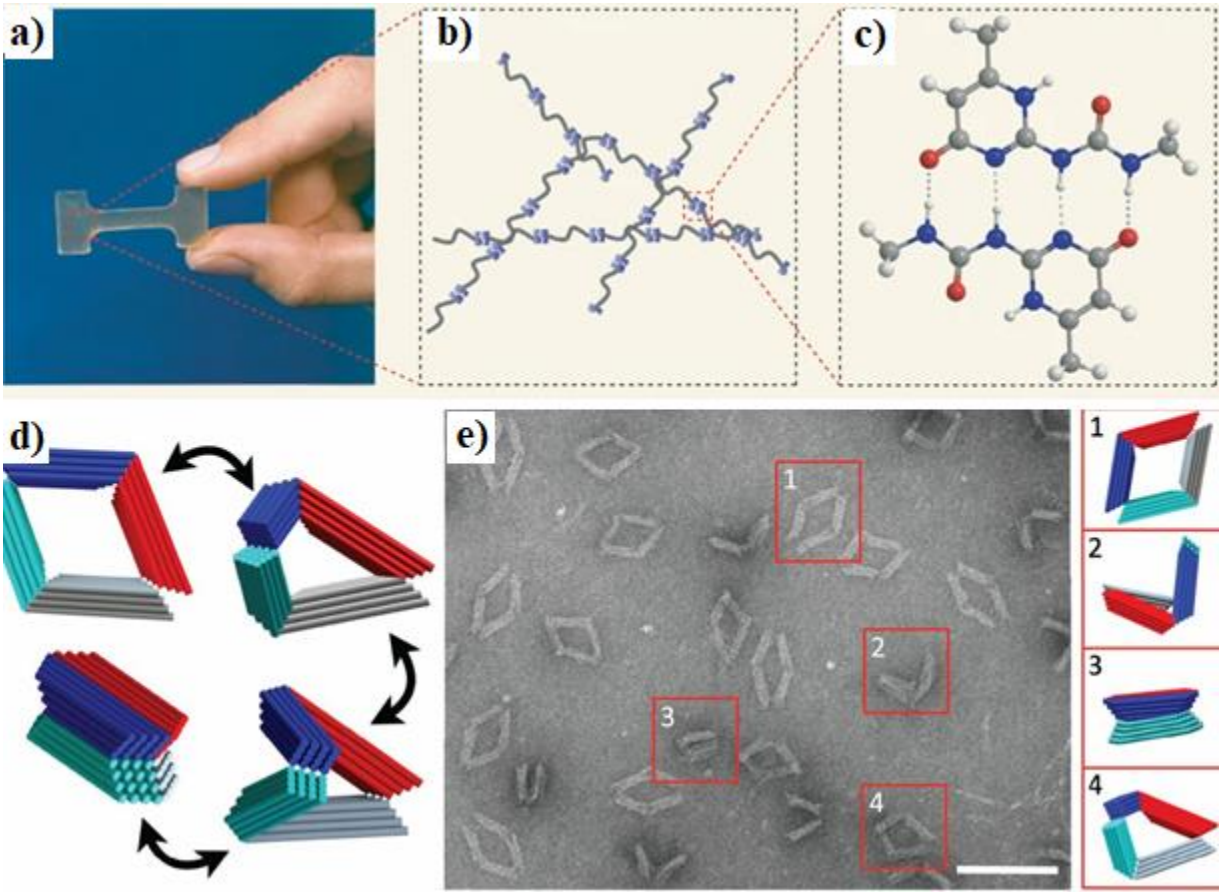


**Figure 2. a)** Plastic component made from supramolecular polymer. **b)** The molecular structure is a network of monomers connected by hydrogen bonds. **c)** Units form hydrogen bonds to each other (dotted lines). Carbon atoms are shown in grey; nitrogen in blue; oxygen in red; and hydrogen in white. **d)** DNA origami mechanism with 3D motion **e)** TEM images confirm well-folded structures.

In the absence of "locking strands" the mechanism fluctuates freely along its motion path. Several structures in different conformations are highlighted. Adapted from [7,67].

In this chapter present a methodology to measure the high-pressure viscoelasticity (HP-LVE) of a supramolecular living polymer by means of DLS-microrheology in the single scattering limit. This limit can be achieved if the contrast of the interrogated solution is low and scattering is mainly due to the added particles [1-5] (at low fraction) and has been reported in the past for DNA-star solutions and gels [29], details given in chapter 1. However, it has not been tested at high pressures and, besides the microrheological data (which can be also obtained via DWS), it provides important information on the dynamic structure via the intermediate scattering function [11-15]. The dynamics and the linear viscoelastic properties of supramolecular living polymers at elevated pressures is presented. The linear viscoelastic spectrum over a wide range of frequencies, temperatures and pressures is obtained by means of passive microrheology at the single scattering limit. Application to 2,4-bis(2-ethylhexylureido)toluene (EHUT) which forms supramolecular living polymers in non-polar solvents, indicates that, pressure may affect their phase behavior and in particular stabilize the tube phase (akin to wormlike micelles). High levels of pressure (in the range 600 to 1000 bars) are found to affect the dynamics much more than the plateau modulus. Specifically, pressure is found to stabilize the tube structure of EHUT assemblies in cyclohexane.

The archetype reversible supramolecular polymer employed is 2,4-bis(2-ethylhexylureido)toluene (hereafter abbreviated as EHUT), based on a bis-urea moiety. Its synthesis, thermodynamic and rheological properties have been discussed quite extensively in the literature **[**30-40**]**. In non-polar solvents, at high enough concentrations and low enough temperatures, EHUT self-assembles into long cylindrical tubes with viscoelastic behavior akin to wormlike surfactant micelles whose rheology depends on the bonding lifetime and overall length (which controls terminal relaxation) **[**38,41**]**. Importantly, a similar bis-urea was recently found to exhibit a high-pressure (about 600 bars) viscosity thickening when dissolved in supercritical propane with significant implications in fracturing fluid processing for enhanced oil recovery operations [42].

The linear viscoelastic properties of living polymers such as the present EHUT assembly were examined in the framework of the classic theory of Cates for living polymers [43-45], which are characterized by two relaxation times, the local breaking time ($\tau_b$) due to the exchange of associating units (lifetime of bonds) and the longer terminal relaxation time ($\tau_t$) of the entire assembly, $\tau_t = (\tau_{rep}$

$\tau_b)^{1/2}$, where $\tau_{rep}$ is the reptation time of the living assembly (this expression holds in the limit $\tau_b << \tau_{rep}$). The model predicts that $\tau_t \sim c^{1.25}$ and $G \sim c^{2.25}$ [43-45]. Experiments under virtually dry conditions confirm the latter that not the former, suggesting a smaller power-law exponent by about 50% [38]. Actually, it was recently reported that humidity can play an important role in speeding-up relaxation via chain scission because of competitive hydrogen bonding [38], which seems to be an important generic phenomenon in organogelators [46].

Given the above developments, and in view of the general need to explore and further exploit the effects of pressure on rheology, application to reversible supramolecular assemblies which combine different length and time scales depending on temperature and concentration, emerges as an outstanding challenge. We address this challenge in this work and focus in particular on the phase behavior and linear viscoelasticity of EHUT solutions in two apolar solvents, dodecane and cyclohexane as functions of pressure and temperature. We first present the high-pressure DLS instrumentation for microrheology and then discuss results obtained with the two different solutions over a range of concentrations, temperatures and pressures.

## II. RESULTS AND DISCUSSION

### A. EHUT IN DODECANE: PRESSURE AFFECTS SOLVENT VISCOSITY

In EHUT/dodecane solutions, tubes are formed and the main effect of pressure reflects the changes in solvent viscosity. In EHUT/cyclohexane solutions, increasing pressure was found to promote filament to tube structure transition. This structural transition is observed at T ~ $49^0$C at ambient pressure [47] and at larger temperature when pressure increased. It was detected in DLS by the presence of a second, slow relaxation process (viscoelastic mode), and use this as a signature of the tube formation in order to construct a phase diagram. The viscoelastic nature of the tube phase was confirmed by microrheology. Fig.3a depicts ISF results from measurements of EHUT / dodecane solutions at different concentrations, 25 $^0$C and pressures of 1 bar (lines) and 1000 (dashed lines) bars. In the system at atmospheric pressure, tube formation for a wide concentration is estiablished in the temperature regime 22 – 68ºC [47]. The effect of high pressure in slowing-down the dynamics is evident across all concentrations. Moreover, with increasing concentration a second relaxation process emerges, which becomes stronger and dominates the solution's response at

higher concentrations. Simple observation of the ISF data suggests that the pressure affects the slow process more substantially compared to the fast one.

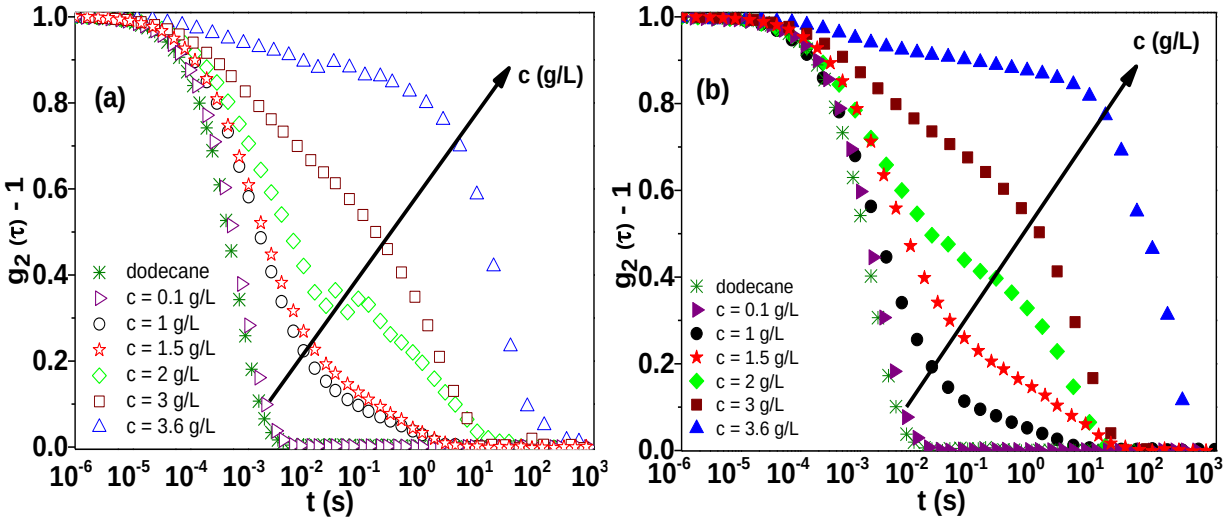


**Figure 3:** ISF of EHUT / dodecane / PMMA probes in (a) 1 (open symbols) and (b) 1000 (filled symbols) bar, at different concentrations at room temperature. The data for the pure solvent (with the PMMA particles) is also shown for reference.

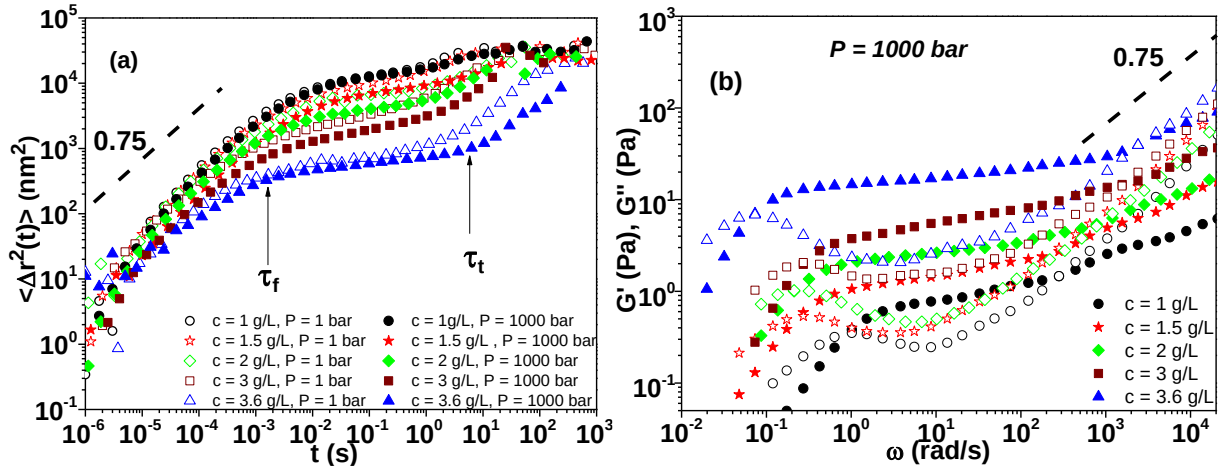


**Figure 4:** (a) Mean square displacement of EHUT solutions in dodecane with added PMMA tracer particles, at different concentrations and pressures (open symbols correspond to 1 bar, filled symbols to 1000 bars) where, $\tau_f$, $\tau_t$ indicate fast and terminal relaxation time, respectively. (b) Respective microrheological frequency-dependent linear viscoelastic moduli of the same solutions at 1000 bars: storage G' (filled symbols) and loss G'' (open symbols). The black dashed line has a slope of 0.75. T = 25 $^0$C.

The respective data of the same solutions with added PMMA particles (at $10^{-4}$ vol%) are shown in Fig.4a in the form of time-dependent mean square displacement, at different concentrations, 25 $^0$C

and pressures of 1 bar (lines) and 1000 (dashed lines) bar. These data were transformed into frequency-dependent LVE moduli as outlined in the Methods section above, which are shown in Fig.4b for P=1000 bar. At all concentrations the terminal regime is captured with G'~$\omega^2$ and G''~$\omega$. Moreover, at the highest frequencies the frequency dependence of G'' appears to conform to a power-law with exponent of about 0.75, as reported for other living and semiflexible polymers [55].

To better appreciate the effects of pressure, it is instructive to compare the LVE spectra at 1 and 1000 bars for two different concentrations. This is indeed depicted in Fig.5 where that impact of pressure on the solvent background is accounted by multiplying the frequency with the pressure-dependent solvent viscosity, the latter being shown in the supplementary materials of this chapter. This normalization collapses both the G' and G'' data at high frequencies, especially at the high-frequency crossover frequency and above, as better observed for 1.5 g/L (Fig.5a), (App. Fig. 1). This confirms that these data reflect local response of the living polymer at times below the breaking time of an association, and the solvent mediates the response (hydrodynamic modes) [56,57]. At the same time, with the two solutions having the same "internal clock", the effect of pressure on the terminal relaxation is evident in this figure and appears to reflect structural change (within the tube region of the phase diagram), as also corroborated by the more extended plateau modulus. This structural change should be associated with the living nature of the self-assembly and the interplay of breaking and terminal times.

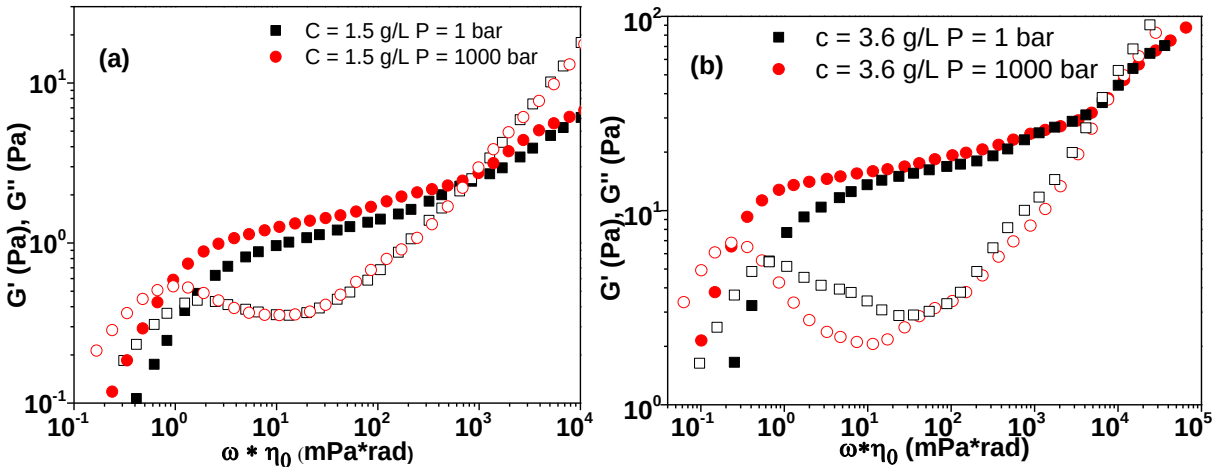


**Figure 5:** G' (filled symbols), G'' (open symbols) for EHUT / dodecane solutions at T = 25 $^0$C, as functions of frequency multiplied by solvent viscosity, at 1 bar (black) and 1000 bar (red). Data are depicted for two different concentrations, (a) 1.5 g/L (a) and (b) 3.6 g/L. Solvent viscosities represent in fig. 6, in appendix.

The latter appears more evident at the higher concentration where the minimum in G'' is shifted to lower frequencies by roughly factor of 1/5, almost the same shift of the terminal crossover frequency, within the experimental uncertainty (Fig. 5b). Note that in the latter case the ISF from obtained from a multi-speckle DLS setup (with a ccd-camera replacing the photomultiplier tube and a linear correlator in order to account for non-ergodicity [51,52, 58,59].

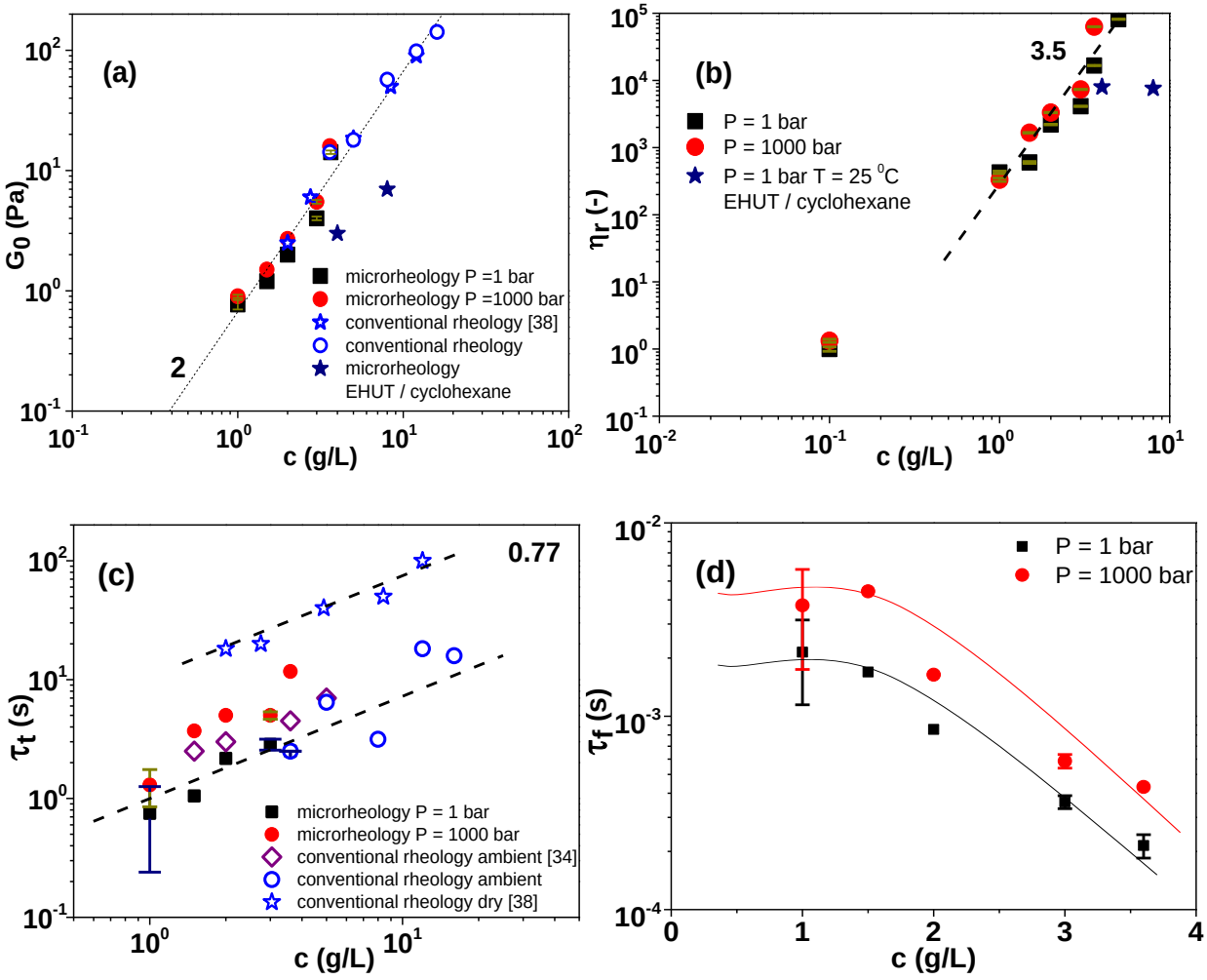


**Figure 6:** (a) Experimental plateau modulus versus concentration at 25 $^0$C. Different data are shown: microrheology at 1 (black squares) and 1000 (red circles) bar, conventional rheology at 1 bar at ambient humidity (open blue circles, and at dry conditions (open blue stars [38]). The line has a slope of 2. (b) Concentration-dependent relative (to solvent) complex viscosity $n^*/n_{solv}$ at 1 (black squares) and 1000 (red spheres) bar. The lines has a slope of 3.5. The open star symbol are microrheological data of EHUT / cyclohexane solution at 1 bar (see text). (c) Respective data of

the terminal relaxation time versus concentration, conventional rheology at 1 bar (filled green stars [38], open purple diamonds [34]). The dashed lines have a slope of 0.77. (d) Fast relaxation time extracted from the high-frequency crossover, as function of concentration at low and high pressure.

The analysis of the LVE spectra reveals the concentration dependence of different material functions, which are presented in Fig.6 for different situations. First, we note in Fig. 6(a) that the value of $G_0$ (extracted at the frequency marking the minimum of G'' [38,39]) is virtually unaffected by pressure and humidity [38]. The power-law dependence $G_0 \sim c^2$ is consistent with theoretical predictions as discussed above [43-45]. Same general remarks hold for the relative complex viscosity data at high concentrations, as seen in Fig. 6(b). The power-law of about 3.5 reflects good solvent conditions. On the other hand, the terminal relaxation time is affected by humidity at ambient pressure but not by pressure, within experimental uncertainty, at ambient humidity, as seen in Fig. 6(c). The latter effect is consistent with the pressure-independence of modulus and zero-shear viscosity, discussed above. It is different from the speed-up of the fast relaxation time with concentration which also becomes slower as the pressure increases (Fig.6d). The latter effect reflects the increase of solvent viscosity with pressure, as already discussed above. Note for completeness, that the effects of humidity were also investigated by DLS-microrheology, confirming the earlier findings [37] (see Fig. 3 in appendix 2).

## B. EHUT IN CYCLOHEXANE: STABILIZATION OF TUBES AT HIGH PRESSURE

We now turn our attention to EHUT solutions is cyclohexane [48]. SANS and IR spectroscopy experiments indicated a structural thickness (tube) transition at $T \approx 50^0$C, P = 1 bar and c = 10 mM. The first task is to investigate the dynamics (Fig. 7a, b) and microrheology (Fig. S7) at atmospheric pressure. As can be seen in Figs.7a and S7, there is a transition from unimodal ISF at high temperatures ($T > 49^0$C) to bimodal ISF at low temperatures ($T \leq 49^0$C). We attribute the presence of second, slow relaxation process to the appearance of self-assembled EHUT tubes, which are known to exhibit strong viscoelasticity accompanied by a plateau modulus [37-39], and use this as a signature of their formation in order to construct a phase diagram, which is depicted in Fig.8. To this end we examine the shape of the ISF of a given EHUT/cyclohexane solution (c=4 g/L) at different temperatures and pressures. For example, at P=325 bars (Fig.7c) we observe a shift of the filament-to-tube transition from ~$50^0$C to $58^0$C, whereas at 600 bars the supramolecular solution

forms only tubes throughout the examined temperature range. Note that for both tubes and filaments, the EHUT solutions were completely transparent without visual hint of phase separation (Fig.7b). More details about the dependence of the average intensity with pressure and temperature can be found in appendix. The interesting finding of Fig.8 is that high pressures (roughly above 300 bar) appear to stabilize further the tubes, which are the only self-assembled structure at this concentration. It is also important to emphasize that the observed filament-tube transitions are reversible and all measurements are performed in equilibrium conditions (very fast kinetics). In general, the effect of pressure can be accounted for by considering a first order transition and invoking the Clapeyron equation:

$$\frac{dP}{dT} = \frac{\Delta H}{T^* \Delta V} \qquad (1)$$

where $T^*$ is the filament-tube transition temperature at reference (atmospheric pressure), $\Delta H$ is the latent heat per molecule associated with the filament-to-tube transition and $\Delta V$ the associated difference in molecular volumes. The experimental results of Fig.8 suggest that increasing the pressure to 300 bars, i.e., $\Delta P \approx 300$ bar, the transition temperature approaches 60ºC, i.e., $\Delta T \approx 10K$. This suggests that $\frac{\Delta H}{\Delta V} \approx 9.7\text{x}10^8$ Pa. Note that $\Delta H$ is about $1.5k_BT$ at 1 bar, and we assume to a first approximation that it has the same dependence on pressure with $\Delta V$. This leads to $\Delta V \approx$ 7.1 Å$^3$/molecule.

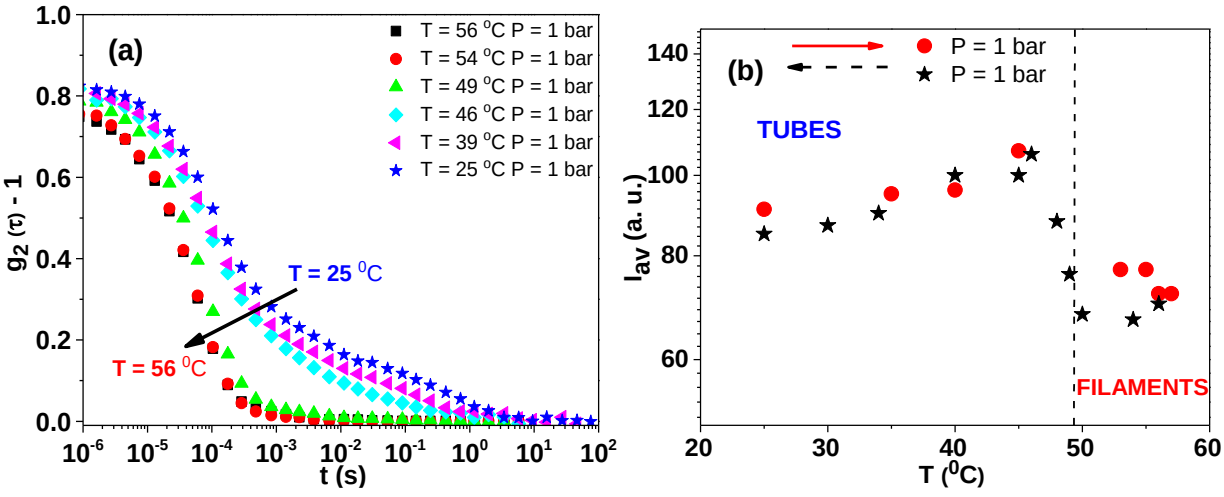

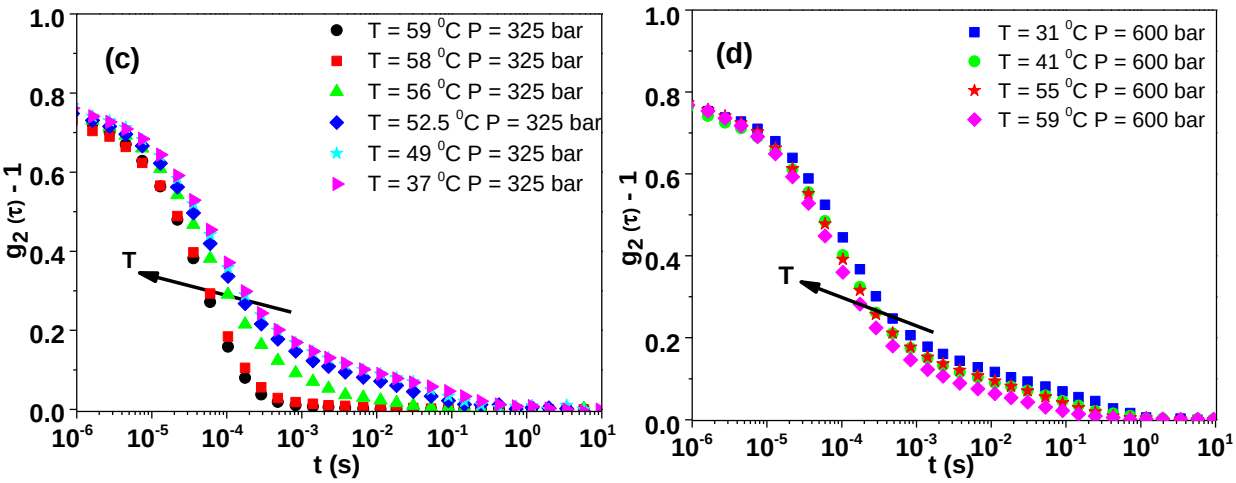


**Figure 7:** ISF of EHUT/cyclohexane solution at 4 g/L. (a) Cooling from 56$^0$C (one process) to 25 $^0$C (slow mode) at 1 bar. (b) corresponding average intensity at 1 bar, red arrow corresponds to heating procedure, black dashed arrow to cooling procedure. (c) ISF for different temperatures upon cooling from 59$^0$C to 37$^o$C at 325 bar (slow mode disappears at high temperatures). (d) Respective data on heating from 31$^0$C to 59$^0$C at 600 bar (slow mode always present).

An important question is whether the stabilization of the tube structure at high pressures reflects a kind of host-guest effect due to more favorable interactions between the tube and the included solvent, or it is a more general phenomenon. Concerning the former situation, we note that solvent interactions inside and outside the tubes have been found to be different [60]. In the latter case, it should occur in other hydrogen bonded assemblies by enhancing bonding at high pressures. This will be investigated in the future.

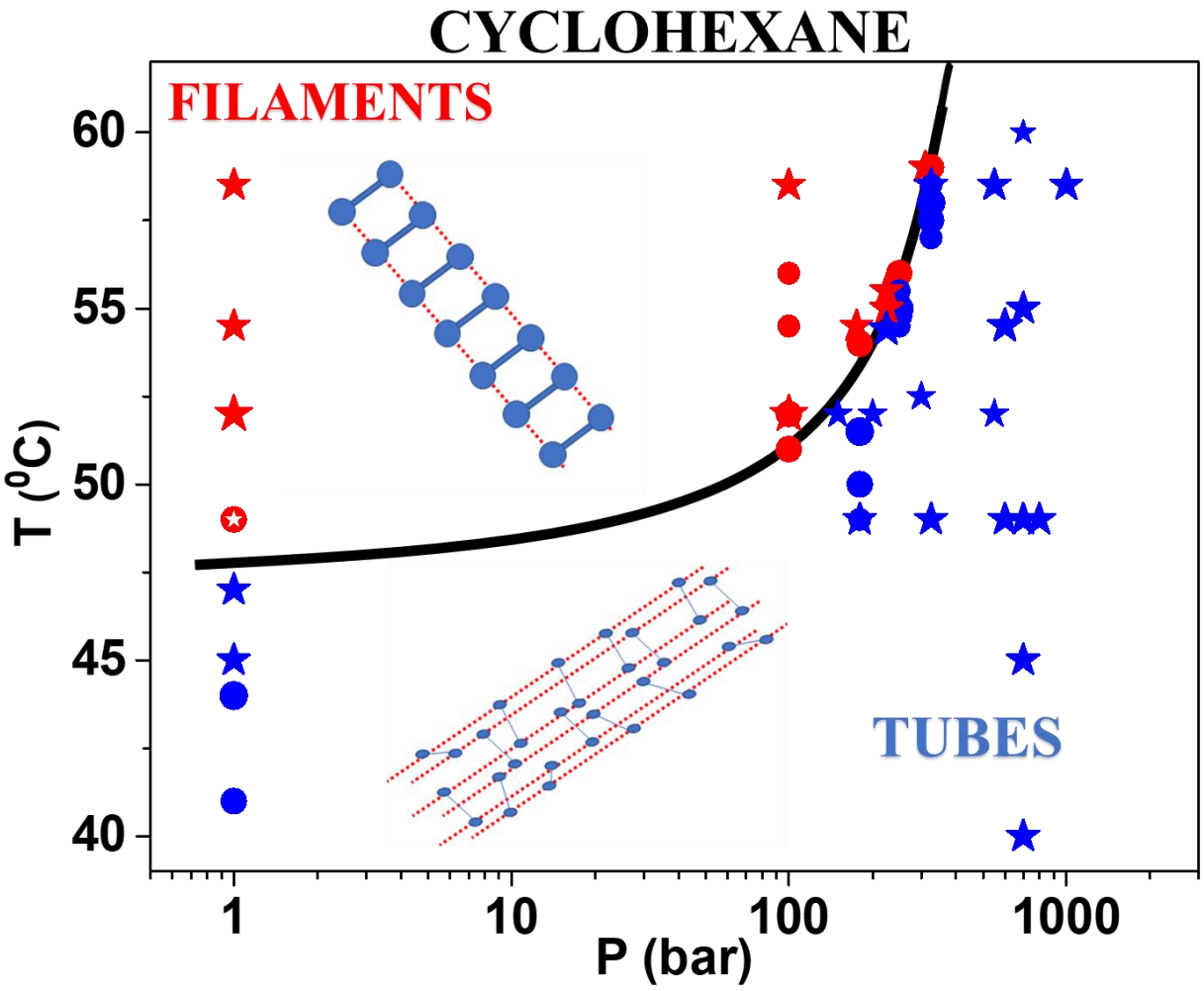


**Figure 8.** Phase diagram of a 4 g/L EHUT / cyclohexane solution in the (T, P) space. Star symbols correspond to microrheological data (with the PMMA particles). Circles correspond to DLS (without added particles). The black line is drawn to guide the eye. Blue color indicates tubes and red filaments.

Fig. 9 summarizes the microrheological results of EHUT/cyclohexane solutions at 4 g/L and different temperatures and pressures. One can follow the evolution of mean square displacement (or associated creep compliance) especially at long times, and its reflection on the LVE spectra, for the same temperature of 49 $^0$C where a transition from filament to tube supramolecular structure takes place at about 180 bar (Fig. 8). Indeed, for the two highest pressures, the data very much resemble those at ambient conditions (1 bar, 25 $^0$C), clearly in the tube regime (Fig. 9a,b). Actually from 600 to 1000 bars the changes in plateau modulus ($G_0$) and terminal relaxation time ($\tau_t$) are

barely discernable (Fig.9 b). On the other hand, at 700 bar the solution forms supramolecular tubes at all temperatures, and this is reflected in the creep compliance and LVE data (Fig.9c,d). In fact, an increase of temperature to 60 $^0$C at constant high pressure (Fig. 9c,d) resulted in a decrease of both the modulus (**$G_0$**) and the terminal relaxation times (**$\tau_t$**) but not in the de stabilization of the tubes.

Figure 10 & 11 contains dynamic and microrheology (PMMA probes addition) data of 8 g/L EHUT/cyclohexane solutions as a function of pressure and temperature. The structure transition found to be unaffected by concentration. The same phase behavior with the 4 g/L solution observed. These results indicate that we have reach a saturation by means of concentration, (see fig. in app. Chapter 2). Questionable remain how pressure can affect this structure in lower concentration closer to binary conditions in dilute regime.

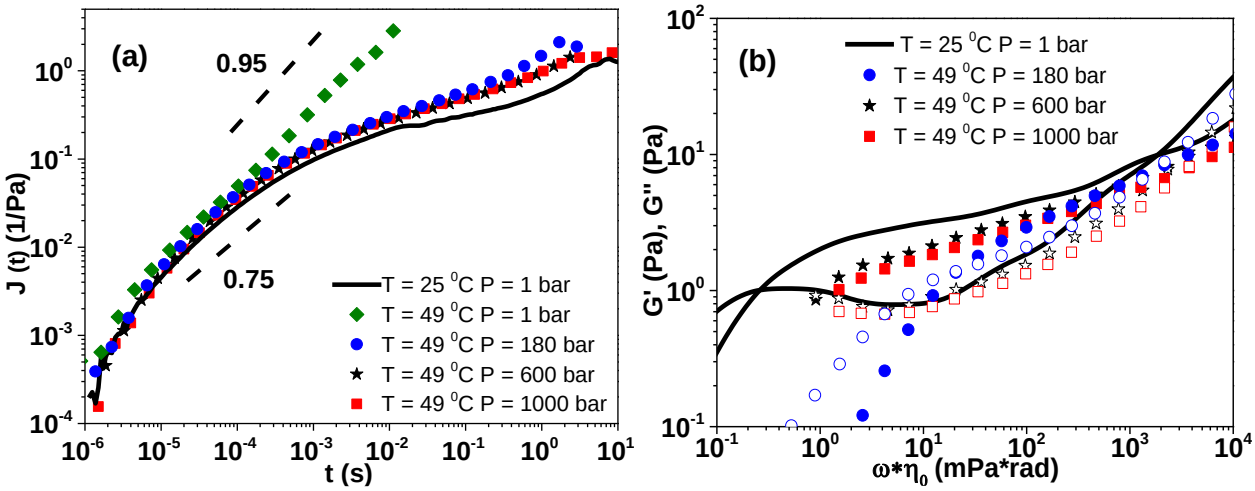

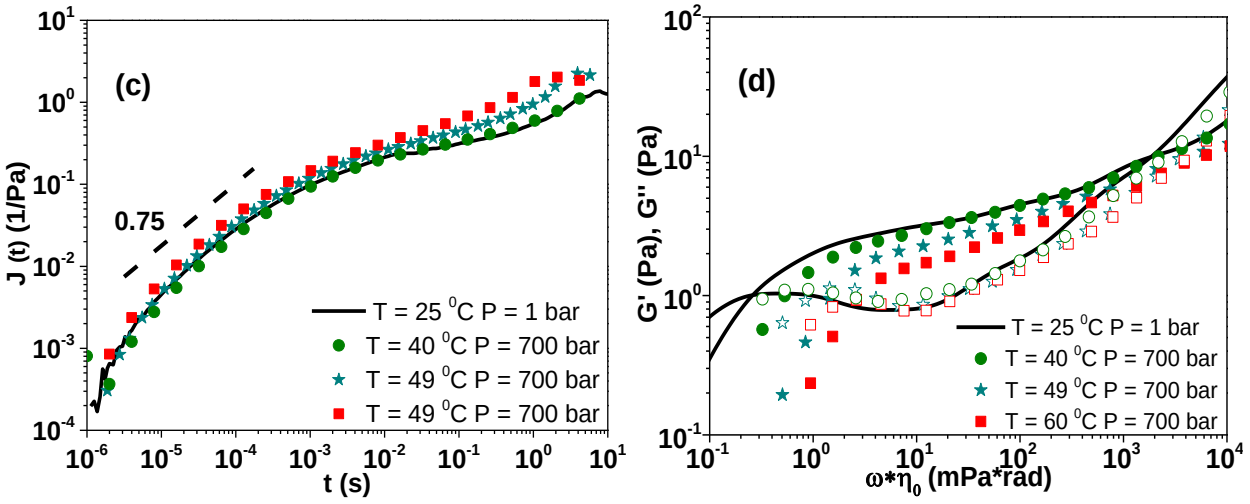


**Figure 9:** (a) Creep compliance of an EHUT/ cyclohexane solution for a specific concentration (c = 4 g/L) and different pressures, for the same temperature of 49$^0$C. Reference data at atmospheric conditions (black line) are also shown, dashed lines have a slope of 0.75 and 0.95, respectively. (b) Respective G', G'' data (49$^0$C) rescaled by solvent viscosity [62-66]. (c) Creep compliance of the same EHUT/ cyclohexane solution at different temperatures for the same pressure of 700 bar. Reference data at atmospheric conditions (black line) are also shown. (d) respective LVE data (700 bar), rescaled by solvent viscosity. Raw data of LVE data (b), (d) in fig. 5 & 7 in app.).

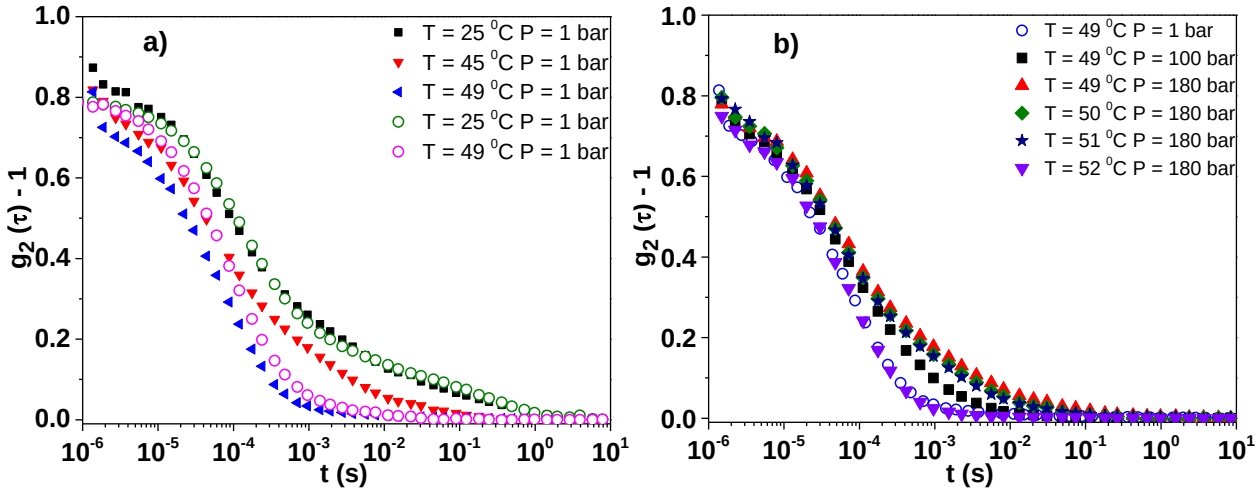


**Figure 10:** ISF of EHUT/cyclohexane solution at 8 g/L. (a) Heating from 25$^0$C (slow mode) to 49 $^0$C (one process) at 1 bar, reference data from a 4 g/L sample (open symbols) are also shown. (b) ISF for different temperatures and pressures (slow mode disappears at 52 $^0$C and 180 bar).

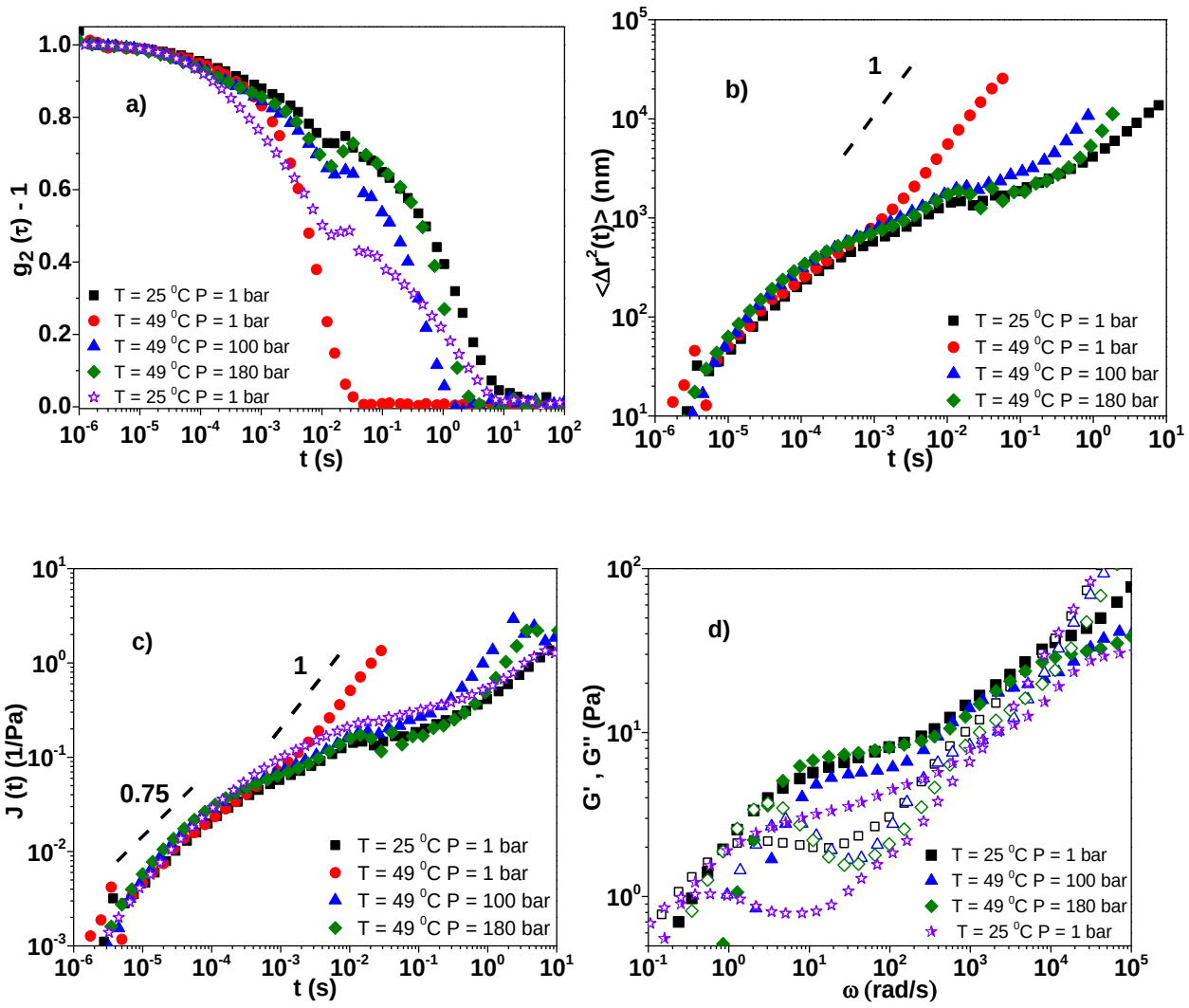


**Fig. 11: (a)** ISF, **(b)** MSD and **(c)** Creep compliance of of an EHUT/ cyclohexane / PMMA solution for a specific concentration (c = 8 g/L) and different pressures, for the same temperature of 49$^0$C. Reference data at atmospheric conditions at 4 (open symbols) and 8 g/L are also shown, dashed lines have a slope of 0.75 and 1, respectively. **(d)** Respective G', G'' data (49$^0$C).

## IV. CONCLUSIONS

High-pressure passive microrheology is emerging as an effective technique for determining the linear viscoelastic properties of a soft materials and represents an important complement to the existing rheometric techniques. In this work we have presented a robust methodology to investigate both the dynamics and linear viscoelasticity of supramolecular living polymers at elevated pressures up to 1000 bars in an appropriate stainless-steel chamber. To this end we employed dynamic light

scattering in the single scattering limit which allows obtaining the intermediate scattering function at different scattering angles (here we used one though), temperatures and pressures. The linear viscoelastic spectrum over a wide range of frequencies was presented for 2,4-bis (2-ethyl-hexyl-ureido) toluene (EHUT) which forms supramolecular living polymers in non-polar solvents. We find that, depending on the solvent's degree of non-polarity, pressure may affect their phase behavior and in particular promote the tube (wormlike micellar) phase. High levels of pressure (in the range 600 to 1000 bars) are found to affect the dynamics much more than the plateau modulus.

## REFRENCES


[1] Xing, Z.; Caciagli, A.; Cao, T.; Stoev, I.; Zupkauskas, M.; O'Neill, T.; Wenzel, T.; Lamboll, R.; Liu, D.; Eiser, E. arXiv preprint arXiv:1712.07956 (2017).

[2] Yasuyuki Kimura, "Microrheology of Soft Matter", J. Phys. Soc. Jpn **78**, 041005-8 (2009).

[3] B. A. Krajina, C. Tropini,, A. Zhu, DiGiacomo, J. L. Sonnenburg, S.C. Heilshorn and A. J. Spakowitz, "Dynamic Light Scattering Microrheology Reveals Multiscale Viscoelasticity of Polymer Gels and Precious Biological Materials," ACS CENTRAL SCIENCE. **3**, (2017).

[4] V. Breedveld, D. J. Pine, "Microrheology as a tool for high-throughput screening," J. Mat. Sci. **38**, 4461-4470, (2003).

[5] B. R. Dasgupta,1 S. Y. Tee, J. C. Crocker, B. J. Frisken, and D. A. Weitz, "Microrheology of polyethylene oxide using diffusing wave spectroscopy and single scattering," P.R.E **65**, 051505 (2002).

[6] Eric. T. Kool, "Hydrogen Bonding, Base Stacking, and steric effects in DNA replication," Annu. Rev. Biophys. Biomol. Struct., **30**, 1-22, (2001).

[7] T. F.A. De Greed & E.W. Meijer, "Supramolecular polymers", Nature, **453**, 8, (2008).

[8] S. Boileau, L. Bouteiller, F. Laupretre & F. Lortie, "Soluble supramolecular polymers based on urea compounds", New J. Chem., **24**, 845-848, (2000).

[9] T. Aida, E. W. Meijer & S.I. Stupp, "Functional Supramolecular Polymers", Science, **335**, (2012).

[10] S. P.W. Wijnands, E. W. Meijer, & Maarten Merk, "DNA-Functionalized Supramolecular Polymers: Dynamic Multicomponent Assemblies with Emergent Properties", Bioconjugate Chem., **30**, 1905–1914, (2019).

[11] T. Kanematsu, T. Sato, Y. Imai, K. Ute, T. Kitayama, "Mutual- and Self-Diffusion Coefficients of a Semiflexible Polymer in Solution", Polymer, **37**, 65, (2005).

[12] M. Adam & M. Delsanti, "Dynamical Properties of Polymer Solutions in Good Solvent by Rayleigh Scattering Experiments", Macromolecules, **10**, 1229, (1977).

[13] T. Cosgrove, J. M. Sutherland, "Self and mutual diffusion measurements in dilute and semi-dilute polystyrene solutions", Polymer, **24**, 534, (1983).

[14] B. W. Brown, P. Zhou, "Solution properties of polyisobutylene investigated by using dynamic and static light scattering and pulsed field gradient NMR", Macromolecules, **24**, 5151, (1991).

[15] C. Le Bon, T. Nicolai, M.E. Kuil, J. G. Hollander, "Self-Diffusion and Cooperative Diffusion of Globular Proteins in Solution", J. Phys. Chem. B, **103**, 10294, (1999).
[16] A.C. Mendes, E.T Baran, R. L. Reis, H.S. Azevedo, "Self-Assembly in Nature: Using the Principles of Nature to Create Complex Nanobiomaterials" Wiley Interdiscip. Rev. Nanomed. Nanobiotechnol., **5**, 582–612, (2013).
[17] Cheng, P.-N.; Pham, J. D.; Nowick, J. S. The Supramolecular Chemistry of β-Sheets. J. Am. Chem. Soc., **135**, 5477–5492, (2013).
[18] Alberts B, Johnson A, Lewis J, Raff M, Roberts K, Walter P. Molecular Biology of the Cell. 5. Garland Press; New York: (2007).

[19] Branden C, Tooze J. Introduction to Protein Structure. 2. Garland Press; New York, (1999).

[20] A.W. Bosman, R.P. Sijbesma, E. W. Meijer, "Supramolecular Polymers at Work." Mater. Today, **7**, 34–39, (2004).
[21] Bas J. G. E. Pieters, Mark B. van Eldijk, R. J. M. Noltea & Jasmin Mecinović, "Natural supramolecular protein assemblies", Chem. Soc. Rev., **45**, 24-39, (2016).

[22] N. C. Seeman, "DNA in a material world", Nature, **421**, 427-431, (2003).

[23] S. M. Douglas, H. Dietz, T. Liedl, B. Hogberg F. Graf, W. M. Shih, "Self-assembly of DNA into nanoscale three-dimensional shapes", Nature, **459**, 414-418, (2009).

[24] Appel, E. A., Biedermann, F., Hoogland, D., del Barrio, J., Driscoll, M. D., Hay, S., Wales, XD. J., and Scherman, O. A., Decoupled Associative and Dissociative Processes in Strong yet Highly Dynamic Host−Guest Complexes, J. Am. Chem. Soc. 139, 12985-12993 (2017).

[25] J. Kohlbrecher, A. Bollhalder, R. Vavrin, G. Meier, Rev. Sci. Instr. **78**, 125101 (2007).
[26] G. Meier, H. Kriegs, Rev. Sci. Instr. **79**, 013102 (2008).
[27] G. Meier, R. Vavrin, J. Kohlbrecher, J. Buitenhuis, M. P. Lettinga, M. Ratajczyk, Mater. Sci. Technol. **19**, 034017 (2008).
[28] K. Dennis, Y. Gao, A. Phathak, P. F. Sullivan, E. M. Furst, J. Rheol. 64, 205-212 (2020).
[29] J. Fernandez-Castanon, S. Bianchi, F. Saglimbeni, R. Di Leonardoab and F. Sciortino, Microrheology of DNA hydrogel gelling and melting on cooling, Soft Matter **14**, 6431-6438 (2018).
[30] Ducouret, G., C. Chassenieux, S. Martins, F. Lequeux, and L. Bouteiller, ''Rheological characterisation of bis-urea based viscoelastic solutions in an apolar solvent,'' Journal of

colloid and interface science **310**, 624-629 (2007).
[31] Lortie, F., S. Boileau, L. Bouteiller, C. Chassenieux, B. Demé, G. Ducouret, M. Jalabert, F. Lauprêtre, and P. Terech, ‘‘Structural and rheological study of a bis-urea based reversible polymer in an apolar solvent,’’ Langmuir **18**, 7218-7222 (2002).
[32] Simic, V., L. Bouteiller, and M. Jalabert, ‘‘Highly cooperative formation of bis-urea based supramolecular polymers,’’ Journal of the American Chemical Society **125**, 13148 13154 (2003).
[33] Bellot, M., and L. Bouteiller, ‘‘Thermodynamic description of bis-urea self-assembly: competition between two supramolecular polymers,’’ Langmuir **24**, 14176-14182 (2008).
[34] Shikata, T., T. Nishida, B. Isare, M. Linares, R. Lazzaroni, and L. Bouteiller, ‘‘Structure and dynamics of a bisurea-based supramolecular polymer in n-dodecane,’’ The Journal of Physical Chemistry B **112**, 8459-8465 (2008).
[35] Sabadini, E., K. R. Francisco, and L. Bouteiller, ‘‘Bis-urea-based supramolecular polymer: The first self-assembled drag reducer for hydrocarbon solvents,’’ Langmuir **26**, 1482-1486 (2009).
[36] Francisco, K. R., C. A. Dreiss, L. Bouteiller, and E. Sabadini, ‘‘Tuning the Viscoelastic Properties of Bis (urea)-Based Supramolecular Polymer Solutions by Adding Cosolutes,’’ Langmuir **28**, 14531-14539 (2012).
[37] Van der Gucht, J., N. Besseling, W. Knoben, L. Bouteiller, and M. C. Stuart, ‘‘Brownian particles in supramolecular polymer solutions,’’ Physical Review E **67**, 051106 (2003).
[38] A. Louhichi, A. R. Jacob, L. Boutteiller, and D. Vlassopoulos, “Humidity affects the viscoelastic properties of supramolecular living polymers”, special issue on Associating polymers, J. Rheol., **61**, 1173-1182 (2017).
[39] Jacob, A. R., A. P. Deshpande, and L. Bouteiller, ‘‘Large amplitude oscillatory shear of supramolecular materials,’’ Journal of Non-Newtonian Fluid Mechanics **206**, 40-56 (2014).
[40] Pinault, T., B. Isare, and L. Bouteiller, ‘‘Solvents with similar bulk properties induce distinct supramolecular architectures,’’ ChemPhysChem **7**, 816-819 (2006).
[41] J. Hendricks, A. Louhichi, V. Merti, R. Fournier, N. Reddy, L. Bouteiller, M. Cloitre, C.Clasen, D. Vlassopoulos, and W. J. Briels, “Non-monotonic stress relaxation after cessation of steady shear flow in supramolecular assemblies,” Phys. Rev. Lett., **123**, 218003 (2019).

[42] M. Hansch, M. Ranfta, A. Dhuwe, R. Enick, “Thickening compressed liquid and supercritical propane with bisurea DMHUT N,N'-(4-methyl-1,3-phenylene)bis[N-(1,5-dimethylhexyl)urea] for enhanced oil recovery or waterless hydraulic fracturing,” J. Supercr. Fluids, **145**, 85-92 (2019).
[43] Cates, M., ‘‘Reptation of living polymers: dynamics of entangled polymers in the presence of reversible chain-scission reactions’’, Macromolecules **20**, 2289-2296 (1987).
[44] Cates, M., and S. Candau, ‘‘Statics and dynamics of worm-like surfactant micelles’’Journal of Physics: Condensed Matter **2**, 6869 (1990).
[45] Cates, M., ‘‘Dynamics of living polymers and flexible surfactant micelles: scaling laws for dilution’’, Journal de Physique **49**, 1593-1600 (1988).
[46] N. J. Van Zee, B. Adelizzi, M. F. J. Mabesoone, X. Meng, A. Aloi, R. H. Zha, M. Lutz, I. A. W. Filot, A. R. A. Palmans and E. W. Meijer, Potential enthalpic energy of water in oils exploited to control supramolecular structure, Nature 558: 100-103 (2018).
[47] Bouteiller, L., Colombani, O., Lortie, F. & Terech, P. “Thickness transition of a rigid supramolecular polymer.” J. Am. Chem. Soc. **127**, 8893–8898 (2005).
[48] Solvents and Solvent Effects in Organic Chemistry, Wiley-VCH Publishers, 3rd ed., N.Y. (2003).
[49] Jacob, A. R., Moghimi, E. & Petekidis, G.” Rheological signatures of aging in hard sphere colloidal glasses.” Phys. Fluids **31**, (2019).
[50] Ferrell, R. T. & Himmelblau, D. M. “Diffusion Coefficients of Nitrogen and Oxygen in Water,” J. Chem. Eng. Data **12**, 111–115 (1967).
[51] E. M. Furst, T. M. Squires, Microrheology, Oxford University Press, NY 2017.
[52] T. G. Mason, “Estimating the viscoelastic moduli of complex fluids using the generalized Stokes-Einstein equation”, Rheol. Acta **39**, 371-378 (2000).
[53] B. G. Alvarenga, M. Raynal, L. Bouteiller, E. Sabadini, “Unexpected Solvent Influence on the Rheology of Supramolecular Polymers,” Macromolecules **50**, 6631-6636 (2017).
[54] Isare, B., Pensec, S., Raynal, M. & Bouteiller, L. “Bisurea-based supramolecular polymers: From structure to properties.” Comptes Rendus Chim. **19**, 148–156 (2016).
[55] N. Willenbacher, C. Oelschlaeger, M. Schopferer, P. Fischer, F. Cardinaux and F. Scheffold, “Broad Bandwidth Optical and Mechanical Rheometry of Wormlike Micelle Solutions” Phys. Rev. Lett. **99**, 068302 (2007).
[56] Th. Athanasiou, G.K. Auernhammer, D. Vlassopoulos and G. Petekidis, “High-frequency

rheometry: validation of the loss angle measuring loop and application to polymer melts and colloidal glasses," Rheol. Acta, **58**, 619-637 (2019).

[57] Schroyen B, Hsu CP, Isa L, Van Puyvelde P, Vermant J., "Stress contributions in colloidal suspensions: the smooth, the rough, and the hairy," Phys Rev Lett **122**, 218001 (2019).

[58] Kirsch, S.; Frenz, V.; Schärtl, W.; Bartsch, E.; Sillescu, H. "Multispeckle Autocorrelation Spectroscopy and Its Application to the Investigation of Ultraslow Dynamical Processes", J. Chem. Phys. **104**, 1758−1761 (1996).

[59] Duri, A.; Bissig, H.; Trappe, V.; Cipelletti, L., "Time-Resolved-Correlation Measurements of Temporally Heterogeneous Dynamics", Phys. Rev. E, **72**, 51401 (2005).

[60] Bouteiller, L., van der Schoot, P., "Probing Weak Intermolecular Interactions in Self-Assembled Nanotubes." J. Am. Chem. Soc. **134**, 1363–1366 (2012).

[61] F.C. MacKintosh, J. Kas, P.A. Janney, "Elasticity of Semiflexible Biopolymer Networks", Phys. Rev. Lett. **75,** 2444254, (1995).

[62] D.R. Caudwell, Martin Trusler, William A. Wakeham, "The Viscosity and Density of n-Dodecane and n-Octadecane at Pressures up to 200 MPa and Temperatures up to 473 K", Int. J. Thermophys., **25**, 1339-1352, (2004).

[63] Zhaohui Liu, J.P. Martin Trusler, Qincheng Bi, "Viscosities of Liquid Cyclohexane and Decane at Temperatures between (303 and 598) K and Pressures up to 4 MPa Measured in Dual-Capillary Viscometer", J. Chem. Eng. Data, (2015).

[64] Wout Knoben, Nicolaas A.M. Besseling, Martien A. Cohen Stuart, "Chain Stoppers in Reversible Supramolecular Polymer Solutions Studied by Static and Dynamic Light Scattering and Osmometry", Macromolecules, **39**, 2643-2653, (2006).

[65] Miguel A. Hernandez-Galvan, Fernando Garcia-Sanchez, Blanca E. Garcia-Flores, and Javier Castro-Arellano, "Liquid Viscosities of Cyclohexane, Cyclohexane + Tetradecane, and Cyclohexane + Benzene from (313 to 393) K and Pressures Up to 60 MPa", J. Chem. Eng. Data, 54, 2831–2838, (2009).

[66] Y. Tanaka, H. Hosokawa, H. Kubota and T. Makita, "Viscosity and Density of Binary Mixtures of Cyclohexane with n-Octane, n-Dodecane, and n-Hexadecane Under High Pressures", Int. Jou. of Thermophysics, 12, 2, (1991).

[67] A.E. Marras, L. Zhou, H.J. Su, C.E. Castro, "Programmable motion of DNA origami mechanics", PNAS, 1-6, (2014).

[68] R. Merindol, S. Loescher & A. Walther, “Pathway-controlled formation of mesostructured all-DNA colloids and superstructures”, Nature nanotechnology, (2018).

[69] H. Dietz, “Folding DNA into Twisted and Curved Nanoscale Shapes”, Science, **325**, 725, (2009).

# ***Chapter 3: Pressure and temperature effect in Solvent selectivity of three-arm diblock star polymer solutions.***

## 3.1 Introduction

We study a three-arm diblock star copolymer in two different selective solvents. They recently have been proposed as a system to realize soft patchy colloids, that would show distinct phase diagram [20-25, 43,44]. Recently, investigations show that we are in the right direction [48]. To achieve this, requires on the one block to be sticky (attractive interaction between the outside blocks) and no strong interaction between the inside locks. It was proposed the use of solvent that is good for the inner block and close to theta for the outer block. Temperature could then be used to tune the interaction through the solvent quality. A recent study has shown the effect of changing solvent selectivity on a Telechelic star polymer using temperature [19]. We are interested here in the effect of high hydrostatic pressure (complementary to T) on the phase diagram of the 3-arm diblock stars. Pressure as a thermodynamic variable would provide a way to tune the intramolecular & intermolecular interactions, through altering the solvent quality/selectivity? (Selectivity refers to the difference of solvent quality between the solvent and the two blocks). This is often embedding $\chi$ parameter in polymer. It represents a mean field approach to the mostly van der walls interaction between the different components [41-42].

Block copolymer have been intensively researched. This is motivated by their remarkable phase diagrams and the ability of synthetic chemistry. Research efforts have included bulk and solutions, including varying solvent quality [1,2]. The discovery of the living character of anionic polymerization offer synthetic polymers with complex architectures. Several studies have looked into the specifics of triblocks in selective solvents. The case of a good solvent for the middle block and bad (or not so good for the outer blocks) has been studied in the context of loop-to-bridge ratio and the existence of gelled phases [3-11, 48]. Formation of spherical micelles were observed (this is an outstanding property of copolymers). The magnitude of these micelles depends on the molecular weight and the fraction of the respective blocks but no so much from polymer concentration (fig 1b), [12-15]. There is a critical micelle concentration, known as CMC. The micellization of such systems are predicted by theoretical models. They were referred that owing to their amphiphilic character of star-blocked copolymers, the formatted micelles may not

participate in dynamic equilibrium. As solvent selectivity increase (temperature decrease) a transition from loose aggregates to flowers observed [13]. Similar behavior for an ABA triblock in heptane, (nonsolvent for the A block, selective for B) are mentioned in [6,18]. A single exponential ISF and micelle (flower-like) formation in dilute regime observed. Increasing the concentration of polymer two extra modes were appearanced. The last mode corresponds to slow rearrangement of the physical micellar network, the intermediate one is connected with the onset of viscoelasticity (fig. 1a).

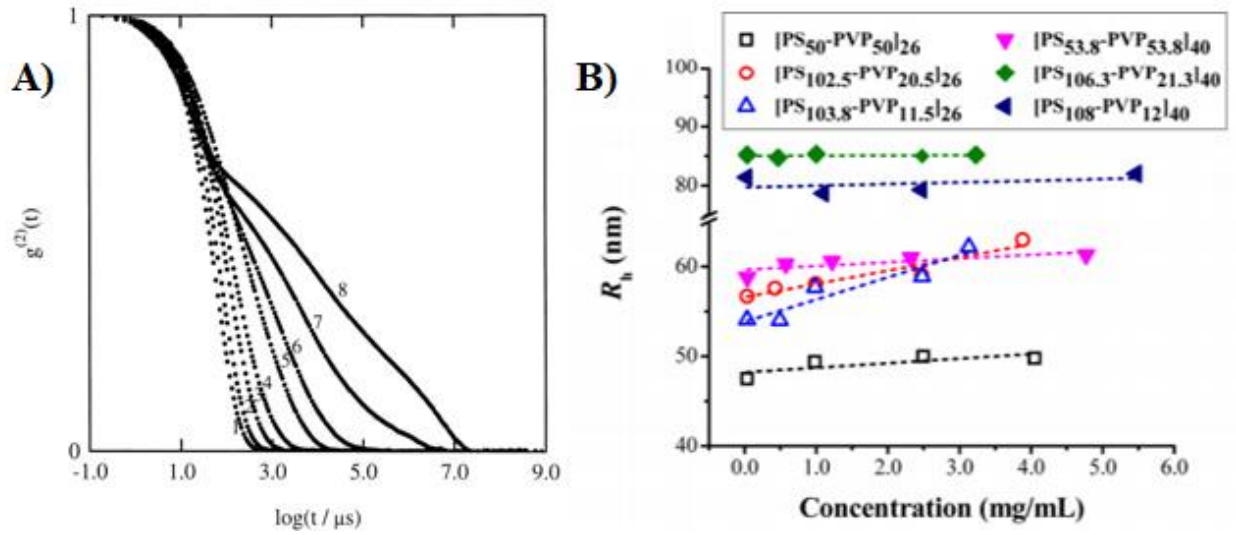


**Figure 1: a)** ISF of triblock copolymer (PS-PEB-PS)/ n-heptane solution. The numbers correspond to different polymer concentrations in wt. % (from 0.49 to 6.9%). **b)** Apparent hydrodynamic radius ($R_H$) versus concentration for 26- and 40-arm stars (PS - PVP) in toluene (bad for PVP, selective for polystyrene) [18,48].

The effect of pressure on solvent quality: due to non-zero compressibility, pressure increase leads to some difference in interaction between polymer and solvent, even in the simple case of van der walls type of interactions. For a thermodynamic description of the case of block copolymer solutions, the compressibilities of the three different components (polymer A, polymer B, solvent) will have to be considered. Already in binary systems, pressure can have settle effects. Even more effects could be expected in block copolymer solvent selectivity [41-42].

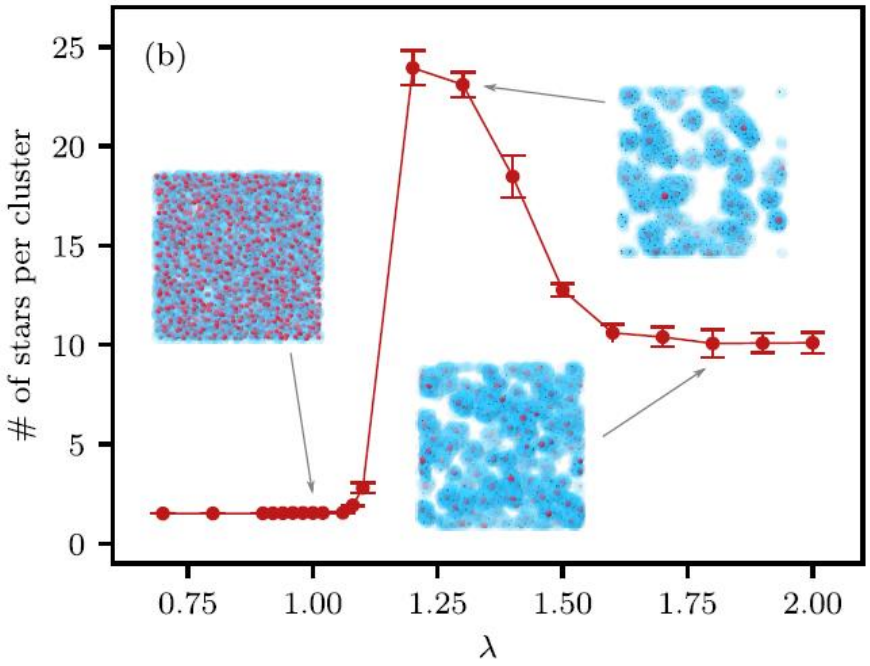


**Figure 2:** Average aggregate size as a function of λ (inverse temperature) extracted from simulations of the coarse-grained blob model. **Insets**: representative configurations of TSPs for indicated λ with the gray arrows (attractive blobs, red; repulsive blobs, light blue; star centers, black). Results correspond to c = 0.11c*. Depicted from [19].

As far as the effect of pressure is concerned, there are plenty of studies in linear polymers, as well as in the phase behavior of more decent systems. However, the pressure effect in materials with more complex structures is under investigation and the studies are limited even know. Most of the studies in the properties of block copolymers emphasize in the effect of pressure in melt conditions and not so much in solutions [35-42]. Jaan Roots and Bo Nyström through DLS experiments were studied PS (Mw = 111000 g/mol) / toluene solutions in dilute and semi-dilute regime and were reported that the value of the hydrodynamic radius was obtained by the diffusion coefficient (D) and it was found to be independent by pressure. Any difference in the value it was in the limit of experimental error [26]. Corey L.Moses and W.A. Van Hook were studied the dependence of pressure by $A_2$ in dilute polystyrene /cyclohexane solutions. In addition, were found a clear dependence between the ($dA_2/dP$) with the Mw. At low molecular weight (25 Kg/mol) from a positive $A_2$ at 41 $^0$C, 1 bar extract negative ($dA_2/dP$). In contrast, for higher Mw (400, 900 Kg/mol) at 29 $^0$C from a negative $A_2$ value extract positive ($dA_2/dP$) [27]. Kenji Kubota et al. was studied the pressure effect in $A_2$ as well the radius of gyration of PDMS/cyclohexyl-bromide in dilute

regime and was found a clear dependence by pressure, where increase of pressure was followed by decrease of $\chi$ parameter, (decrease of theta point by ~3 $^0$C/ 400 Kg/cm$^2$) [28]. Through cloud point measurements H. Hosokawa et. al. was reported to a non – monotonic behavior of critical solution temperature by pressure for a series of concentrations for a polystyrene / methylcyclohexane solution [29], where W.A. Van Hook and co – workers were argued the complicated pressure, molecular weight dependence in polystyrene cyclohexane solutions in semi-dilute regime [30]. In dilute and semi-dilute regime K. Erdogan was reported the density variation both in low (50 Kg/mol) as well as in high molecular weight polystyrene /methylcyclohexane solutions [31].

On the effect of pressure in the micellization of block copolymers solutions, D. A. Ylitalo and C.W. Frank were reported the increase of the CMC (always positive $\Delta V_{mix}$) with pressure for two low molecular weight PS-PEP samples in selective solvent (n -heptane) [32]. Micellar solutions of PS-b-PI & PS-b-PB in supercritical propane were found to exhibit significantly lower cloud pressures than the corresponding nonmicellar solutions (linear homopolymers) which is an indication that the polymer solubility is enhancement due to micelle formation [50]. It's not provocative someone to say that pressure was found to leads in decrease of $\chi$ parameter (increase of polymer solubility) in general. In our study, an opposite effect by pressure between the 3-arm diblock star solutions and the respective linear polymers were observed, (fig. 9). For a better characterization and the understanding of the phase behavior of this specific sample more experiments were needed. The construction of an analytic phase diagram with binodal and spinodal curves (vs T, P, c) is out of the limit of this work. In the frame of this thesis, our interest is around the pressure effect on block copolymers and how the Flory-Huggins ($\chi$) parameter can change [45-47]. Polymers itself are really complex materials (macromolecules). Even know, isn't clear why application of pressure in polymer solutions should lead in better solvent conditions or in worst. Thermodynamics can give an answer (owing to changes in volume of mixing) but literature studies they don't give a clear answer. From my point of view, the result of the application of pressure connected strongly and is a combination of the molecular weight, glass transition (Tg), fraction of the composites, as well as the chemistry of the specific polymer.

## 3.2 Results and discussion

### 3.2.1 Dilute regime: Pressure stabilizes loose aggregates (clusters) in Telechelic star polymer solutions

We studied the effect of pressure and temperature in 3-arm diblock star solutions as well as in the respective linear polymers in selective solvents. We use DLS to measure hydrodynamic radius of the aggregates over a range of pressures. Two different regimes were identified. At low pressure (1 bar) increase of temperature lead to increase of $R_H$ of the clusters and eventually a total dissolution at 60 $^0$C. At high pressure (1kbar) the $R_H$ is independent by temperature (fig. 9 b) and dissolution take place at 55$^0$C. This behavior is discussed in terms of evolution of solvent selectivity and interaction parameter with temperature and pressure [7]. In linear polymers (PS (126 Kg/mol), PB) increase of pressure (at constant temperature) was found to lead to macro - phase separation of samples as depicted in figure 3 & 4. In the case of diblock stars, increase of pressure leads to dissolution (as a consequence of better solvent condition) and stabilization of the loose aggregate (cluster).

**A. DLS of linear polymers solutions under pressure**

Wu use DLS at 90$^o$ to evaluate the phase and possibly the evolution of solvent quality. $R_H$(P) and I 90$^o$(P). In the "good" solvent regime, correlation function shows a single decay that is interpreted as diffusion of single chains, providing a measure of $R_H$ = 10.6 nm. As the solvent quality decreases, larger intensities are measured, and the IACF becomes more complex, as a slow mode appears, signs of strong slower fluctuation. The correlation functions measured for PB and PS in phenyldodecane in different P and T are shown in figure 3 & 4. They allow to establish the pressure and temperature dependence of the onset of phase separation as depicted in Fig 11. We found that increasing pressure lead to an increase of critical temperature in polybutadiene and polystyrene solutions. Well in the one phase regime (single mode decay) we found $R_H$ to decrease with increasing pressure, which we attribute to a decrease of solvent quality.

We first report the case of solutions of pure polymers (polystyrene & polybutadiene) in the selected solvent (phenyldodecane). We did measurements in dilute regime (c = c*/12) where at ambient

pressure $T_\Theta \sim 51, 21^0$C, for PS and PB respectively). At high temperature, single exponential IAF were observed and the average intensity is as expected from the single chains scattering. We observe that increased pressure leads to a reduction of $R_H$ by up to ~20% by increase of pressure to 1 kbar, from Rh=10.44 nm (T = $60^0$ C, P = 1 bar) to 8.6 nm (T = $60^0$ C, P = 1 kbar) (fig. 8). At lower temperatures presence of a second mode was observed in IACF. At lower T, stronger intensity was measured and IACF was a single slow mode. We took this as the onset of phase separation. The phase separation lines are reported for PS and PB in fig 11. Similar behavior was observed in PB solutions with however lower theta temperature (fig. 4).

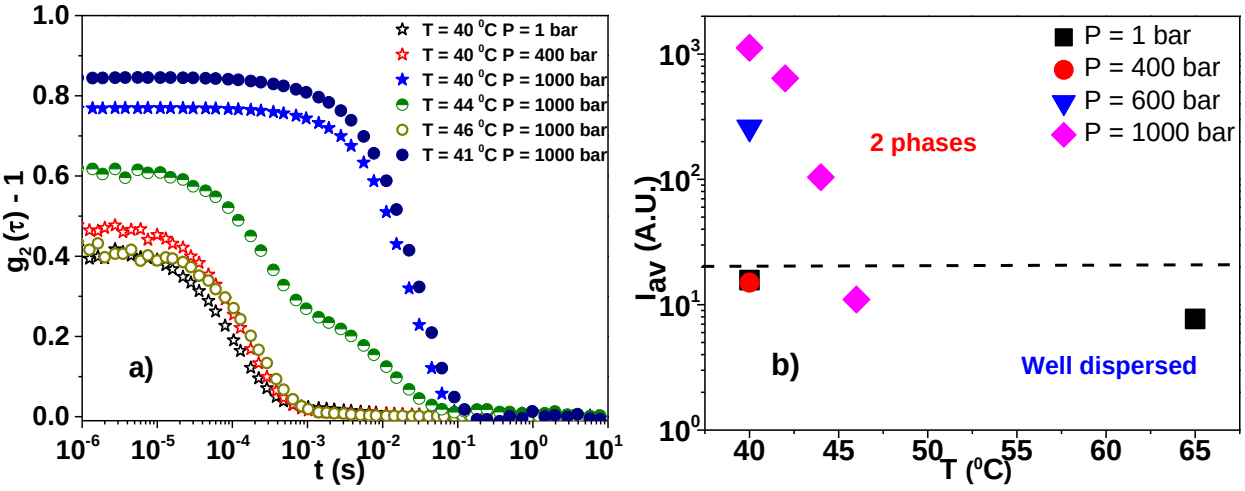


**Figure 3: a)** ISF of Linear Polystyrene / Phenyl-dodecane solutions. stars correspond to pressures from 1 → 1000 bar at constant Temperature (40 $^0$C). circles correspond to constant Pressure at 1000 bar, for Temperature jumps at 40 → 46 → 41 $^0$C. **b**) Average Scattering intensity as a function of Temperature. The results show a reversible transition by temperature at 1 kbar (magenta symbol).

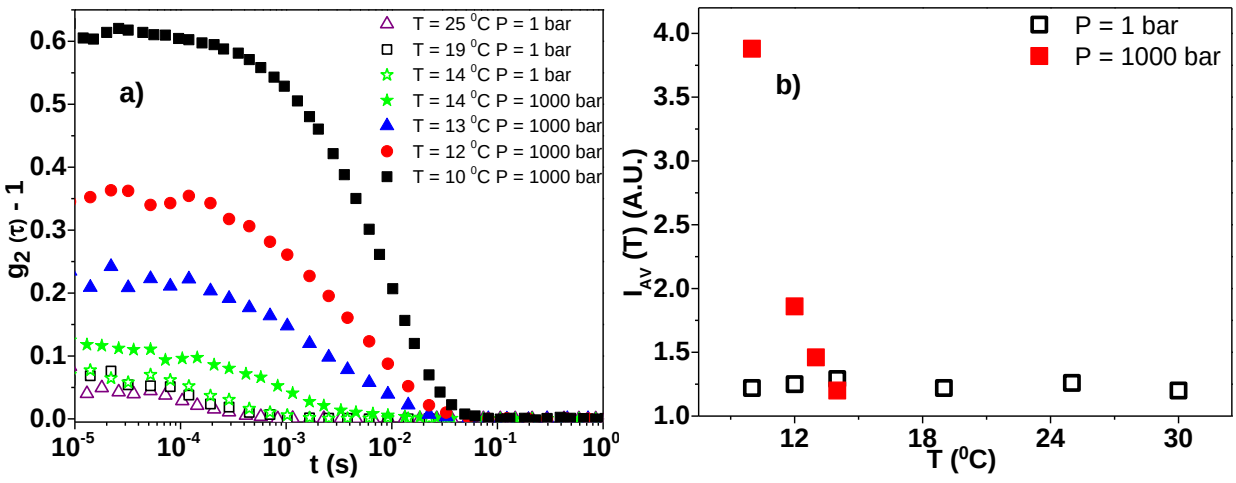


**Figure 4: a)** ISF of dilute Linear Polybutadiene / Phenyl-dodecane solutions at different temperatures and pressures **b)** Average intensity versus temperatures at 1 (open symbols) and 1000 bar (filled symbols).

### B. DLS of 3-arm diblock star solutions under high-hydrostatic pressure

We use dynamic light scattering to characterize the evolution of 3-arm diblock star solutions with temperature and pressure. Two systems with varying fraction block lengths and similar overall molecular weight were investigated. The intensity autocorrelation functions characterized with a two-step decay (fig 5a). We attribute the fast mode to single diblock star diffusion motion. The second mode attributed to the formation of cluster as a result of the sticky ends (outer blocks). The effect of pressure studies were limited in the dynamic properties (hydrodynamic radius and average intensity) though to the only 3 available scattering angles in the HP cell.

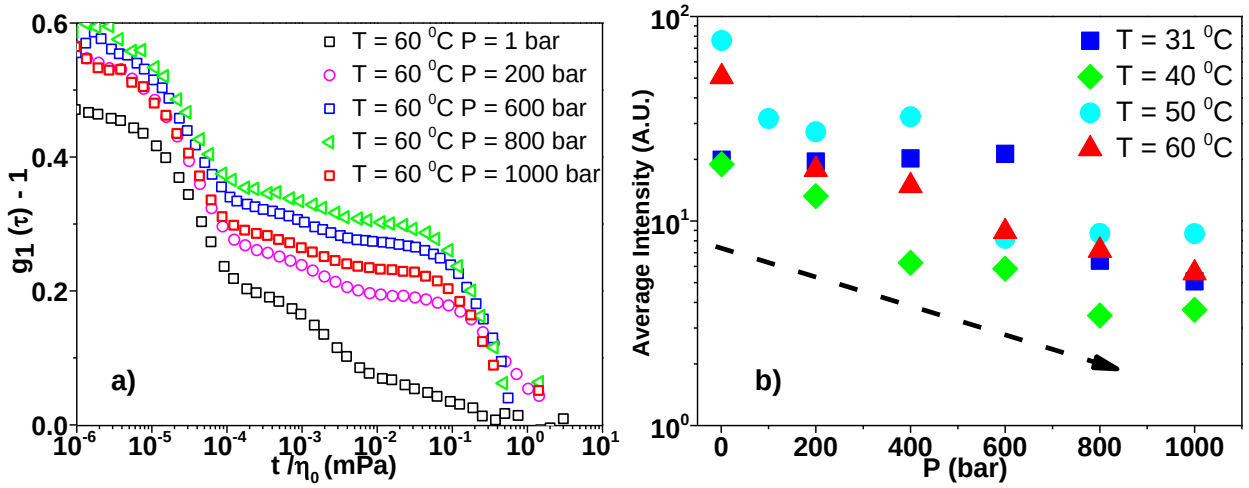


**Figure 5: a)** Field correlation function of Sample A/ phenyldodecane solutions at constant temperature (T = 60 $^0$C) for different pressures, (1→ 1000 kbar). **b)** Average scattering intensity for different Temperatures, Pressures.

The pressure effect in FAF for the two different samples illustrated in fig 5 & 6. The FAF showed a two-step decay as already mentioned. The data are rescaled by solvent viscosity. The average intensity decreases by increase of pressure (fig.6b). The presence of the third relaxation time (fig 5a) is possibly an artifact. During the measurements no spikes or inhomogeneities or sharp changes observed in the average intensity. The big difference in the scattering intensities between figure 5b & 10 are owing to change of the photo counter.

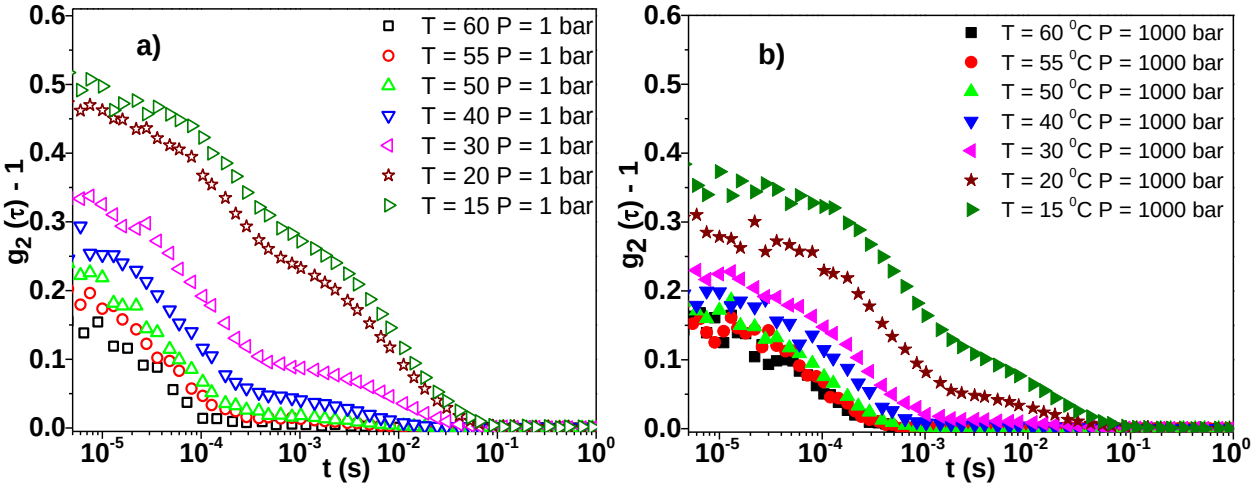


**Figure 6:** ISF of Sample B for different temperatures at **a**) 1 bar **b)** 1000 bar.

Increase of pressure was found to lead to the dissolution of the cluster (red curve, fig 7b) at high temperatures and to decrease of the hydrodynamic radius of the cluster in lower temperatures (50

to 15 $^{0}$C) (fig.6b). For pressures higher than 600 bar the hydrodynamic radius was found to be independent of temperature. We still have cluster at lower temperature but possibly under high hydrostatic pressure there is no dynamic exchange of associating blocks. For a sample with higher fraction of polystyrene, a similar effect of pressure in the hydrodynamic radius of the cluster was observed.

The second general observation is that compare with the temperature where cooling lead to decrease of cluster magnitude (fig. 9) and increase of the $R_H$ of the single star (fig. 8), increase of pressure followed by cluster i) dissolution close to binary conditions – high temperatures ii) decrease/stabilization of the magnitude of this loose aggregate (cluster) iii) decrease of the hydrodynamic radius of the single star. In addition, decrease in the scattering intensity observed. Furthermore, increase of pressure find to lead in drop of the scattering intensity originated from the second mode in the IAF (fig. 10 b). The last achieved by analyzing the data through inverse Laplace transform (Contin) analysis whereas, the intensity of the fast relaxation process remains constant with temperature and pressure (fig. 10a). An indication that the fast process corresponds truly in 'single' star. This doesn't happen in the case of TSP/heptane solutions. Heptane is non-solvent for polystyrene and thermodynamic good for polybutadiene. From dynamic data we observe a single exponential function (indication for monodisperse micelle formation). In this case the intensity of the fast mode varies with the temperature because the fast mode corresponds to the micelle, not in single star (see in app. Chapter 3). The hydrodynamic radius of the micelle increases with decrease of the temperature as a consequence of the aggregation number increase owing to change in solvent selectivity (fig. 8 b).

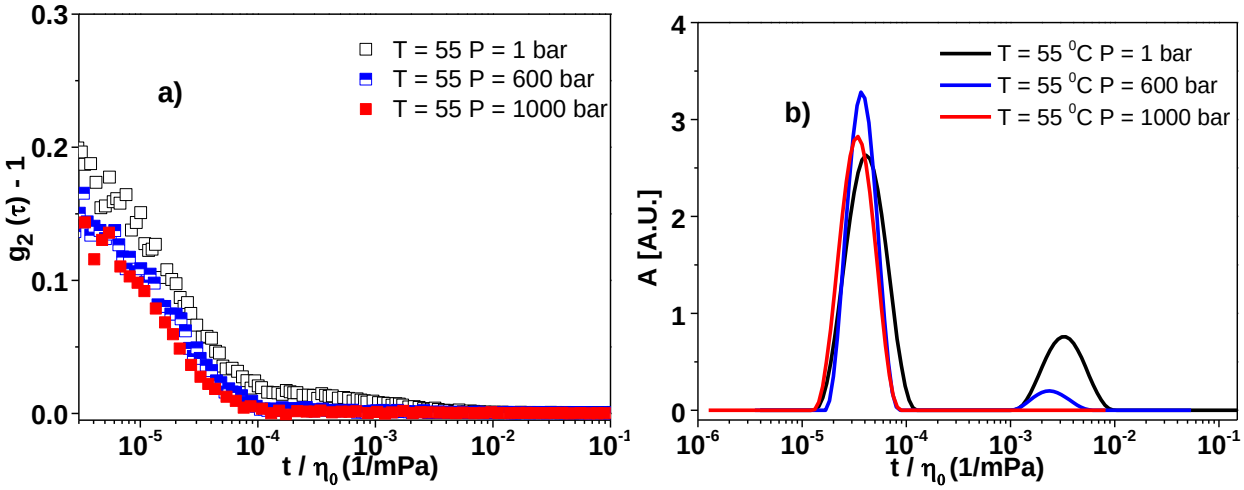

**Figure 7: a)** ISF of Sample B for different pressures at T = 55 $^0$C. **b)** Distribution functions of relaxation times through Contin analysis. The data are rescaled by solvent viscosity.

The aggregation number of the micelle is estimated to be around 10 based on the differences in the scattering intensity. This is in good agreement with the measured Rh and the corresponding hydrodynamic volume, $V_H = (4\pi/3)R_H^3$. $V_H$ of micelle ~10 $V_H$ single chain)

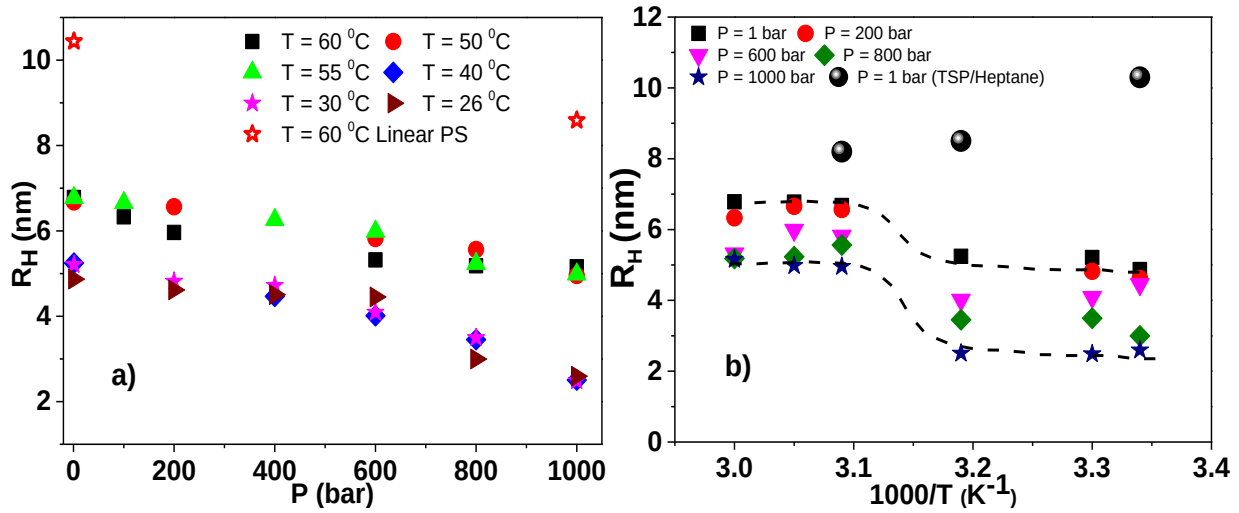


**Figure 8**: Hydrodynamic radius ($R_H$) of 'single star' of sample A as a function of **a)** pressure for different temperatures **b)** inverse temperature for different pressures. Black spheres correspond to Sample B/ heptane solution (micelle formation).

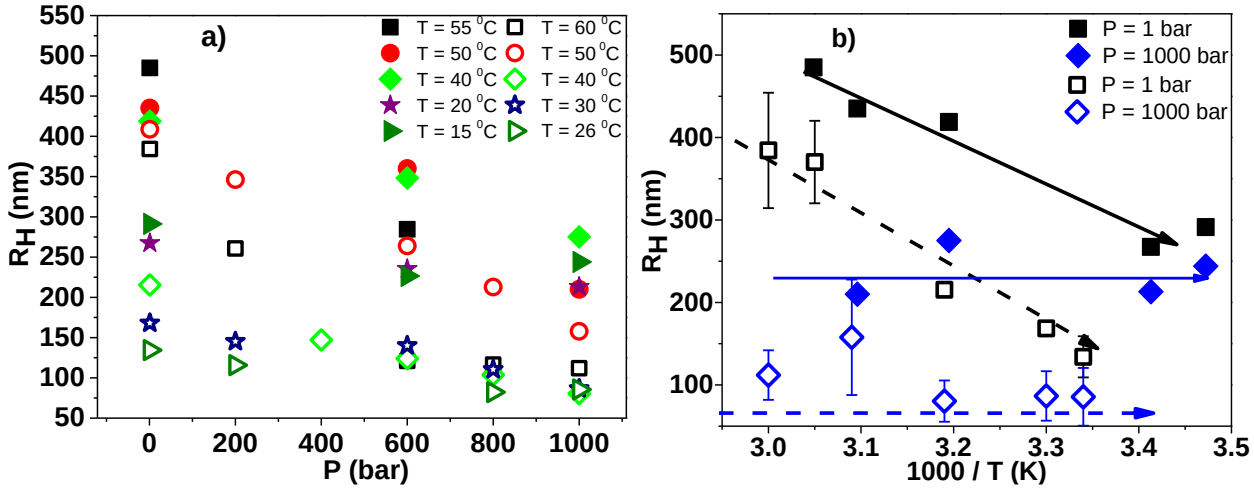


**Figure 9:** Rh of clusters as a function of **a)** pressure for different temperatures. **b)** inverse temperature for different pressures. Open symbols correspond to Sample A, filled symbols to Sample B.

The effect of pressure and temperature in diffusion coefficient observed to be negligible both in 'single star' and in formatted clusters (see in app. Chapter 3). The hydrodynamic radius extracted from dynamic light scattering experiments in dilute solutions through the Stokes- Einstein-Sutherland relation. We expect because we are in dilute regime the main friction which play a role to be from the solvent viscosity, so we use the solvent viscosity in the SES equation. Consequently, the main effect on the magnitude of the hydrodynamic radius is owing to changes in solvent viscosity (P, T).

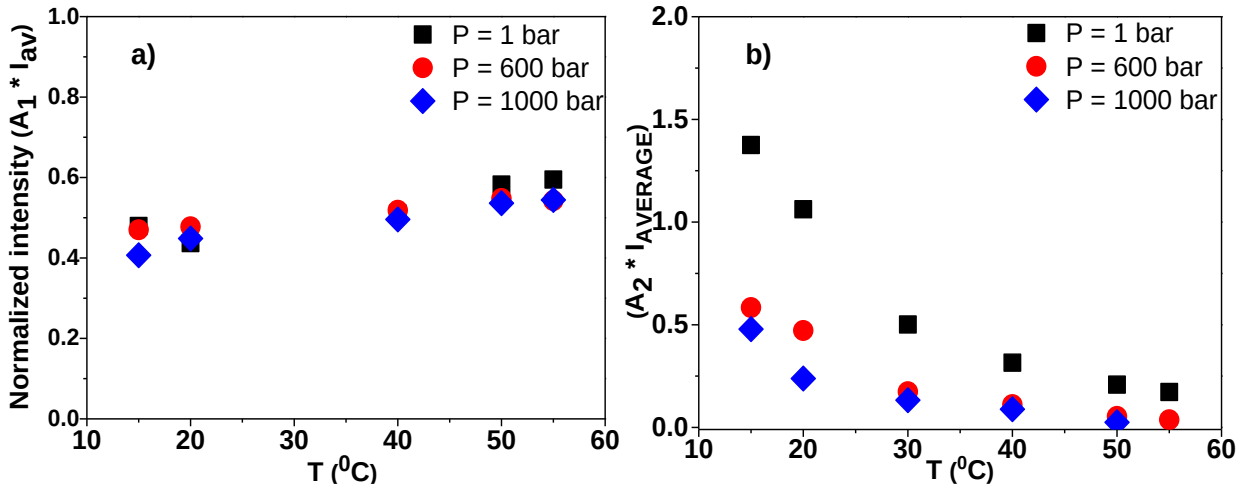


**Fig. 10:** Normalized intensity multiply by amplitude of the respective mode in Sample B, **a)** Single star (I1 * A1) **b)** cluster (I2 * A2).

A general illustration and a phase diagram in pressure and temperature space for dilute samples are in table 1 & fig. 11. Interesting is the fact that an opposite effect by application of pressure observed between the linear and the 3-arm diblock star polymer solutions.

**Table 1: General overview**

| **Parameter** | **$R_H$ single star** | **Intensity single star** | **$R_H$ cluster** | **Intensity cluster** |
|---|---|---|---|---|
| *Temperature (increase)* | *Increase* | *Constant* | *Decrease* | *Decrease* |
| *Pressure (increase)* | *Decrease* | *Constant* | *Decrease* | *Decrease* |

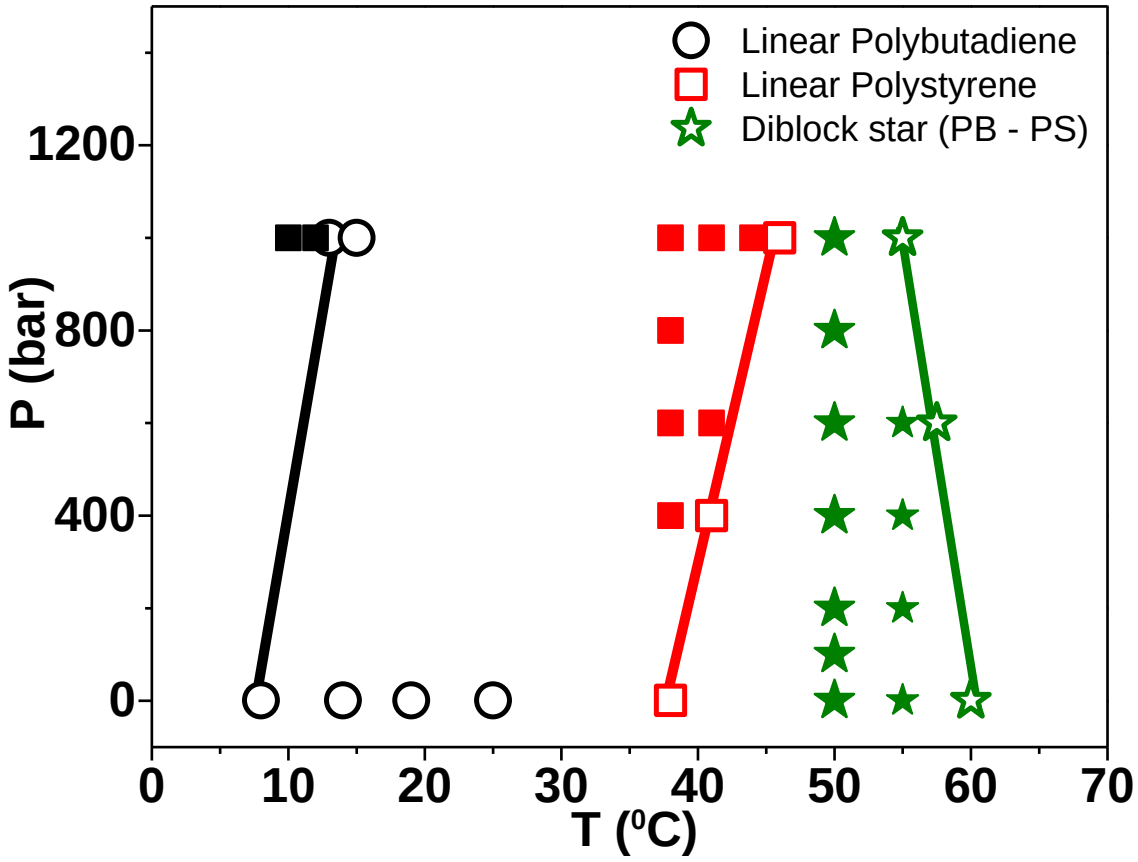


**Fig. 11:** Phase diagram in P-T space of linear (squares, circles) and star (star symbols) polymer solutions in phenyldodecane in dilute regime. Open symbols correspond to single phase, closed to phase separation.

**C. Microrheology of three-arm diblock star in Cyclohexane: An alternative? case**

We would like to know of the consequences of the attraction and formation of cluster on the rheological properties of the solutions especially at higher concentration, in particular to check for the possible formation of percolated structure that should form weak gels, the effect of pressure on the rheological properties. We attempt to do microrheology. This is difficult to do in samples dissolved in phenyldodecane that almost index match the PMMA probe particles (see materials and methods). We moved to solutions in cyclohexane owing to retrieve the PMMA probes MSD from the IAF. Microrheology was found to be feasible in this case. Cyclohexane solutions were found to

have comparable dynamic behavior with the phenyldodecane in intermediate and semi-dilute regime.The data in dilute regime fill the gap and was improved DLS data.

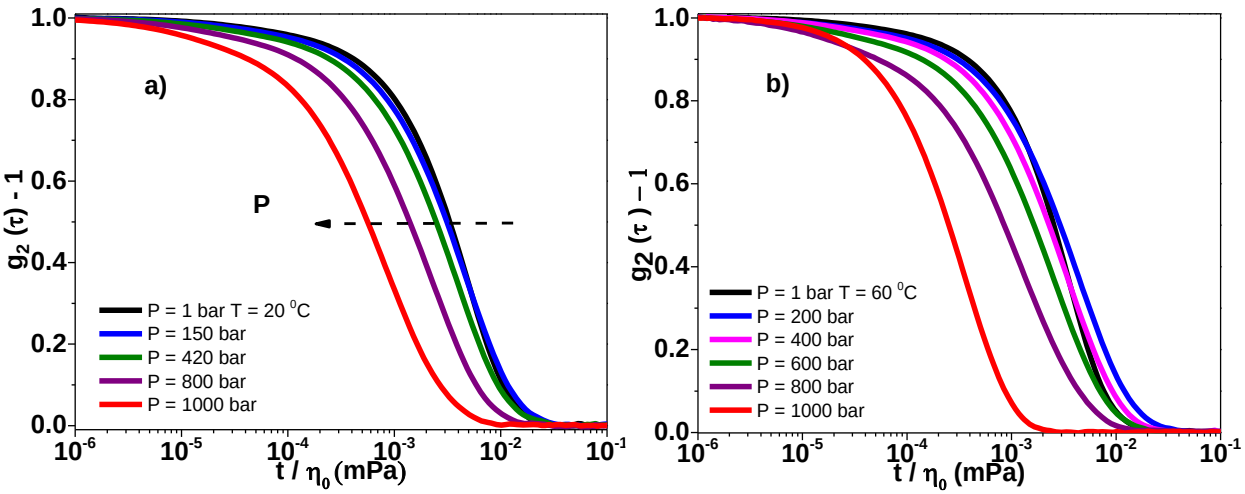


**Figure 12:** ISF of Sample A / cyclohexane / PMMA probes in **(a)** 20 and **(b)** 60$^0$C, at different pressures. The data are shifted by solvent viscosity. c = 0.6 c*.

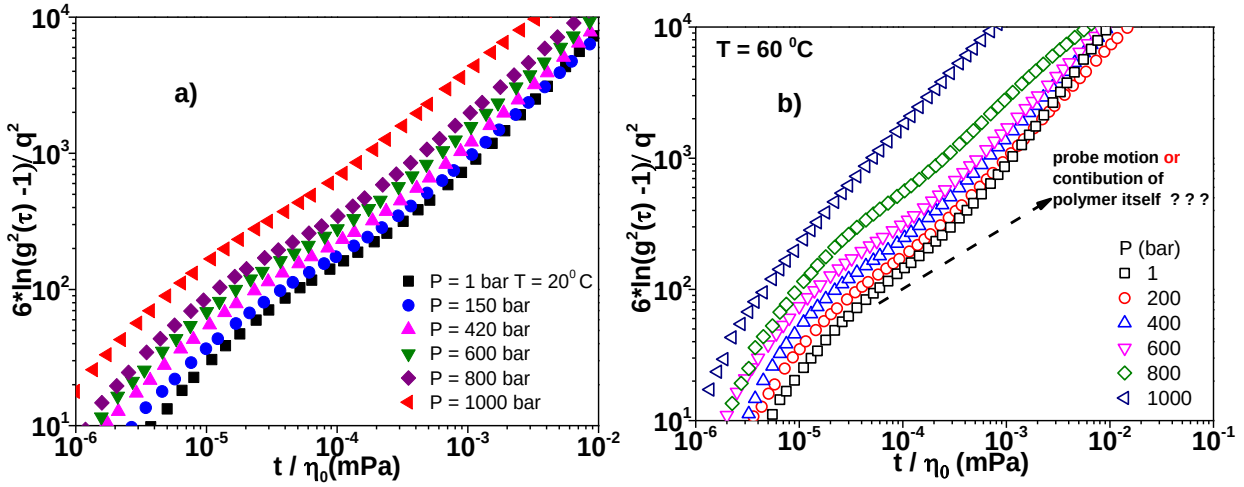


**Figure 13:** ISF of Sample A / cyclohexane / PMMA probes in **(a)** 20 and **(b)** 60$^0$C, at different pressures. The data are shifted by solvent viscosity. c = 0.6 c*.

Similar temperature effect in relative viscosity was observed with [19]. As pressure increases the decrease of the relative viscosity was observed. No elastic plateau modules exist. We were observed the formation of viscous samples in the studied temperature-pressure range. At 1 kbar and 60 $^0$C the relative viscosity is almost unit, indicating that no presence of cluster exists under such conditions (fig. 15b). If exist, doesn't have a contribution in the viscosity of the sample.

Furthermore, the samples in cyclohexane look to be weaker comparing with the samples in phenyldodecane, (this observation can be visible also from naked eyes). From the technical part, is important to mention the presence of two diffusive motions, where a sub-diffusive motion observed in between (fig. 13). Two possible scenarios for this strange behavior of the motion of the probe exist, i) the probe particle undergo this sub-diffusive motion at short times due to the dynamic exchange of the clusters (give a slope of  0.75), ii) the material itself contribute enough in the scattering intensity as a result the observation of this non-diffusive motion of the probe.

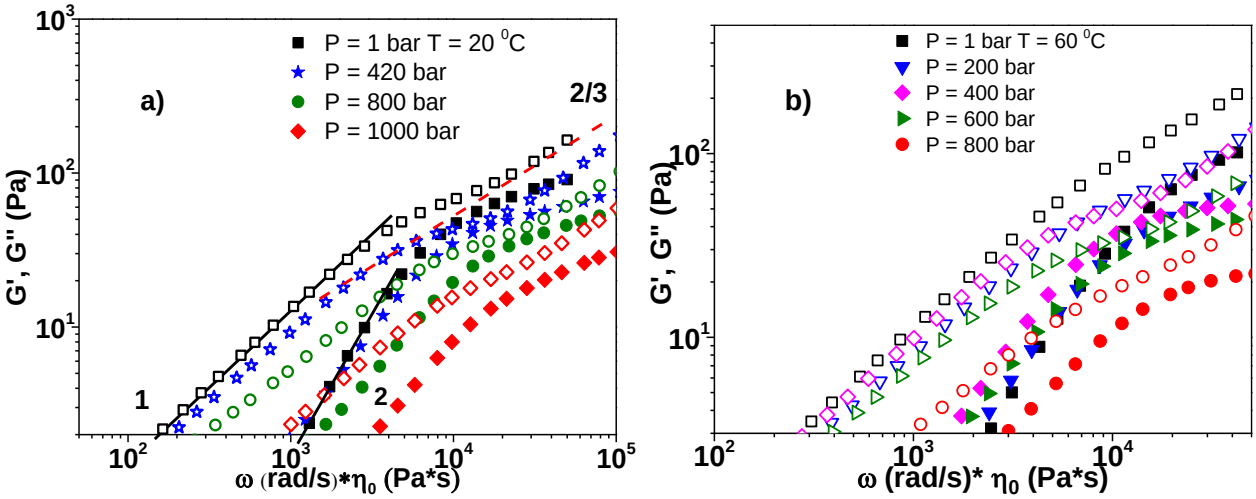


**Figure 14:** Frequency dependent viscoelastic spectra of Sample A / cyclohexane / PMMA probes in **(a)** 20 and **(b)** 60$^0$C, at different pressures. The data are shifted by solvent viscosity. c = 0.6 c*.

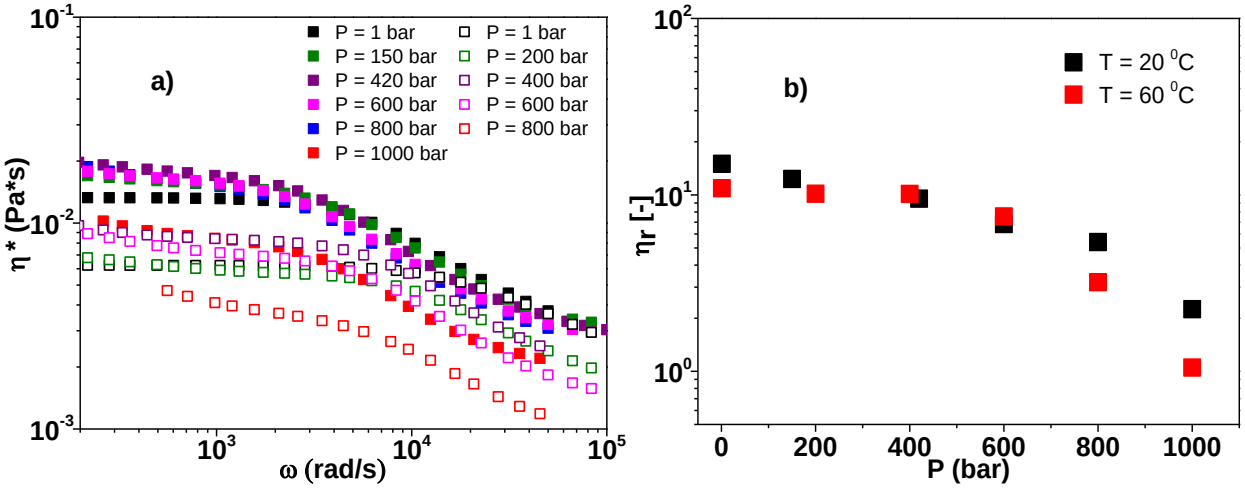


**Figure 15:** Frequency dependent complex viscosity of Sample A / cyclohexane / PMMA probes in **(a)** 20 and 60$^0$C, at different pressures. **(b)** Relative viscosity versus pressure at 20 (black squares) and 60 $^0$C (red squares). The data are shifted by solvent viscosity. c = 0.6 c*.

### 3.2.2 Semi-dilute Regime: Loose aggregates remains unaffected by Pressure and temperature

The pressure and temperature effect in the dynamics of loose aggregate are smaller as the polymer concentration increases in a level higher than the overlap concentration (fig. 16). Still we don't have any hint about the formation of a viscoelastic (transient) network, but the interactions of the formatted clusters seem to be enough stronger. By increase of pressure at 1kbar we observe a small decrease in the diffusion coefficient but use of Stokes-Einstein relation (extraction of hydrodynamic radius) isn't the proper one in this concentration limit (fig. 17 & 18).

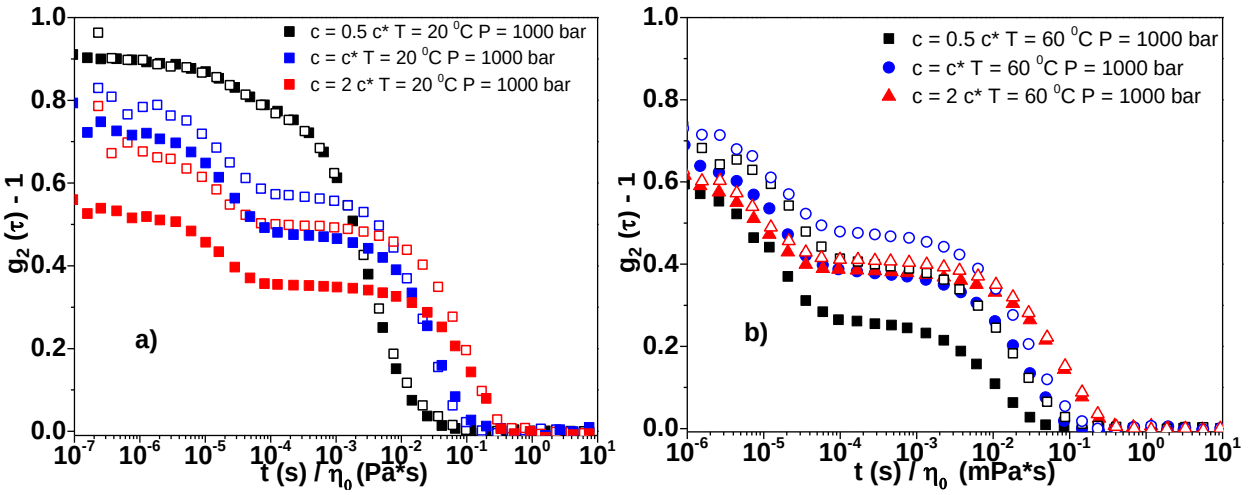


**Figure 16:** Normalized intensity correlation functions at different concentrations at **a)** 20 and **b)** 60 $^0$C of sample A/phenyldodecane. Open and filled symbols correspond to 1 and 1000 bar respectively. The data is shifted by solvent viscosity.

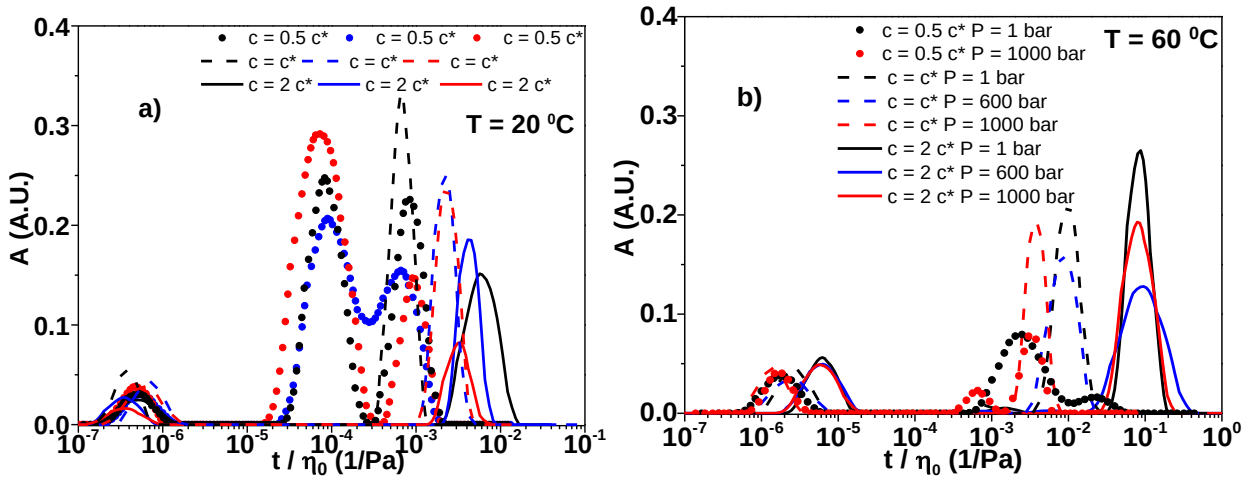


**Figure 17:** Distribution functions of relaxation times at different concentrations and pressures at **a)** 20 and **b)** 60 $^0$C of sample A/phenyldodecane solutions. The data is shifted by solvent viscosity.

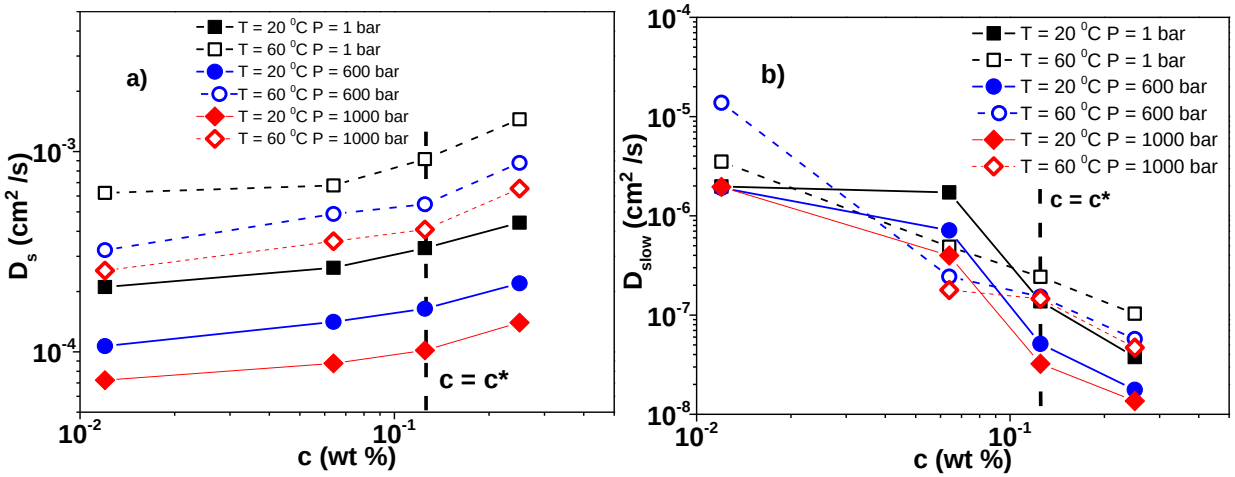


**Figure 18: a)** short time and **b)** cooperative diffusion at 20 (filled symbols) and **b)** $60^0$ C (open symbols) at different pressures versus mass concentration of sample A/phenyldodecane solutions.

A similar concentration dependence between 3-arm diblock star copolymers and triblock copolymers [10] from the literature observed. Also, by increase of temperature we observe that the scattering intensity drops down. The cluster formation observed in higher polymer concentration from 0.1 at 20 $^0$C to 0.3 c* 60 $^0$C. The peak in the scattering intensities observed to be independent by the temperature and observed in the same polymer concentration (fig 19b). Furthermore, a diffusive motion (q-independent) in the fast as well as in the slow process observed. This probably is owing to the small molecular weight of the 3-arm diblock stars (fig. 20 & 21).

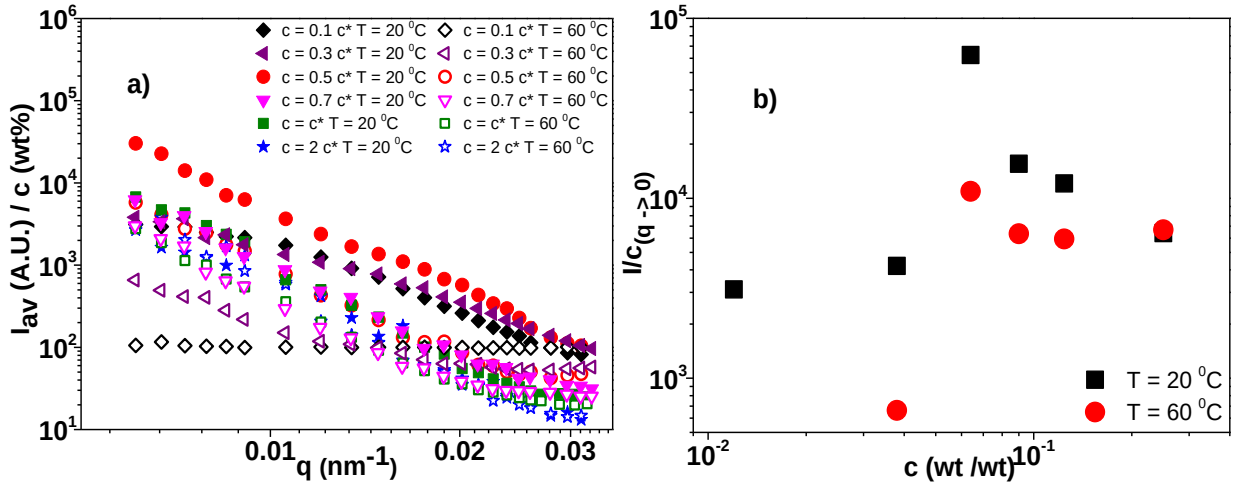


**Figure 19: a) (Static)** Scattered intensity versus the transfer vector for different concentrations at 20 (open symbols) and 60 $^0$C (filled symbols) of sample A/phenyldodecane solutions. **b)** Scattered

intensity at q→0 versus concentration, black squares and red circles corresponds to 20 and 60 $^0$C, respectively. The data is renormalized by polymer concentration.

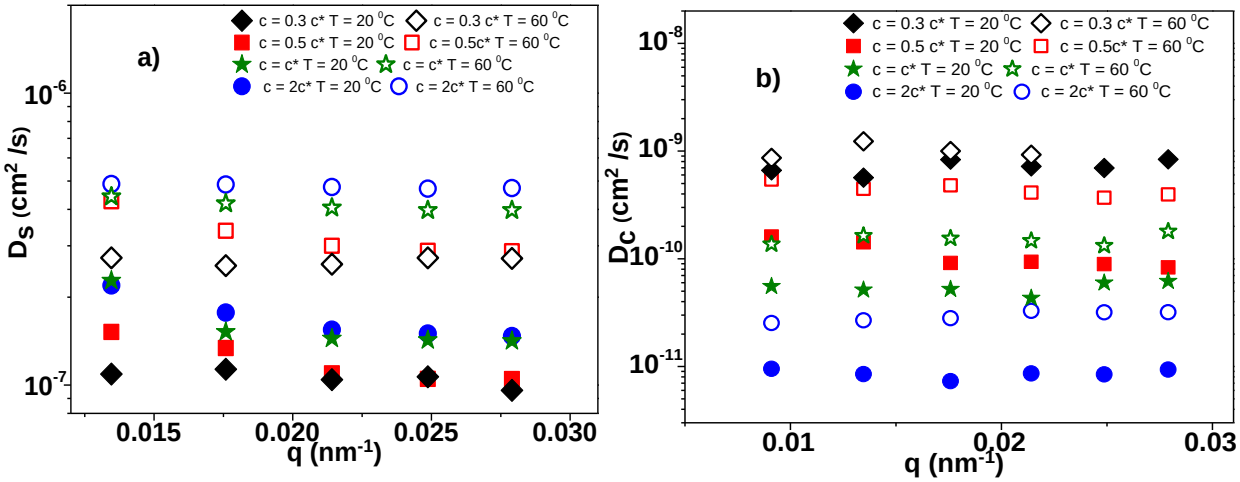


**Figure 20:** angular dependence of **a)** short time and **b)** cooperative diffusion at 20 (filled symbols) and 60$^0$ C (open symbols) for different concentrations of sample A.

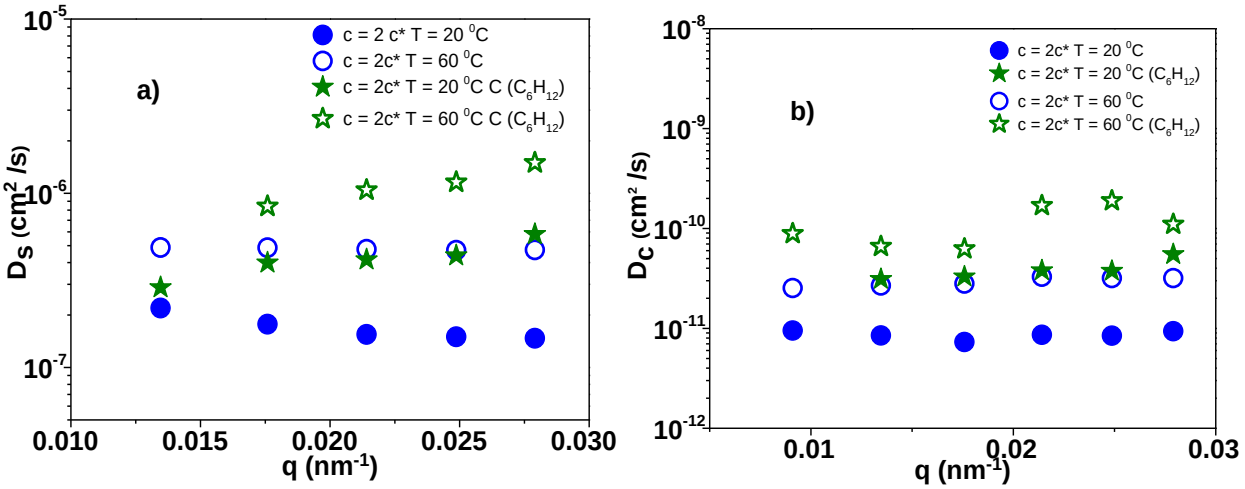


**Figure 21:** angular dependence of **a)** short time and **b)** cooperative diffusion at 20 (filled symbols) and 60$^0$ C (open symbols) at 2c* star symbols correspond to Sample A/cyclohexane, circles to Sample A/Phenyldodecane solutions.

‘

## 3.3 Conclusions

In homopolymer / phenyldodecane solutions (polystyrene PS & polybutadiene PB) the cloud point (identified by a sharp increase in the scattered intensity) was observed to increase as pressure increases of 4$^{o}$C in both cases. From ~40 $^{0}$C at 1 bar to 44$^{0}$C at 1000 bar in PS and from 10 to 14 $^{0}$C in PB. Three-arm diblock star known to form temperature sensitive clusters in phenyldodecane. We checked on the effect of pressure compare to the effect of temperature. The hydrodynamics radius of the single star (fast mode) was found to decrease as pressure increases (~20% / kbar). The scattering intensity of the fast mode was found to be independent of temperature & pressure. The hydrodynamic radius of the cluster (slow mode in IAF) was found to decrease as temperature decreases at 1 bar. Increase of pressure lead to the decrease of the cluster hydrodynamic radius (from 500 nm at 1 bar to 250 nm at 1kbar in sample A and from 400 to almost 100 in sample B). The hydrodynamic radius of the cluster (250 nm) became independent to temperature at high pressure (1kbar). The scattering intensity to the cluster (slow mode) decrease as pressure increases. In addition, the clusters dissolution observed at 60$^{o}$C at 1 bar was found to happen at 55$^{o}$C at 1kbar. In larger concentration (semi-dilute regime) the dynamics of the 3-arm diblock star were observed to be less sensitive to temperature & pressure. Strong angular dependence of the scattered intensity was found with I~q-4. Microrheology was attempted in cyclohexane ($C_6H_{12}$) solutions in intermediate regime (0.6c*). $C_6H_{12}$ (as a replacement of Phenyldodecane) was chosen for contrast reason. The solutions were found to be viscous, with relative viscosity almost independent of temperature decrease and decreasing with increasing pressure (15 at 1 bar to 1 at 1kbar). At higher concentration (2c*) the MSD of the micro-rheology probes was no-longer Brownian, preventing the simple application of Stokes Einstein equation for microrheology. Interestingly dispersion of 3-arm diblock star in heptane (a bad solvent for PS) in the dilute regime lead to the formation of monodisperse micelles at 1 bar, with decreasing $R_H$ (aggregation number) with increasing temperature (Rh from 11 nm to 8 nm from 20$^{o}$C to 50$^{o}$C, $N_{agg}$ around 10). with a narrow distribution function were observed. No angular (q) dependence with the diffusion coefficient exists.

## References

[1] T. P. Lodge, B. Pudil, & K. J. Hanley, "The Full Phase Behavior for Block Copolymers in Solvents of Varying Selectivity", Macromolecules, **35**, 4707-4717, (2002).

[2] D. A. Vega, J.M. Sebastian, Y.L. Loo & R. A. Register, "Phase Behavior and Viscoleastic Properties of Entangled Block Copolymer Gels", J. Pol. Sci.: part B: Pol. Phys. **39**, 2183-2197, (2001).

[3] Kell Mortensen. "Structural properties of self-assembled polymeric micelles" Cur. Op. in Col. & Int. Sci., vol:**3**, pp: 12-19, 1998.

[4] J. Bang, T. Lodge et Al. "Sphere, Cylinder and Vesicle Nanoaggregates in Poly(styrene-b-isoprene) Diblock Copolymer Solutions", Macromolecules, vol: **39**, pp: 1199-1208.

[5] C. Konak, M. Helmstedt, R. Bansil, "Temperature dependence of dynamics of solutions of triblock copolymer in a selective solvent", Polymer, vol. **41**, pp: 9311-9315, (2000).

[6] C. Konak, G. Fleischer, Z. Tuzar, R. Bansil, "Dynamics of Solutions of Triblock Copolymers in a selective solvent: Effect of Varying Copolymer Concentration" J. Pol. Sci. Part B:Pol. Phy. Vol: **38**, pp: 1312-1322, (2000).

[7] D. Lairez, M. Adam, E. Raspaud, J.P. Carton, J.P. Bouchaud, "TRIBLOCK COPOLYMERS IN A SELECTIVE SOLVENT: DILUTE AND SEMI-DILUTE SOLUTIONS", Macromol. Symp,. **90**,203-229, (1995).

[8] F. Xu, T. Li, J. Xia, F. Qiu, Y. Yang, "(Polystyrene-g-polyisoprene)-b-polystyrene comb-coil block copolymer in selective solvent", Polymer, vol:48, pp: 1428-1434, 2007.

[9] E. Raspaud, J. Pierre Carton, et. al., "Triblock Copolymers in a Selective Solvent. 1. Aggregation Process in Dilute Solution", Macromolecules, vol:27, pp: 2956-2964, 1996.

[10] E. Raspaud, J. Pierre Carton, et. al., "Triblock Copolymers in a Selective Solvent. 2. Semidilute Solutions", Macromolecules, vol:29, pp: 1269-1277, 1996.

[11] J. P. Hinestrosa, J. Alonzo, M. Osa, S.M. Kilbey II, "Solution Behavior of Polystyrene-Polyisoprene Miktroarm Block Copolymers in a Selective Solvent for Polyisoprene", Macromolecules, vol:43, pp: 7294-7304, 2010.

[12] J. Bang, K. Char et. Al., "Temperature-dependent micellar structures in poly(styrene-b-

isoprene) diblock copolymer solutions near the critical micelle temperature" J. Chem. Phy. Vol: 121, pp: 11489, 2004.

[13] D. Lairez, M. Adam, J.P. Cartoon and E. Raspaud, "Aggregation of Telechelic Triblock Copolymers: From Animals to Flowers", Macromolecules, vol: 30, pp: 6798-6809, 1997.

[14] T. P. Lodge & J. Bang, "Origin of the thermoreversible fcc-bcc transition in block copolymer solutions", Phys. Rev. Let., **92**, 145501-1-4, (2004).

[15] T. Lodge, M. Hamersky, K.J. Hanley and C. I Huang, "Solvent Distribution in Weakly-Ordered Block Copolymer Solutions", Macromolecules, vol: 30,pp: 6139-6149, 1997.

[16] J. Huh, K. H. Kim, C. H. Ahn, & W. H. Jo, "Micellization behavior of star-block copolymers in a selective solvent: A brownian dynamics simulation approach", J. Chem. Phys., **121**, 4998, (2004).

[17] Y. Wang, W.L. Mattice, D. H. Napper, "Simulation of the Self-Assembly of Symmetric Triblock Copolymers in Dilute Solution", Macromolecules, **25**, 4073-4077, (1992).

[18] J. Plestil, D. Hlavat, J. Hrouz and Z. Tuzart, "Dilute and semidilute solutions of ABA block copolymer in solvents selective for A or B blocks: 1. Small-angle X-ray scattering study*", Polymer, **31**, 2112, (1990).

[19] Esmaeel Moghimi, Iurii Chubak, Antonia Statt, Michael P. Howard, Dimitra Founta, George Polymeropoulos, Konstantinos Ntetsikas, Nikos Hadjichristidis, Athanassios Z. Panagiotopoulos, Christos N. Likos and Dimitris Vlassopoulos, 'Self-Organization and Flow of Low-Functionality Telechelic Star Polymers with Varying Attraction', ACS Macro Lett., vol: 8, pp: 766−772, 2019

[20] F. L. Verso, A. Z. Panagiotopoulos & C. N. Likos, "Phase behavior of low-functionality, telechelic star block copolymers", Faraday Disc., **144**, 143-157 (2010).

[21] P. Adamczyk, P. Polanowski & A. Sikorski, "Percolation in polymer-solvent systems: A monte Carlo study", J. Chem. Phys., **131**, 234901, (2009).

[22] F.L. Verso & C. N.Likos, "End-functionalized polymers: Versatile building blocks for soft materials", Polymer, **49**, 1425-1434 (2008).

[23] B. Capone, I. Coluzza, F. L. Verso, C. N. Likos, R. Blaak, "Telechelic star polymers as self-assembling units from the molecular to the macroscopic scale", Phys. Rev. Let., **109**, 238301, (2012).

[24] F.L. Verso, C. N. Likos, C. Mayer & H. Lowen "Collapse of Telechelic Star Polymers to Watermelon Structures", Phys. Rev. Let., **96**, 187802, (2006).

[25] E. Bianchi, R. Blaak & C. Likos, "Patchy colloids: state of the art and perspectived", Phys. Chem. Chem. Phys., **13**, 6397-6410, (2011).

[26] J. Roots and B. Nyström, "Photon Correlation Spectroscopy on Polystyrene Solutions under High Pressure," *Macromolecules*, vol. 15, no. 2, pp. 553–556, 1982.

[27] C. L. Moses and W. A. Van Hook, "Pressure dependence of the second virial coefficient of dilute polystyrene solutions," *J. Polym. Sci. Part B Polym. Phys.*, vol. 41, no. 23, pp. 3070–3076, 2003.

[28] Kenji Kubota, Kenji Kubo and Kazuyoshi Ogino, ''The Pressure and Temperature Dependence of the Second Virial Coefficients and the Chain Dimensions of Polydimethylsiloxane Solutions,'' J. of Chem. Soc. Of Jap., vol. 49, pp. 2410-2418, 1976.

[29] H. Hosokawa, M. Nakata, and T. Dobashi, "Coexistence curve of polystyrene in methylcyclohexane. VII. Coexistence surface and critical double point of binary system in T-p-φ space," *J. Chem. Phys.*, vol. 98, no. 12, pp. 10078–10084, 1993.

[30] W.A. Van Hook, H. Wilczura and Luis P.N. Rebelo, ''Dynamic Light Scattering of Polymer/Solvent Solutions Under Pressure. Near-Critical Demixing (0.1< P/MPa < 200) for Polystyrene/Cyclohexane and Polystyrene/Methylcyclohexane,'' Macromolecules, vol.32, p.p. 7299 – 7311, 1999.

[31] S. Do Yeo and E. Kiran, "High-pressure density and viscosity of polystyrene solutions in methylcyclohexane," *J. Supercrit. Fluids*, vol. 15, no. 3, pp. 261–272, 1999.

[32] D.A. Ylitalo and C.W. Frank, ''The effect of pressure on block copolymer micelle formation: fluorescence and light scattering studies of poly(styrene – b – ethylene propylene) in heptane,'' Polymer, vol. 37, No. 22, pp. 4969 – 4978, 1996.

[33] Ute Zettl, Sebastian T. Hoffman, Matthias Ballauff, " Self-Diffusion and Cooperative Diffusion in semidilute Polymer Solutions As Measured by Fluorescne Correlation

Spectroscopy'', Macromolecules, vol. 42, pp:9537-9547, 2009.

[33] N.P. Balsara, P. Stepanek, T.P. Lodge, M. Tirrell, "Dynamic Light Scattering from Microstructured Block Copolymer Solutions" Macromolecules, vol: 24, pp: 6227-6230, 1991.

[34] J. Fang and Erdogan Kiran,"Thermoreversible Gelation and Polymorphic Transformations of Syndiotactic Polystyrene in Toluene and Toluene + Carbon Dioxide Fluid Mixtures at High Pressures", Macromolecules, vol:41, pp: 7525-7535, 2008.

[35] G. Fytas, G. Meier, T. Dorfmuller and A. Patkowski, "Separation of Two Relaxation Processes in Bulk Polymers Using Photon Correlation Spectroscopy at High Pressures", Macromolecules, vol: 15, pp: 214-216, 1982.

[36] J. Lee, T. Wang, K. Shin, J. Cho, "High-Pressure neutron scattering and random-phase approximation analysis of a molten Baroplastic diblock copolymer" Polymer, vol: 175, pp: 265-271, 2019.

[37] G. Cheng, B. Hammouda and D. Perahia, "Polystyrene-block-Polyisoprene Diblock-Copolymer Micelles: Coupled Pressure and Temperature Effects" Macromol. Chem. Phys., vol: 215, pp: 776-782, 2014.

[38] D. Y. Ryu, D. J. Lee, J. K. Kim, K.A. Lavery, T. P. Russell, Y. S. Han, B. S. Seong, C. H. Lee, P. Thiyagarajan, "Effect of hydrostatic pressure on closed-loop phase behavior of block copolymers", Phys. Rev. Lett., **90**, 235501, (2003).

[39] W. Winoto, S. P. Tan, Y. Shen, M. Radosz, K. Hong & J. W. Mays "High-Pressure Micellar Solutions of Polystyrene-block-polybutadiene and Polystyrene-block-polyisoprene in Propane Exhibit Cloud-Pressure Reduction and Distinct Micellization End Points", Macromolecules, **42**, 3823-3826, (2009).

[40] D. A. Hajduk, S. M. Gruner, S. Erramilli, R. A. Register, & L. J. Fetters, "High-Pressure Effects on the Order−Disorder Transition in Block Copolymer Melts", Macromolecules, **29**, 1473–1481, (1996).

[41] E. M. Masnada, G. Julien, D.R. Long, "Miscibility Maps for Polymer Blends: Effects of Temperature, Pressure, and Molecular Weight", J. Pol. Sci. Pol. Phys., **52**, 419-443, 2014.

[42] S. Merabia & D.Long, "Heterogeneous Dynamics and Pressure Dependence of the Dynamics

in van der Waals Liquids", Macromolecules, **41**, 3284–3296, (2008).

[43] I. Wadgaonkar & A. Chatterji, "Network formation and gelation in telechelic star polymers", J. Chem. Phys., **146**, 084906, (2017).

[44] D. Vlassopoulos, T. Pakula, G. Fytas, M. Pitsikalis & N. Hadjichristidis, "Controlling the self-assembly and dynamic response of star polymers by selective telechelic functionalization", J. Chem. Phys. **111**, 1760 (1999).

[45] W. A. Van Hook, "Phase diagrams and thermodynamics of demixing of polystyrene/solvent solutions in (T,P,X) space", New York, (2000).

[46] X. Xiong, J. Eckelt, & B. A. Wolf, "Linear versus Three-Arm Star Polybutadiene: Effects of Polymer Architecture on the Thermodynamic Solution Behavior", Macromolecules, **45**, 9539–9546, (2012).

[47] D. J. Kozuch, W. Zhang & S.T. Milner, "Predicting the Flory-Huggins $\chi$ Parameter for Polymers with Stiffness Mismatch from Molecular Dynamics Simulations", Polymers, **8**, 241, (2016).

[48] J. L. Davis, X. Wang, K. Bornani, J. P. Hinestrosa, J. W. Mays & S. M. Kilbey, "Solution Properties of Architecturally Complex Multiarm Star Diblock Copolymers in a Nonselective and Selective Solvent for the Inner Block" , Macromolecules, **49**, 2288−2297, (2016).

[49] A. Sikora, Z. Tuzar, "Association of Two-Block Copolymer Polystyrene-block-poly(2-vinylpyridine) in Toluene", Makromol. Chem., **184**, 2049-2059 (1983).

[50] W. Winoto, S. P. Tan, Y. Shen, M. Radosz, K. Hong & J. W. Mays, "High-Pressure Micellar Solutions of Polystyrene-block-polybutadiene and Polystyrene-block-polyisoprene in Propane Exhibit Cloud-Pressure Reduction and Distinct Micellization End Points", Macromolecules, **42**, 3823-3826, (2009).

## *Chapter 4: Conclusions and future work*

## 4.1 Conclusions

High-pressure passive microrheology is emerging as an effective technique for determining the linear viscoelastic properties of soft materials and represents an important complement to the existing rheometric techniques. In this work we have presented a robust methodology to investigate both the dynamics and linear viscoelasticity of soft matter systems, mainly polymer solutions, of complex materials such as i) supramolecular living polymers (chapter 2), ii) diblock stars (TSP) (chapter 3) and gelatin aqeous solutions at elevated pressures up to 1200 bar.

We employed dynamic light scattering with varying temperatures and pressures. A good agreement between dynamic and microrheological data they were found. Note that multiple scattering diffusion wave scattering (DWS limit) for high pressure microrheology has also been tested successfully.

Our data in ambient pressure confirm literature microrheological data of living polymer solutions as well as were found to have perfect agreement with rheology data. Pressure was found to have small effect on self-assemble structure (mainly affect the solvent viscosity) when we are clearly in one regime (tube). In contrast, a structure transition from filaments (weak viscous samples) to tubes was observed in cyclohexane. Increase pressure has effect on the interaction balance. High pressure favors the tube structure (compare to the filament ones). These investigations are relevant not only for the scientific community but also for industrial purposes as supramolecular polymers used in industry (drilling fluids) as thickeners.

In the case of block copolymer stars, the Van der Waals attraction between polymer in a bad solvent lead to formation of aggregates in dilute solutions, that depends on the precise balance of interaction. We were investigated the influence of pressure on the formation of the loose aggregate as well on the mechanical properties of viscous solutions. Increase of pressure leads in the decrease of the i) aggregation number of the clusters ii) relative viscosity in dilute regime. We concluded that this is a consequence of the solvent selectivity decrease with increase of pressure.

Passive Microrheology offers a powerful way to investigate viscoelasticity and its evolution under high pressure. It is however limited to rather low modulus. The technique is not able to resolve Brownian motion of probes in large modulus materials (including most polymer melt). It offers also the ability to follow well and with high precision the evolution of viscoelasticity in kinetic processes, in particular pressure induced changes.

Despite this limitation it can be applied to a large number of dispersions and solutions, including emulsions, biopolymers, hydrogels. Indeed, we have performed preliminary studies and feasibility

tests on several samples, including emulsion for drilling fluids, gelatin sol-gel transition, PNIPAM based temperature responsive core-shell particles. Some of the preliminary data can be found in Appendix 3.

# ***Appendix***

## I. Complementary results in EHUT dispersions

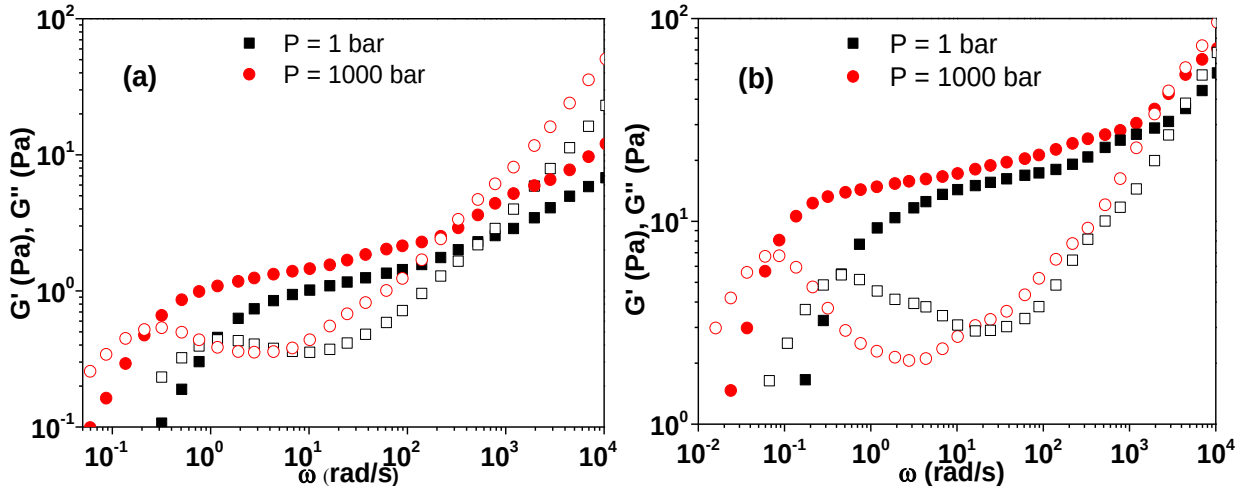


**Figure 1.** Frequency dependence of elastic G' (filled symbols) and loss G'' moduli (open symbols) for EHUT / Dodecane solutions in ambient (black squares) and 1000 (red circles) bar for different concentrations 1.5 g/L (a), 3.6 g/L (b).

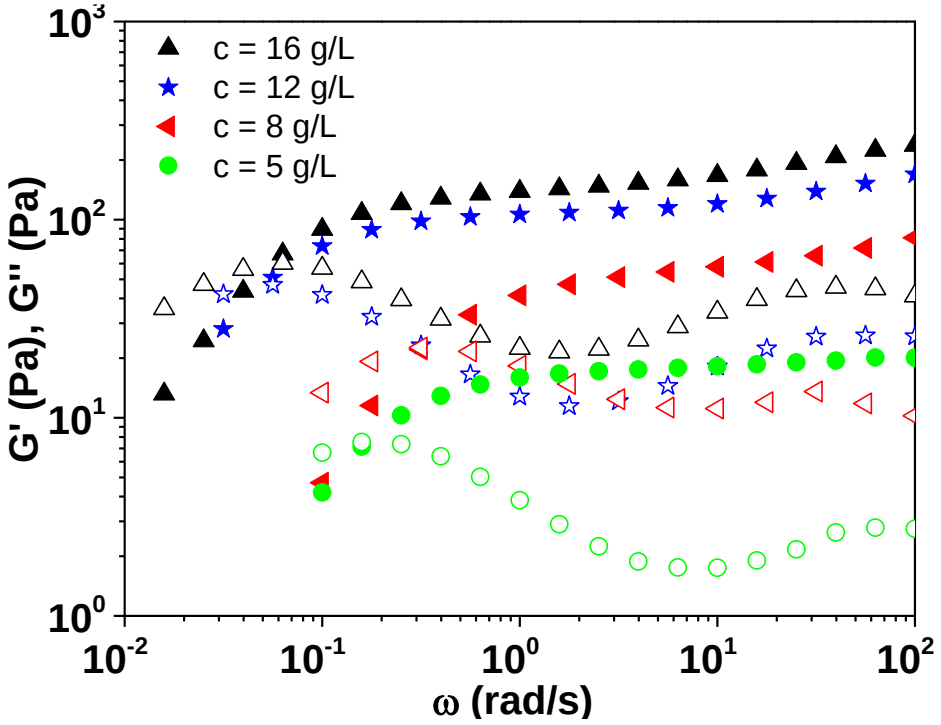


**Figure 2:** Linear viscoelastic spectra of EHUT / dodecane solutions G' (filled symbols), G'' (open symbols) in high concentrations, extracted from bulk (conventional) rheological measurements at ambient conditions (T = 25 $^{0}$C, P = 1 bar, humidity ~ 40%).

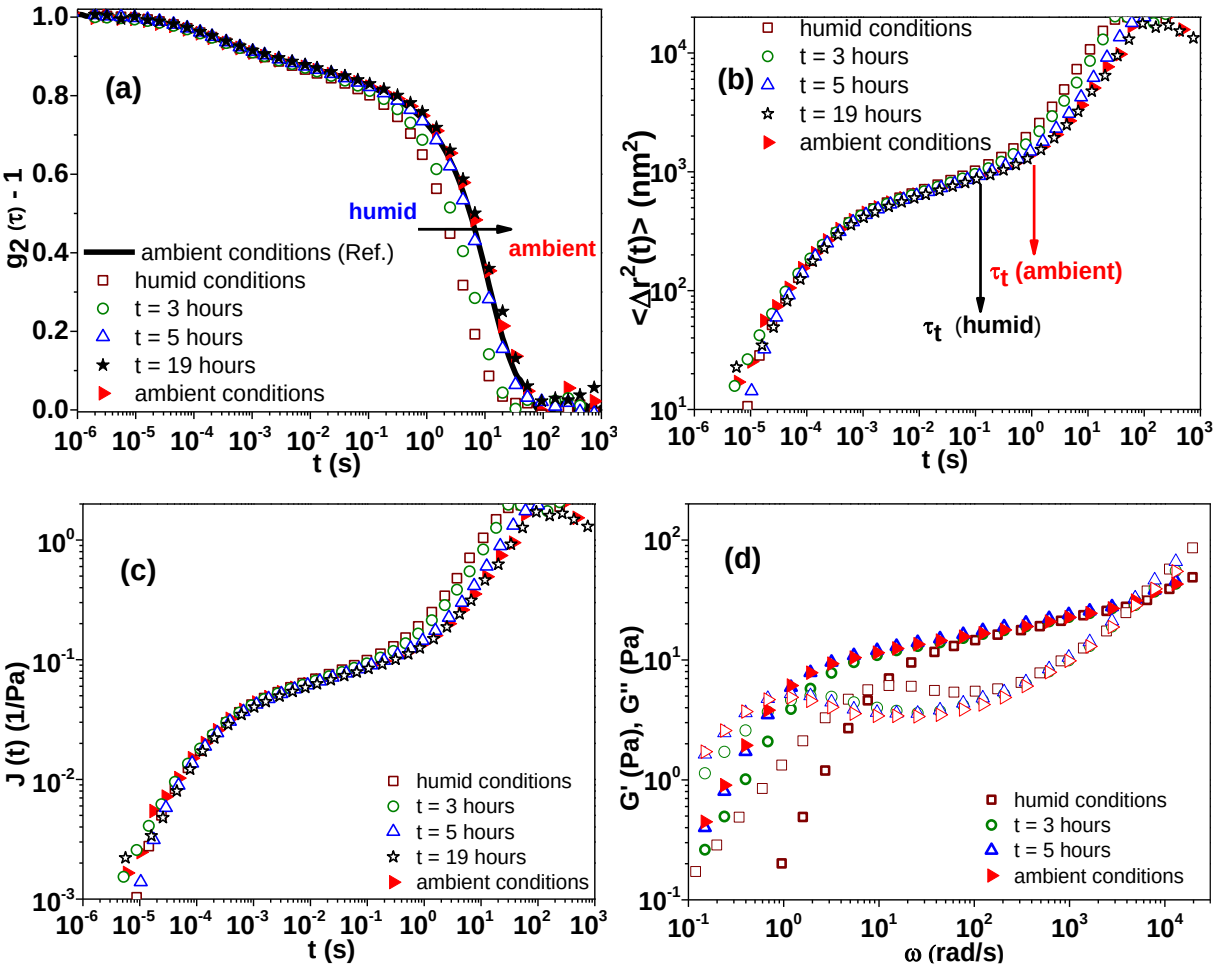


**Figure 3.** Humidity effects on EHUT/ dodecane/ PMMA solutions. ISF (a) and Mean Square Displacement (b) for EHUT / dodecane solutions in different humidity contents (c = 3.6 g/L), $\tau_t$ indicate the terminal relaxation time. Respective creep compliance (c) and Frequency dependent linear viscoelastic moduli, storage G' (filled symbols) and loss G'' moduli (open symbols) for EHUT / dodecane solutions at different levels of relative humidity (d). Ambient conditions (reference measurements, Ref.) correspond to T = 25 $^0$C, P = 1 bar, relative humidity ~ 43 %. Humid conditions correspond to relative humidity ~93 %. Intermediate measurements (t = 3, 5 and 19 hours) were conducted upon removing the top cup of the sample cell (being at ambient conditions) in order to expose the sample to humid conditions that follow the changing dynamics due to changing environmental conditions. Between measurements at different times the cup was put back and the sealed sample had different humidity compared to ambient. The black line in (a) corresponds to reference measurement in ambient conditions before the change of the humidity.

Experimental account of humidity effects: In order to assess the role of humidity, we loaded the closed sample cell to a closed beaker (filled with water) and we left it for 36 hours. At this point the relative humidity was constant at about 93 %. The first microrheological data under "ambient

conditions" are shown in Fig.S5 (wine squares). Then, we removed the cup of the sample cell and measurements took place at different times (3,5,19 hours), corresponding to different humidity levels. During each measurement we added the cup to reduce changes of humidity during the measurement.

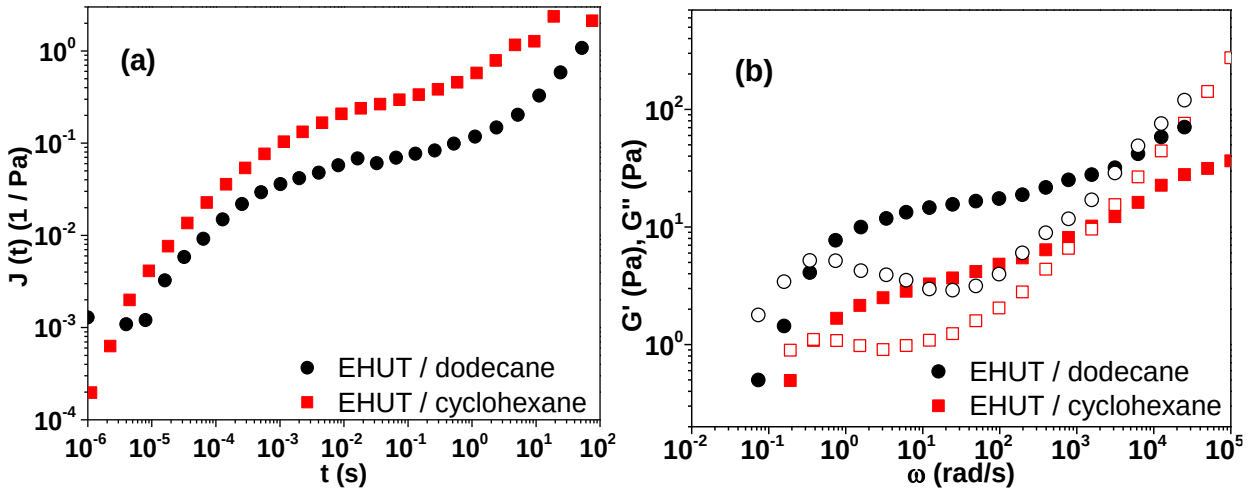


**Figure 4.** Comparison between EHUT / cyclohexane (c =4 g/L) and dodecane (c = 3.6 g/L) / PMMA solutions at ambient conditions (T = 25 $^0$C, P = 1 bar), creep compliance (a) and LVE spectra (b).

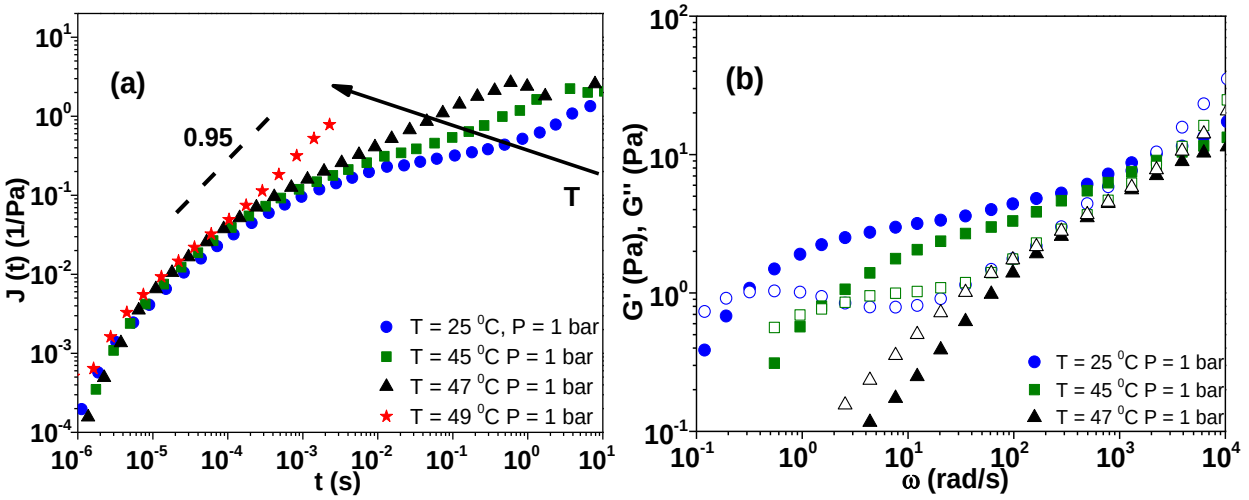


**Figure 5.** Creep compliance (a) and Frequency dependence (b) of the elastic G' (filled symbols) and loss G'' moduli (open symbols) for 4 g/L EHUT / cyclohexane / PMMA solutions in different temperatures and ambient pressure.

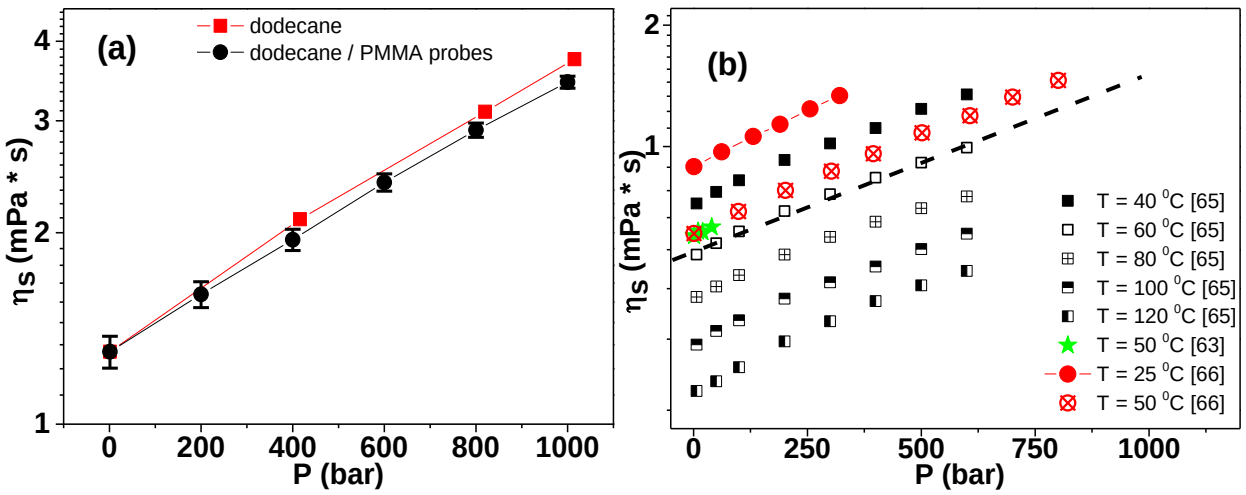


**Figure 6:** Solvent viscosities as a function of pressure (a) at room temperature for dodecane [62]. Red squares correspond to literature, Black circles and stars are data extracted from DLS microrheology measurements with dilute PMMA suspensions in dodecane, (b) cyclohexane (T, P) [63, 65, 66].

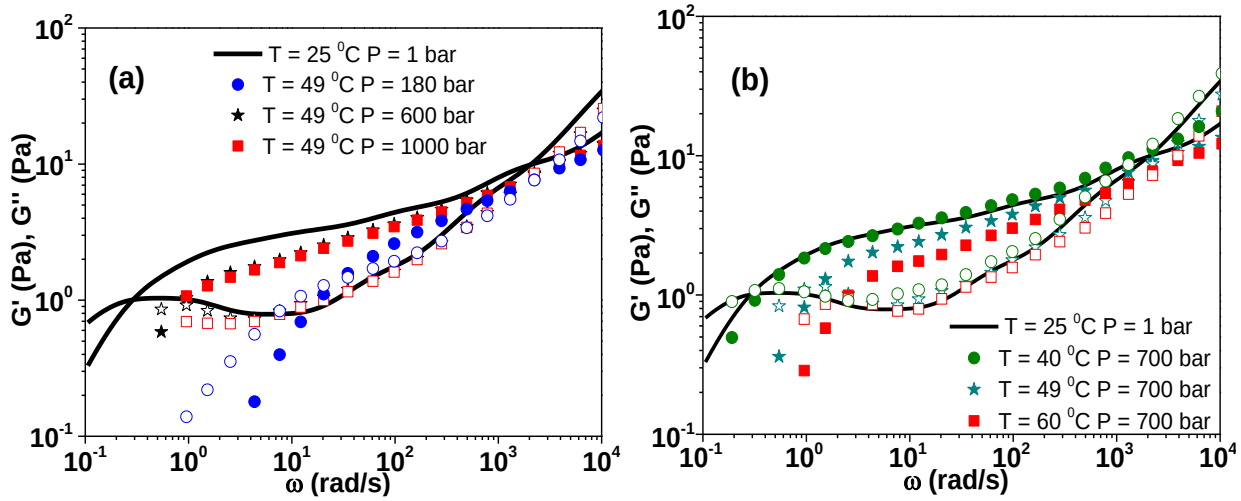


**Figure 7:** LVE of an EHUT/ cyclohexane solution for a specific concentration (c = 4 g/L) and different pressures, (a) for constant temperature of $49^0$, (b) at different temperatures and constant pressure of 700 bar. Reference data at atmospheric conditions (black line) are also shown.

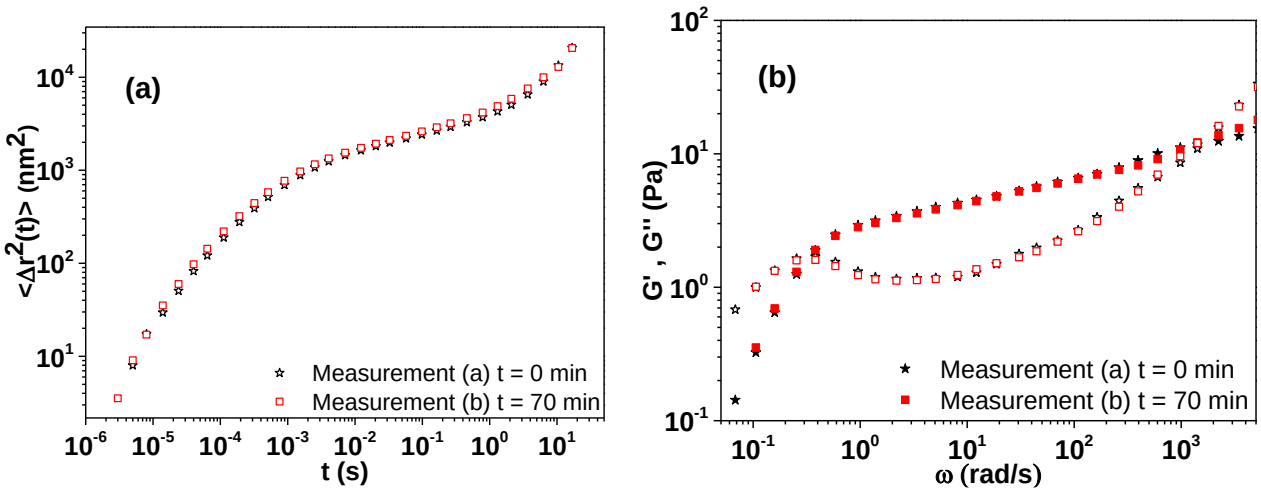


**Figure 8:** MSD of an EHUT/ dodecane / PMMA solution for a specific concentration (c = 3 g/L) at 1000 bar and room temperature, Different measurements (a), respective LVE data (b). Measurement duration 4200 sec.

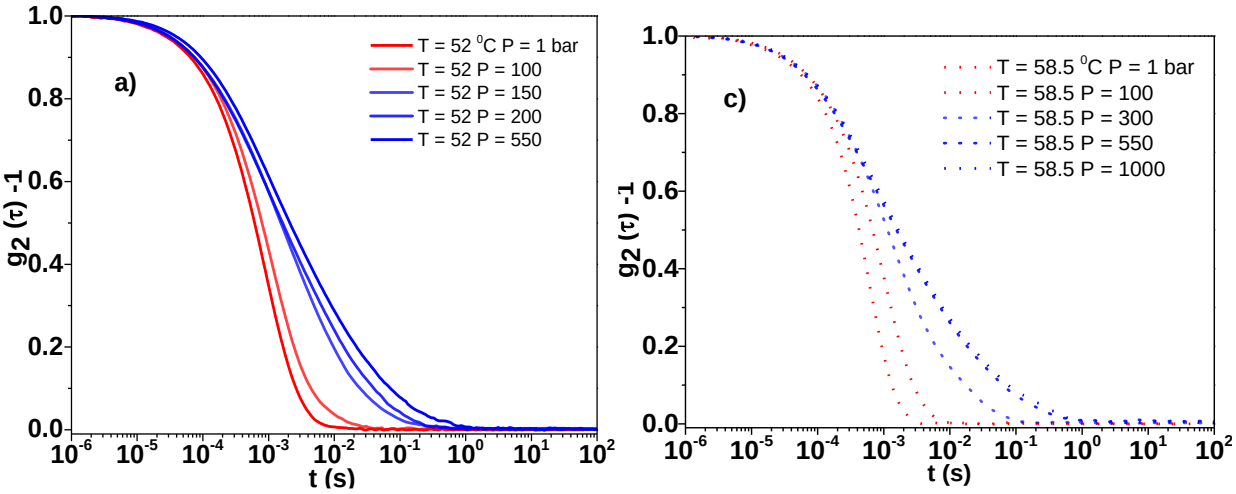


**Figure 9:** ISF of EHUT/cyclohexane/PMMA Solutions for different temperatures pressures – Transition points indicating by blue curves.

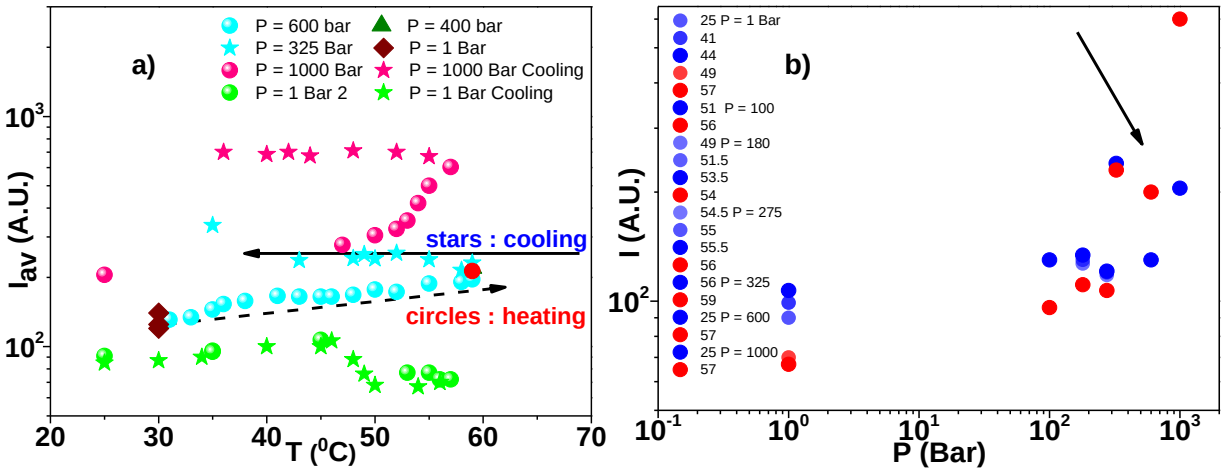


**Figure 10: a)** Scattering intensity as a function of Temperature at: ambient pressure (green), 600 bar (cyan) and 1000 bar (pink). **b)** intensity values as a function of Pressure, indicates the structure transition, blue correspond to tubes – red to filaments. For higher pressures no transition from tube to filaments observed – also, no transition in the intensity values (increase of temperature lead to increase of intensity).

## II. Complementary results in Three-arm diblock star polymer solutions

### Phenyl-dodecane viscosity (P, T)

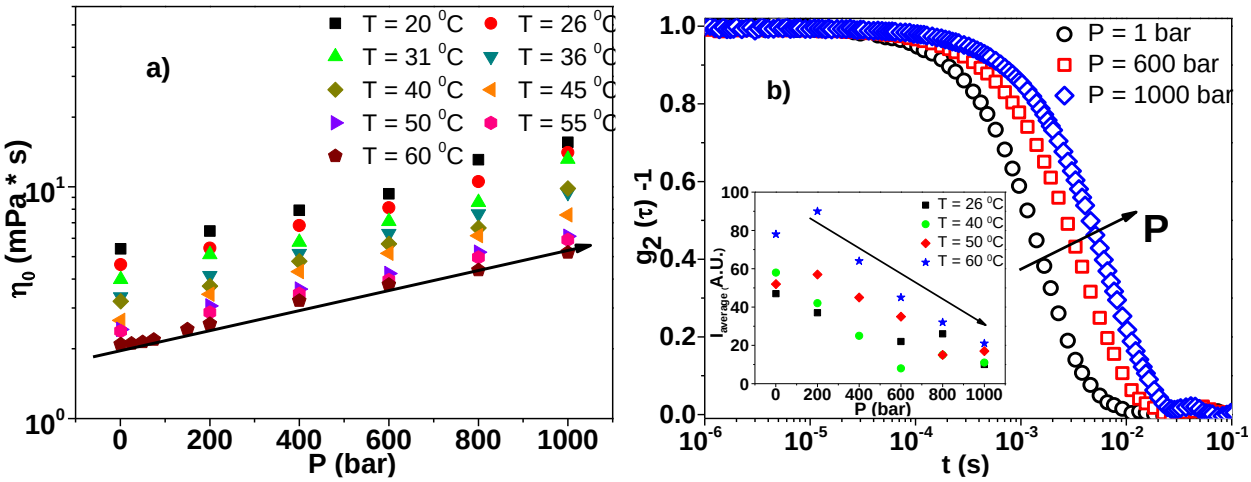


**Figure 1:** a) Viscosity of phenyl dodecane solvent (P, T), b) ISF of PMMA particles dispersed in phenyl dodecane, T = 26$^0$C. **Inset**: Average Intensity of ISF.

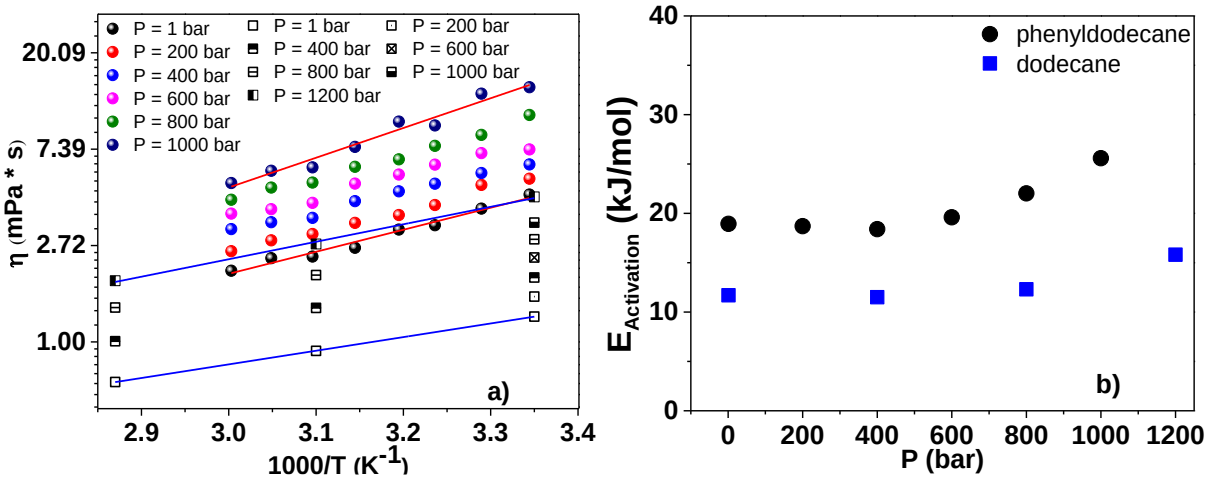


**Figure 2: a)** Viscosity values of phenyldodecane (spheres), dodecane (black open symbols) **b)** Activation energy ($E_A$) vs P of phenyldodecane (spheres) and dodecane (circles).

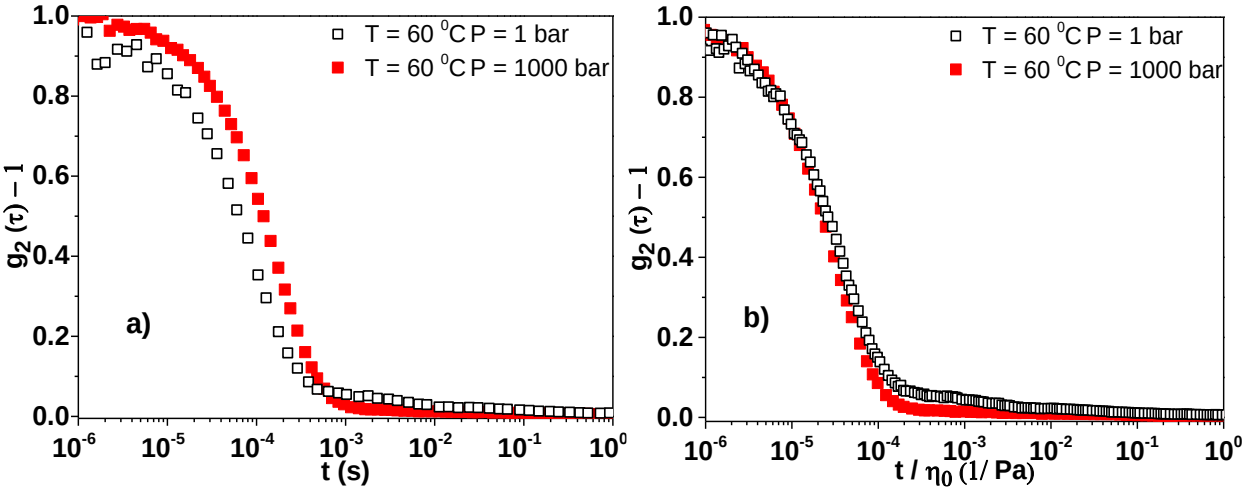


**Figure 3: a)** ISF of dilute Linear Polystyrene / Phenyl-dodecane solutions at T = 60 $^0$C, **b)** rescaled by solvent viscosity.

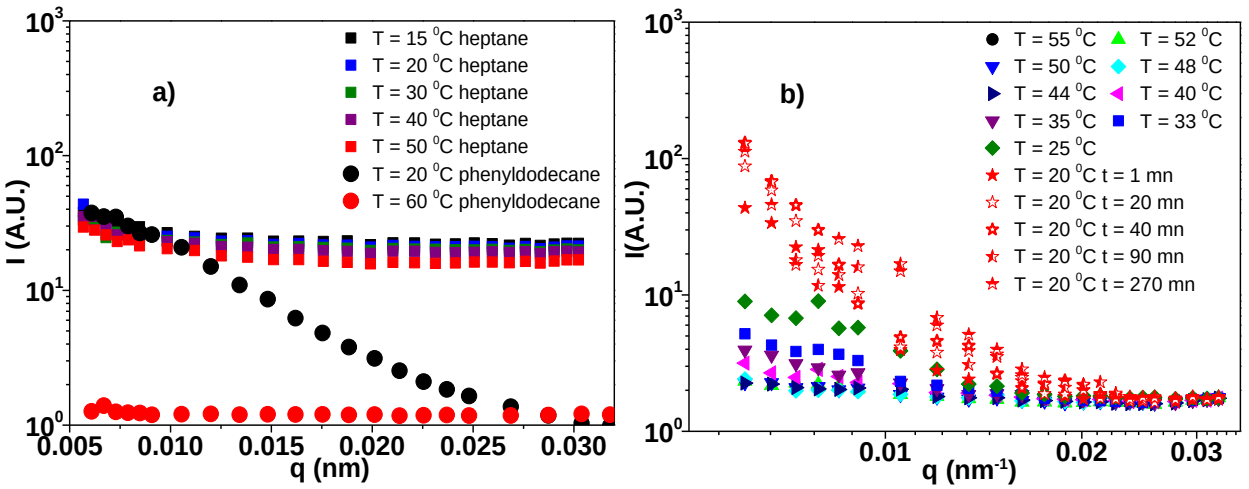


**Figure 4:** (Static) Scattered intensity versus the transfer vector for **a)** different temperatures at heptane (open squares) and (phenyldodecane) **b)** temperature ramp in phenyldodecane of sample A.

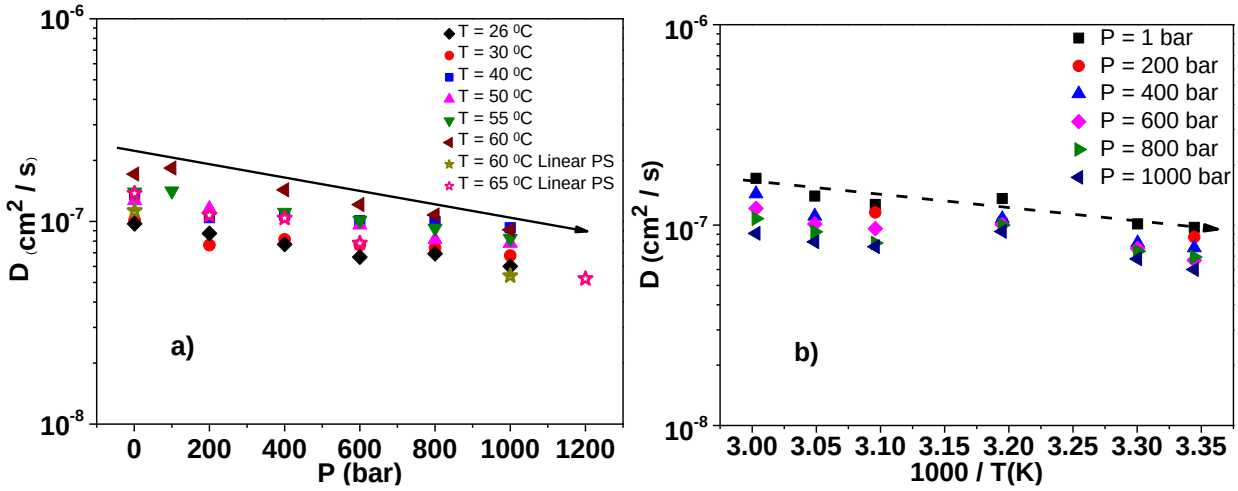


**Figure 5:** diffusion coefficient of single star as a function of pressure **a)** and temperature **b)**.

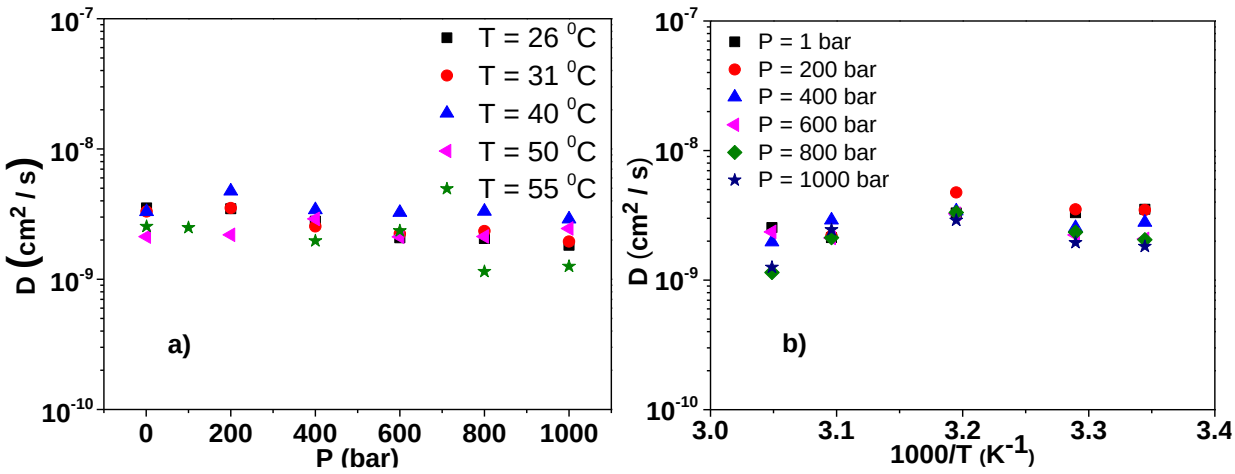


**Figure 6:** Diffusion coefficient of cluster (slow process) as a function of pressure **a)** and temperature **b)**.

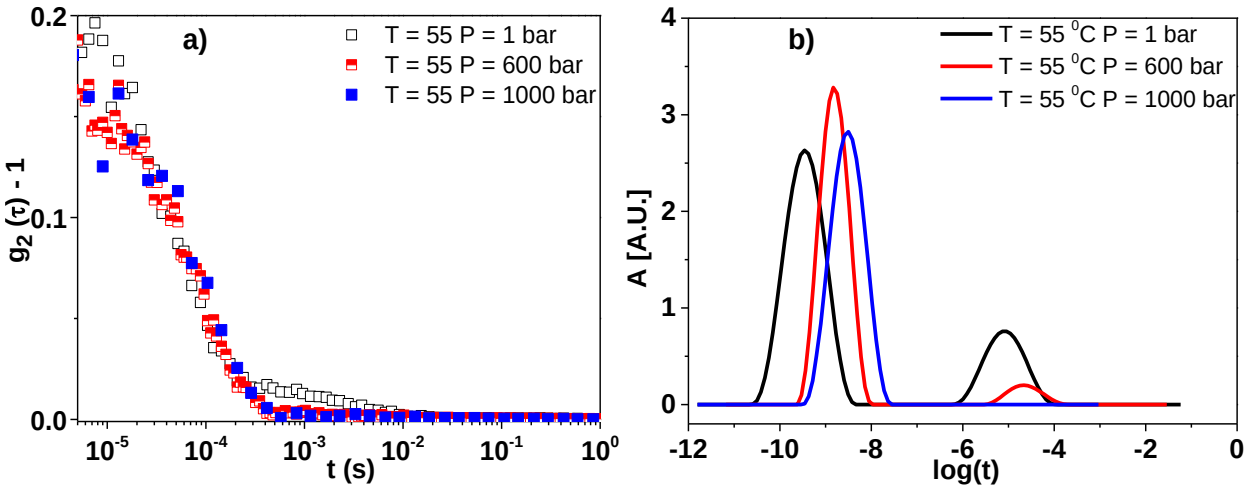


**Figure 7: a)** ISF of Sample B for different pressures at T = 55 $^0$C. **b)** Contin analysis.

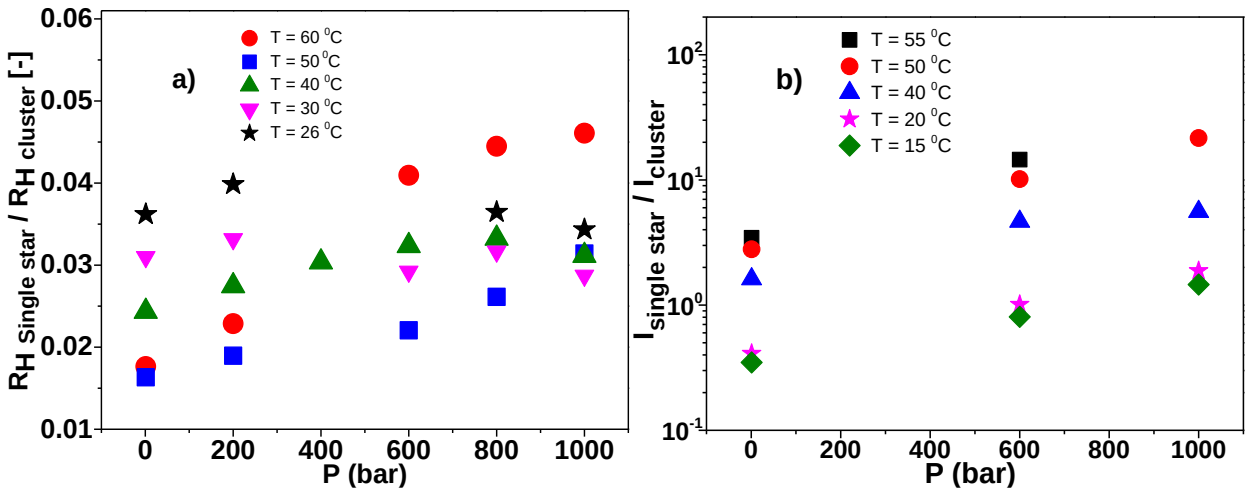


**Figure 8:** a) Hydrodynamic radius ratio of single star / cluster star of sample A. b) Intensity ratio of single star / cluster of Sample B.

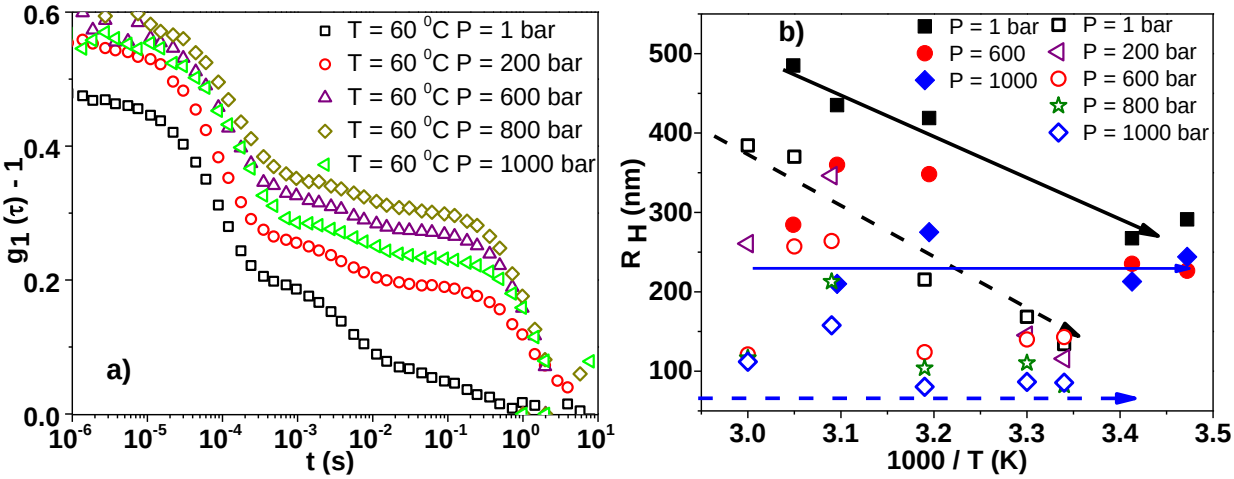


**Figure 9: a)** Field correlation function of Sample A/ phenyldodecane solutions at constant temperature (T = 60 $^0$C) for different pressures, (1→ 1000 bar). **b)** Rh of clusters as a function inverse temperature for different pressures. Open symbols correspond to Sample A, filled symbols to Sample B (in phenyldodecane).

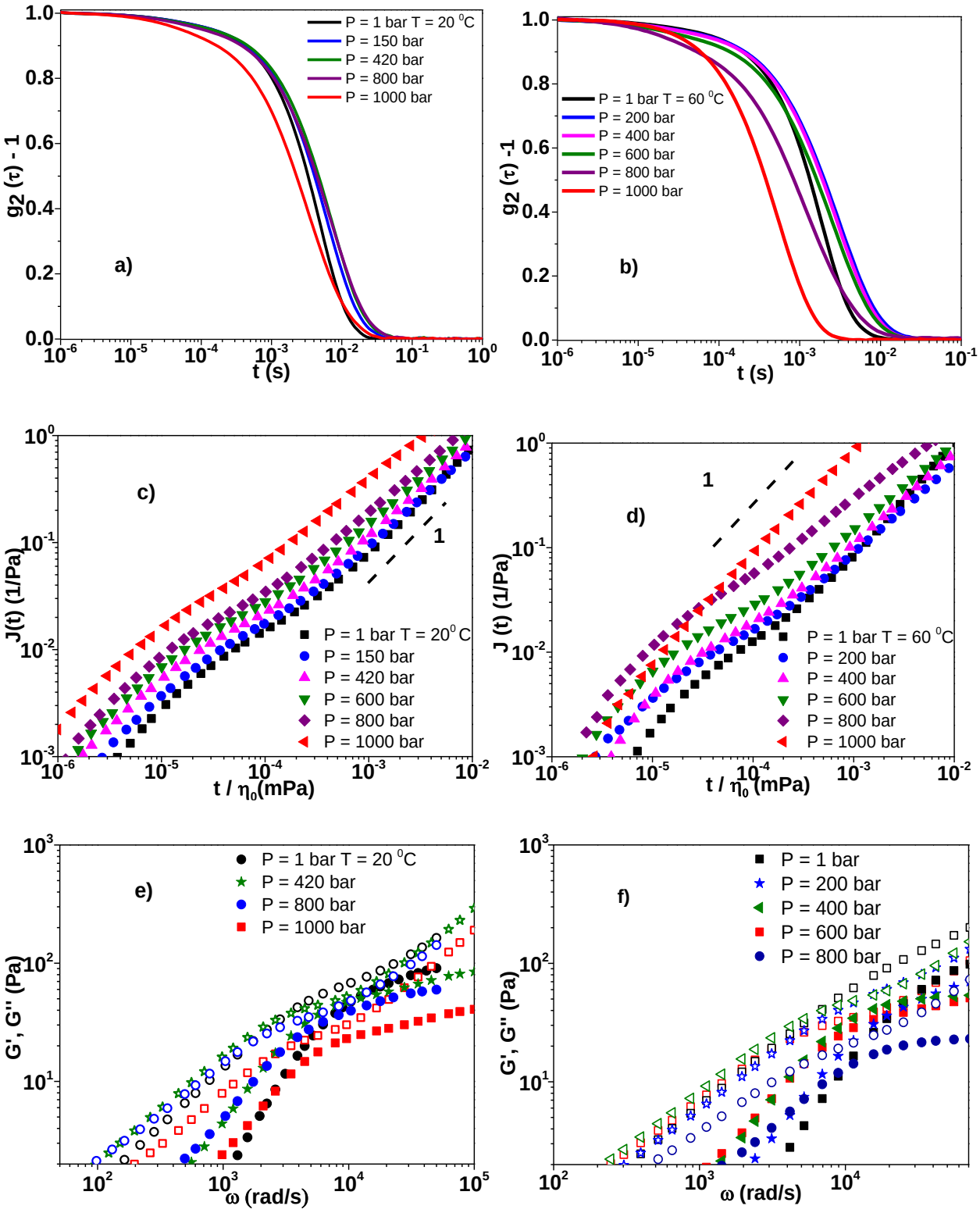


**Figure 10:** Raw data of 3 arm star / cyclohexane / PMMA probes at 2 c* at **a,c,e)** 20 and **b,d,f)** 60 $^0$C. **a,b)** ISF, **c,d)** creep compliance **e,f)** G' and G'' respectively.

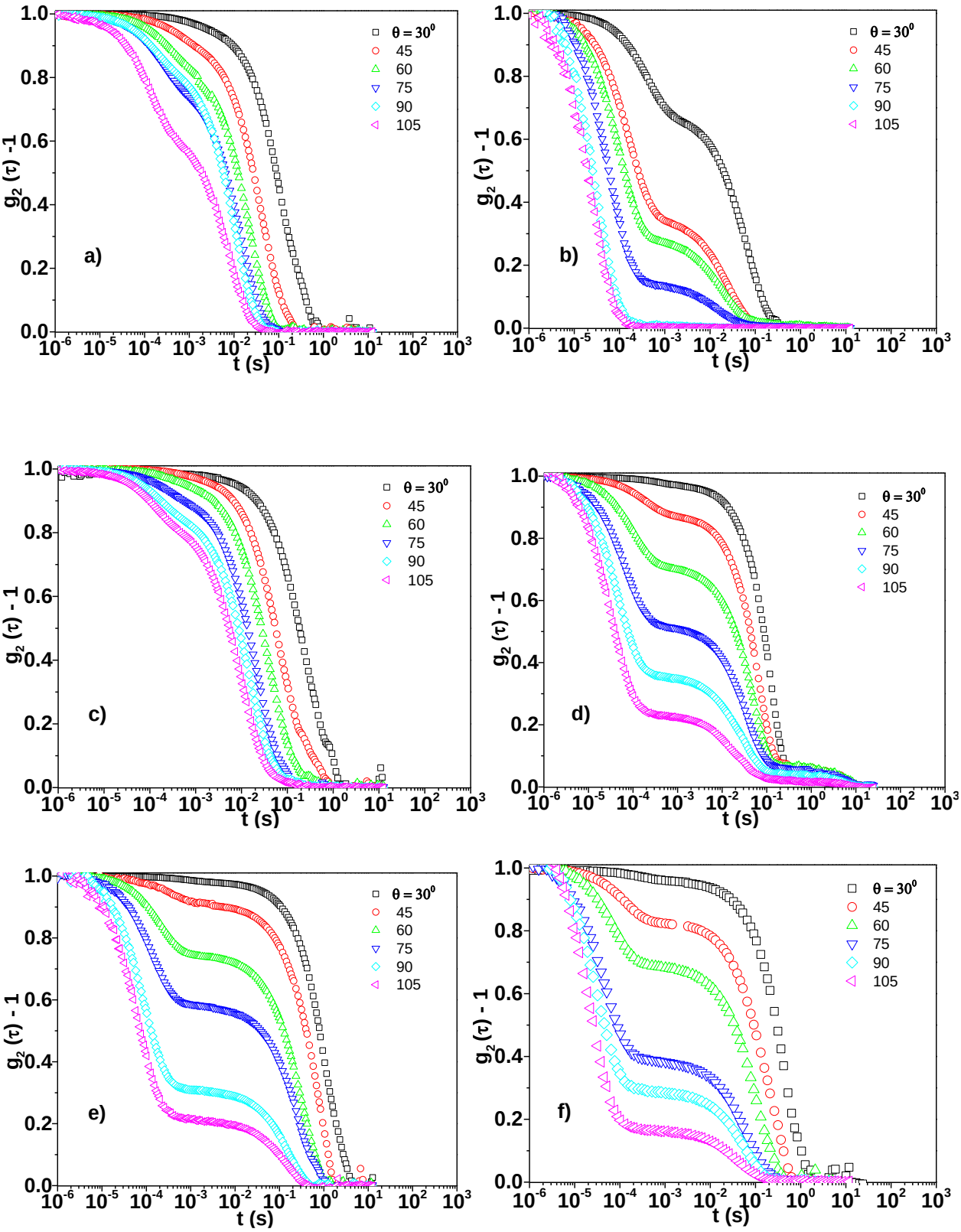
a)
b)
c)
d)
e)
f)
θ = 30⁰
45
60
75
90
105
g2 (τ) - 1
t (s)

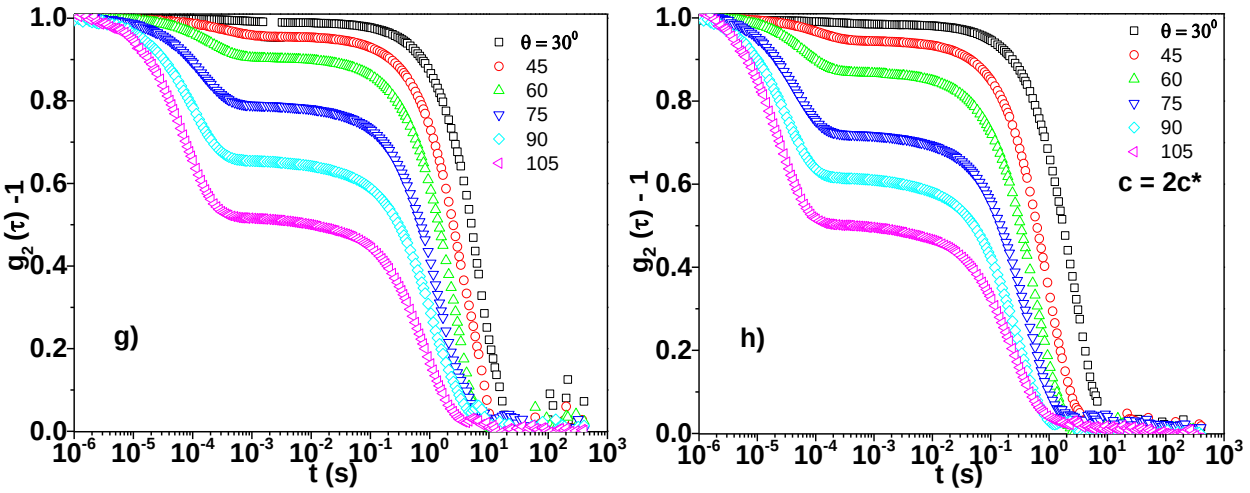


**Figure 11:** Normalized intensity correlation functions at different scattering angles at **a)** 0.3 **c)** 0.5 **e)** c* and **g)** 2 c* at 20 and **b, d, f, g)** 60 $^{0}$C of sample A.

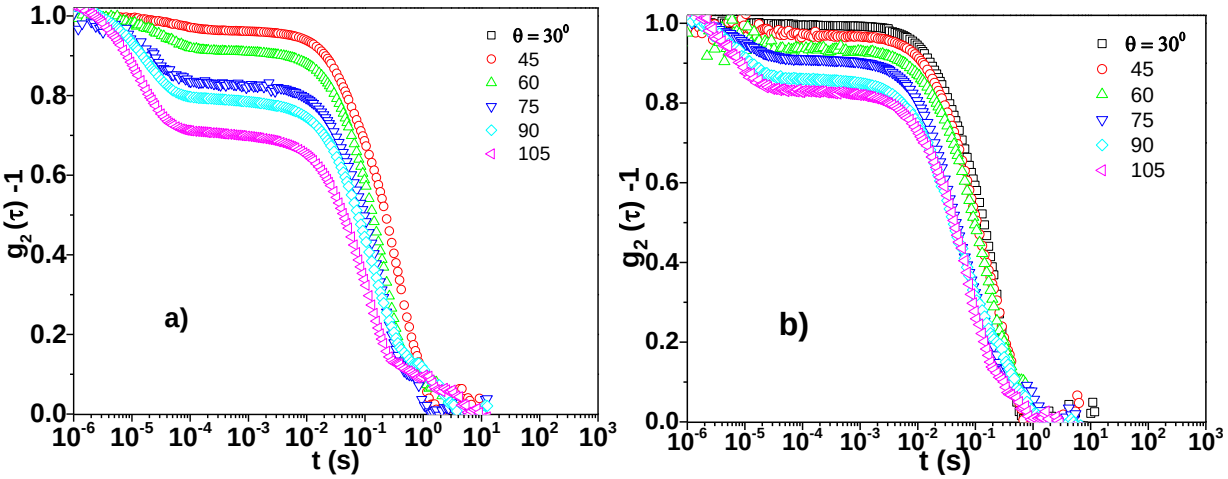


**Figure 12:** Normalized intensity correlation functions of Sample A/ cyclohexane at different scattering angles at 2 c* at **a)** 20 and **b)** 60 $^{0}$C of sample A.

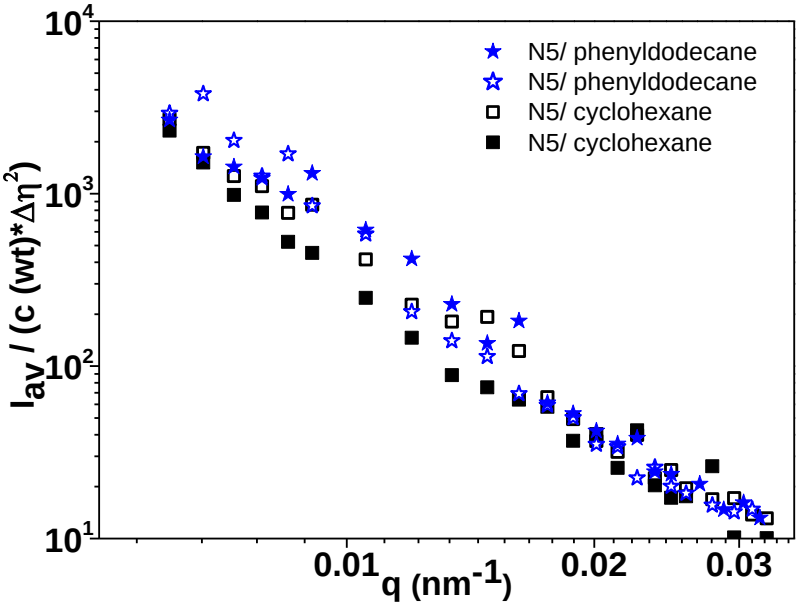


**Figure 13:** Static light scattering intensity of 3 arm diblock star / phenyldodecane (blue stars) and cyclohexane (black squares) solutions. The data are normalized by concentration and refractive index mismatch. Open symbols correspond to 60, closed to 20 $^0$C.

**Three-arm diblock star polymers in other solvents (cyclohexane-heptane)**

Questionable remain the exact mechanism and the origin of the values of β ~ 1.3 (stretched exponent) in intensity correlation function of 3-arm diblock star/ cyclohexane / PMMA solutions in semidilute regime. In contrast with the experiments in dilute (0.6 c*) in this case the value of β isn't <1 (indication for sub-diffusive motion of the probe) nor 1 (indication for the diffusion motion of the probe) nor 2 (ballistic probe motion). Passive microrheology remain unknown if works well in samples with different domains-areas (reach A block and poor B). Important to mention that all the necessary conditions for a good microrheology experiment looks valid and works well. A possible scenario for the 1.3 value of beta is that hopping of the probe due to the dynamic exchange of the cluster happens.

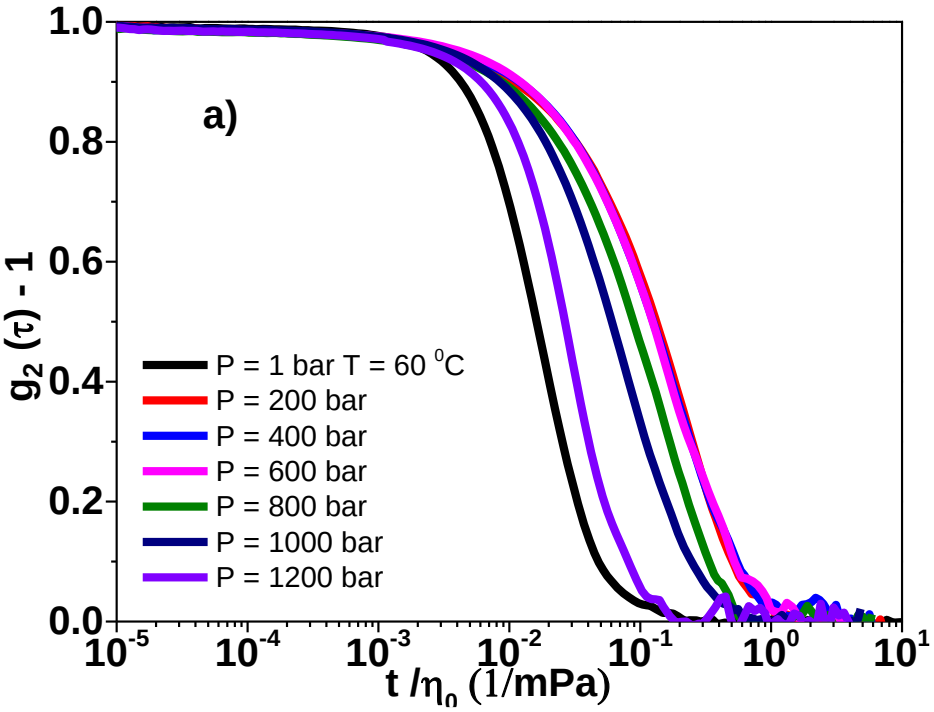


**Figure 14:** ISF of sample A / cyclohexane / PMMA probes at 2c*. Pressure dependence. The data are shifted by solvent viscosity.

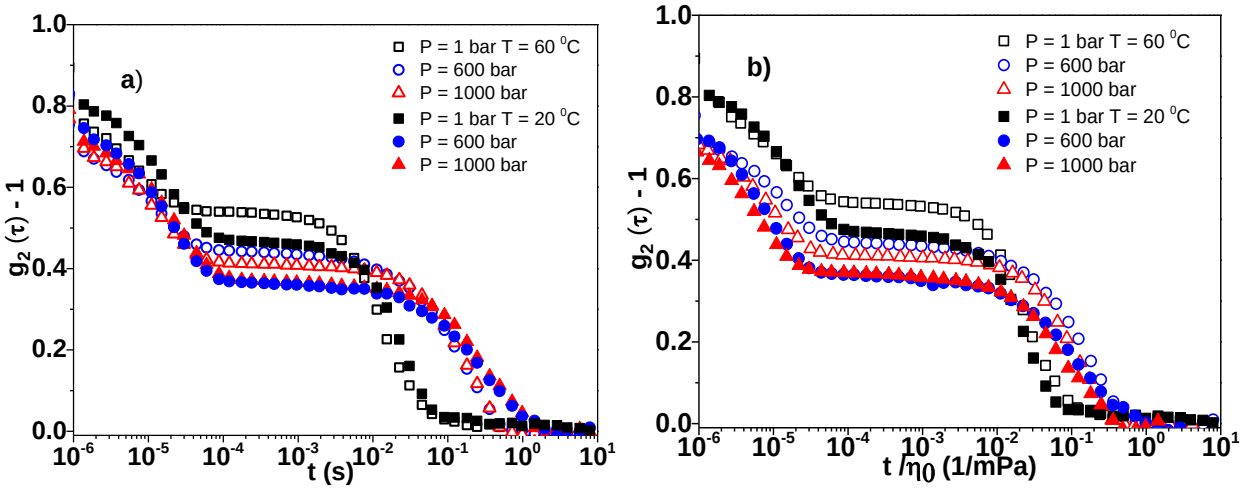


**Figure 15:** ISF at **a)** 2c* (~26 wt%) at 20 (filled symbols) and 60 $^0$C (open symbols) of sample A/cyclohexane solutions at different pressures. **b)** Shifted data by solvent viscosity.

In contrast with the case of TSP/phenyldodecane solutions, in case of TSP/cyclohexane samples, both from dynamic and microrheology experiments a non-monotonic behavior by increase of pressure observed (fig 14 & 15). Interesting is what happen in pressure regime at 5-6 kbar. Probably

the stronger the interactions and the formatted network, the higher the appropriate pressure for the cluster dissolution.

**Three-arm diblock star polymers in heptane**

The extreme case: Bad solvent for the Polystyrene – Good solvent for the PB. Open question: How the solvent selectivity varies with temperature and pressure in highly selective solvent. Owing to nitrogen solubility, pressure experiments it wasn't feasible to take place.

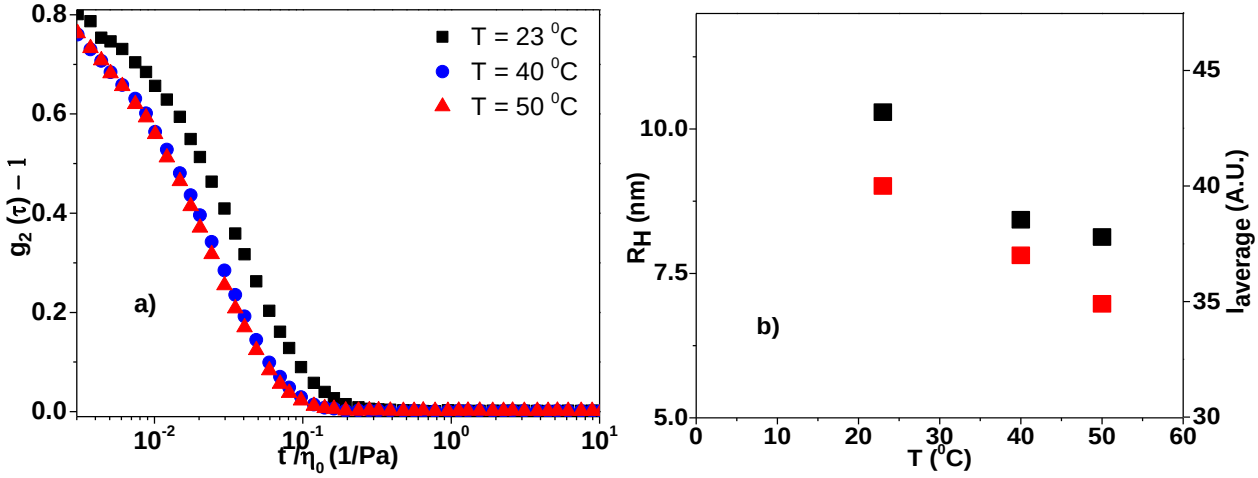


**Figure 16: a)** ISF of Sample A / heptane at different temperatures. **b)** Hydrodynamic radius (red squares- left axis) and average intensity (black squares-right axis) versus temperature. The data are shifted by solvent viscosity.

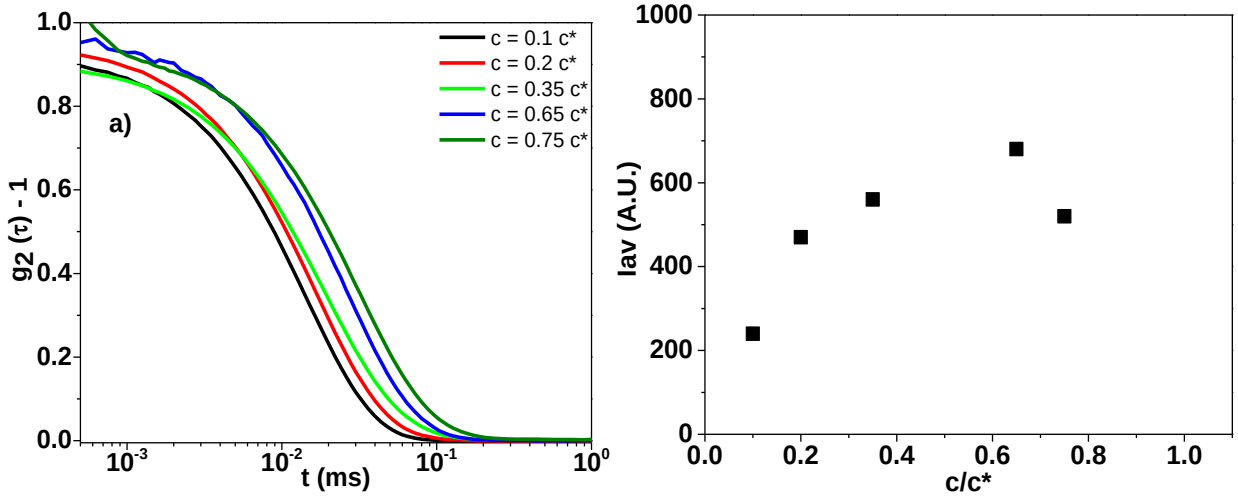


**Figure 17:** Concentration dependence of 3-arm diblock star/ Heptane solution **a)** ISF **b)** respective average intensities.

## Preliminary results in other systems

### I. Core-shell Pnipam-Polystyrene

Preliminary experiments in dilute regime in core-shell PNIPAM-PS microgels are shows that pressure have an impact in the interactions. As a result, changes in hydrodynamic radius observed. All the experiments performed in dilute regime.

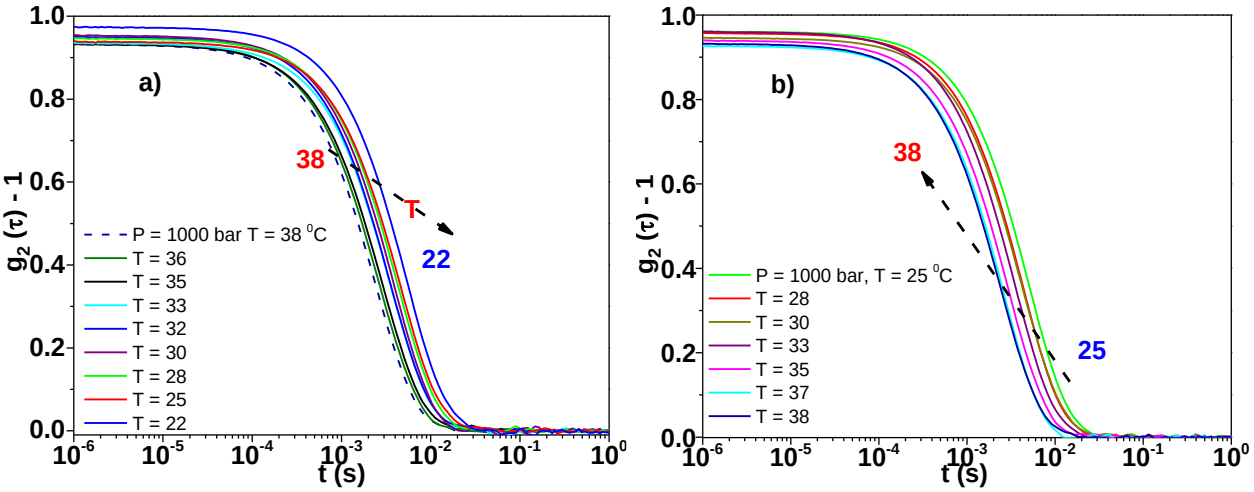


**Figure 1:** ISF of PNIPAM TFEMA microgels for different temperatures at 1000 bar. Experiments performed in single scattering limit.

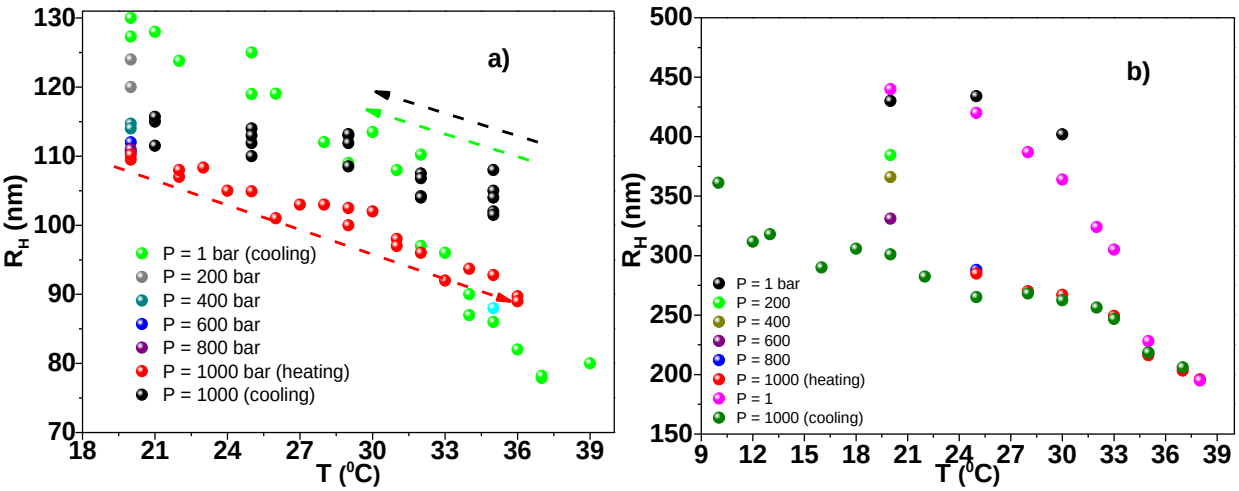


**Figure 2:** Hydrodynamic radius as a function of temperatures for different pressures of **a)** PS-PNIPAM **b)** TFEMA- PNIPAM core-shell particles in dilute regime.

Emulsions are another interesting category for studying their mechanical properties under high hydrostatic pressure. Owing to the big changes in the volume fraction by hydrostatic pressure application, big changes in the viscoelasticity of the sample are possible to observed.

## II. Gelatin aqeous solutions

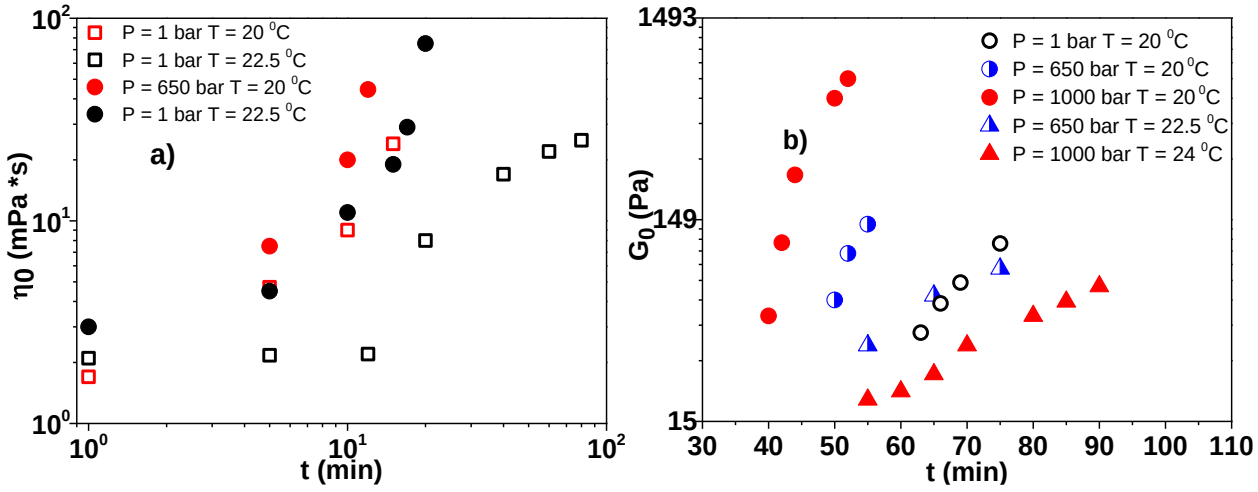


**Figure 2: a)** viscosity & **b)** plateau modulus of gelatin / $H_2O$, solutions, c = 2 wt. %, as a function of time for a series of pressures and Temperatures. Viscosity values extracted in the single scattering limit, plateau modulus in the multiple scattering limit by means of passive microrheology.

In gelatin gels solutions we were investigated through DLS and microrheology the effect of hydrostatic pressure in the formation of the triple helix. Microrheology experiments were performed in single scattering limit (low probes concentration) as well as in multiple scattering (~1% wt probes concentration). Changes in scattering intensity (Mw) & in mechanical properties (increase of plateau modules) of gelatin gels were found to connected with the changes in the formation of the triple helix. Pressure was found to alter the kinetic process as well leads in the formation of stronger gels. A better knowledge about the mechanical properties of Gelatin gels under high hydrostatic pressure will be helpful for food industry purposes. We were observed a good agreement between DLS and microrheology.